FGI PUBLICATIONS N:O 174

Characterizing Boreal Forest Structure and Estimating Above-Ground Biomass with Helicopter-borne Ku-band Profiling Radar

BY Ziyi Feng

NLS
FINNISH GEOSPATIAL
RESEARCH INSTITUTE
FGI

Aalto University publication series
Doctoral Theses 237/2026

Characterizing Boreal Forest Structure and Estimating Above-Ground Biomass with Helicopter-borne Ku-band Profiling Radar

Ziyi Feng

A doctoral thesis completed for the degree of Doctor of Science (Technology) to be defended, with the permission of the Aalto University School of Electrical Engineering, at a public examination held at the lecture hall H304 of the school on 08 October 2026 at 12 noon.

Aalto University
School of Electrical Engineering
Department of Electronics and Nanoengineering

Finnish Geospatial Research Institute
Department of Remote Sensing and Photogrammetry

Supervising professor
Associate Professor Jaan Praks, Aalto University, Finland

Thesis advisors
Professor Juha Hyyppä, Finnish Geospatial Research Institute, National Land Survey, Finland
Professor Yuwei Chen, Hangzhou Institute for Advanced Study, University of Chinese Academy of Sciences, China

Preliminary examiners
Professor Johan Fransson, Linnaeus University, Växjö, Sweden
Professor Andreas Reigber, German Aerospace Center (DLR), Germany

Opponent
Professor Johan Fransson, Linnaeus University, Växjö, Sweden

Aalto University publication series
Doctoral Theses 237/2026

© Ziyi Feng

FGI Publications N:o 174

ISBN 978-952-64-3410-0 (soft cover)
ISBN 978-952-64-3409-4 (PDF)
ISSN 1799-4934 (print)
ISSN 1799-4942 (PDF)
http://urn.fi/URN:ISBN:978-952-64-3409-4

ISBN 978-951-48-0298-0 (print)
ISBN 978-951-48-0299-7 (electronic)
ISSN 2342-7345 (print)
ISSN 2342-7353 (electronic)

Cover image generated with ChatGPT (OpenAI), 2026.

PunaMusta Oy
Helsinki 2026
Finland

Acknowledgements

I started this long journey in 2015, when I had the opportunity to conduct my master's thesis at the Finnish Geospatial Research Institute (FGI) under the supervision of Prof. Yuwei Chen. Yuwei introduced me to research, from general research methods to radar hardware and data processing, and guided me through my first research conference and journal publication. After my master's thesis, I continued working on the profiling radar project, and in 2017, he encouraged me to pursue a doctoral degree. I sincerely thank him for his continuous guidance and encouragement, which helped me begin my research career at FGI.

I would also like to express my deepest gratitude to my advisor, Prof. Juha Hyyppä. As the head of the Department of Remote Sensing and Photogrammetry at FGI, he has played an important role in creating the research environment in which this work was carried out. Juha contributed to developing the research ideas, interpreting the results, and improving both the published articles and this dissertation through extensive comments and suggestions. Beyond his direct scientific guidance, I have been deeply impressed by his dedication to scientific work and his strong support for young researchers. His encouragement has been an important source of motivation throughout my doctoral studies.

I sincerely thank my supervising professor at Aalto University, Prof. Jaan Praks. With his strong expertise in radar remote sensing, Jaan provided valuable guidance on both the scientific direction of the thesis and the doctoral study process. Whenever I approached him for advice regarding doctoral studies, course requirements, or thesis writing, he always offered generous support and guidance. His advice helped me improve the structure of my dissertation, clarify its scientific focus, and finally bring the thesis to completion.

I am also grateful to my co-authors who contributed to the research presented in this dissertation. Teemu Hakala made important contributions throughout the Tomoradar research and was always generous with his help and support. Xiaowei Yu provided valuable scientific support and advice during the study. Eetu Puttonen and Yunsheng Wang contributed useful ideas and discussions at different stages of the research, while Mika Karjalainen provided important support in project management. I would also like to sincerely thank all the other co-authors whose efforts, contributions, and support were essential to the completion of the studies included in this dissertation.

During the past years, I have also participated in research projects that were not directly included in this dissertation. I would particularly like to thank Aimad El Issaoui and Matti Lehtomäki for the many discussions and collaborations we shared, from which I gained knowledge and experience that also benefited my doctoral research. I am also grateful to Prof. Harri Kaartinen, Prof. Antero Kukko, and Prof. Jarkko Koskinen for their leadership and for helping to create a supportive research environment. My thanks also go to all my other colleagues at FGI for the many scientific discussions, informal conversations, friendships, and enjoyable moments over the years. Together, these interactions created a friendly and inspiring working and research atmosphere at FGI.

I gratefully acknowledge the financial support from the Academy of Finland through the projects "Interaction of Lidar/Radar Beams with Forests Using Mini-UAV and Mobile Forest Tomography", "Centre of Excellence in Laser Scanning Research", "Forest-Human-Machine Interplay", "Capturing structural and functional diversity of trees and tree communities for supporting sustainable use of forests", and "Feasibility of Inside-Canopy UAV Laser Scanning for Automated Tree Quality Surveying". I also acknowledge the support from the European Community's Seventh Framework Programme and the scholarship from Maanmittausalan edistämissäätiö that supported the finalization of this thesis.

I am sincerely thankful to Prof. Andreas Reigber and Prof. Johan Fransson for serving as the pre-examiners of this dissertation. Their valuable comments and suggestions helped me substantially improve the thesis during its final revision. I would also like to express my special gratitude to Prof. Johan Fransson for accepting the invitation to serve as the opponent at my doctoral defense.

Finally, I would like to thank my friends and family. Some of my longtime friends have settled in China, Finland, or other European countries. Although we are often separated by distance, I have always received their warm greetings and continuous encouragement throughout this long journey, for which I am deeply grateful. Over the past years, I have also shared many wonderful moments with my friends Aimad, Karla, Mariana, Fabricio, Raquel, Roope, and Leticia. Thank you for all the great conversations, dinners, relaxing moments, and the many ways you have supported me in everyday life. Your friendship has brought warmth and joy to many difficult and dark winter days. My deepest thanks go to my parents for their continuous support in every aspect of my life. I would also like to thank my dear husband, Jin, for all the wonderful moments we have shared and for his constant emotional and practical support throughout this journey.

Espoo, September 2026
Ziyi Feng

Contents

Acknowledgements ..... **iv**

List of Publications ..... **viii**

Author's Contribution ..... **ix**

List of Abbreviations ..... **xi**

1 Introduction **1**

1.1 Motivation and background **1**

1.2 Objectives and overview of the thesis **4**

2 Literature review **7**

2.1 Optical remote sensing **7**

2.2 LiDAR data **8**

2.3 Radar data **13**

2.3.1 Radar–forest interaction and AGB retrieval 13

2.3.2 Synthetic Aperture Radar 15

2.3.3 Profiling radar 19

3 Materials **22**

3.1 Study areas and field reference **22**

3.2 Remote sensing data **23**

3.2.1 Tomoradar system overview 23

3.2.2 Reference LiDAR data 26

4 Methods **27**

4.1 Remote sensing data processing **27**

4.2 Terrain and canopy top elevation estimation **28**

4.3 Ku-band signal penetration in boreal forests **30**

4.4 Plot-level forest attribute extraction **32**

5 Results and discussion **34**

5.1 Terrain and canopy top elevation estimation **34**

5.1.1 Terrain elevation estimation 34

5.1.2 Canopy top elevation estimation 36

5.2 Ku-band signal penetration in boreal forests **38**

5.3 Plot-level forest attribute estimation **41**

5.4 Scientific and practical implications **44**

5.5 Limitations and future research 46
6 Conclusions 51
References 53

List of Publications

This doctoral thesis is based on the following publications, which are referred to in the text by their Roman numerals. The articles are reprinted with permission from the publishers.

I Feng, Z., Chen, Y., Hyyppä, J., Hakala, T., Zhou, H., Wang, Y., Karjalainen, M., 2018, Estimating Ground Level and Canopy Top Elevation With Airborne Microwave Profiling Radar. IEEE Transactions on Geoscience and Remote Sensing, 56(4), 2283–2294, https://doi.org/10.1109/TGRS.2017.2778024.

II Zhou, H., Chen, Y., Feng, Z., Li, F., Hyyppä, J., Hakala, T., Karjalainen, M., Jiang, C., Pei, L., 2018, The Comparison of Canopy Height Profiles Extracted from Ku-band Profile Radar Waveforms and LiDAR Data. Remote Sensing, 10(5), 701, https://doi.org/10.3390/rs10050701.

III Chen, Y., Feng, Z., Li, F., Zhou, H., Hakala, T., Karjalainen, M., Hyyppä, J., 2020, Lidar-aided analysis of boreal forest backscatter at Ku band. International Journal of Applied Earth Observation and Geoinformation, 91, 102133, https://doi.org/10.1016/j.jag.2020.102133.

IV Zhou, H., Chen, Y., Hu, N., Dong, Y., Xu, X., Feng, Z., Hakala, T., Hyyppä, J., 2020, The Determination of Effective Beamwidth of Ku Band Profiling Radar Based on Waveform Matching Method in the Boreal Forest of Finland. Remote Sensing, 12(17), 2710, https://doi.org/10.3390/rs12172710.

V Feng, Z., Yu, X., Chen, Y., Puttonen, E., Hakala, T., Jiang, C., Hyyppä, J., 2024, Feasibility of using Ku-band helicopter-borne microwave radar for stem volume and biomass estimation in boreal forest. International Journal of Applied Earth Observation and Geoinformation, 131, 103966, https://doi.org/10.1016/j.jag.2024.103966.

Author's Contribution

Publication I: Estimating Ground Level and Canopy Top Elevation With Airborne Microwave Profiling Radar

Ziyi Feng processed the remote sensing data, developed the ground and canopy top elevation estimation methods and analyzed the results. Yuwei Chen conducted the data collection and assisted in method development and results analysis. Juha Hyyppä advised on the entire study, participated in the results analysis, and arranged the resources. Teemu Hakala conducted the data collection. Hui Zhou and Yunsheng Wang assisted in the method development. Mika Karjalainen supervised the project. Ziyi Feng and Yuwei Chen wrote the first draft of the manuscript and all other authors assisted in reviewing the manuscript.

Publication II: The Comparison of Canopy Height Profiles Extracted from Ku-band Profile Radar Waveforms and LiDAR Data

Ziyi Feng, Fashuai Li and Changhui Jiang processed the remote sensing data for the study. Hui Zhou and Yuwei Chen planned the study, developed the study methods, analyzed the results, and wrote the major part of the manuscript. Juha Hyyppä reviewed and contributed to the study methodology. Mika Karjalainen designed the practical field test. Yuwei Chen and Teemu Hakala designed the Tomoradar system and conducted the field test and data collection. Ling Pei assisted with writing and reviewing the manuscript.

Publication III: Lidar-aided analysis of boreal forest backscatter at Ku band

Ziyi Feng assisted in data collection, processed the data, and contributed to results analysis and visualization. Yuwei Chen designed the study, developed the methods, analyzed and visualized results. Fashuai Li developed and validated the methods, and analyzed and visualized the results. Hui Zhou was responsible for the study methods and results analysis, visualized results. Yuwei Chen and Fashuai Li prepared the major draft of the manuscript with Ziyi Feng and Hui Zhou assisting in reviewing and revising. Teemu Hakala was responsible for data collection, contributed to data processing and results analysis. Mika Karjalainen managed the project, and Juha Hyyppä supervised the whole work and acquired the funding.

Publication IV: The Determination of Effective Beamwidth of Ku Band Profiling Radar Based on Waveform Matching Method in the Boreal Forest of Finland

Ziyi Feng was responsible for data collection and assisted in results validation. Hui Zhou designed the study, developed the methods, analyzed and visualized the results. Yuwei Chen designed the study, planned the field measurements, developed the study methods, validated the model, supervised the study and managed the whole project. Nan Hu

developed study methods and provided the required study resources. Yuandan Dong assisted in the method development. Xinmin Xu assisted in study results analysis and provided the required resources. Teemu Hakala contributed to data collection and field measurements planning. Juha Hyyppä managed the project and acquired the funding. Hui Zhou generated the main draft of this manuscript; Yuwei Chen and Yuandan Dong reviewed and improved it, and all other authors checked it.

Publication V: Feasibility of using Ku-band helicopter-borne microwave radar for stem volume and biomass estimation in boreal forest

Ziyi Feng collected and managed the study data, processed the data, developed the study methods, and analyzed and visualized the results. Xiaowei Yu developed the study method, analyzed and visualized the results. Yuwei Chen planned the field measurement, collected data and assisted in results analysis. Eetu Puttonen assisted in the results analysis. Teemu Hakala contributed to the field measurement and data collection. Changhui Jiang helped to review and improve the manuscript. Juha Hyyppä designed the study, supervised the work, managed the project, assisted in the results analysis and acquired the funding. Ziyi Feng generated the main draft of the manuscript assisted by Xiaowei Yu and Juha Hyyppä, and all the other authors checked the manuscript.

List of Abbreviations

AEBW	Average effective beamwidth
AGB	Above-ground biomass
ALS	Airborne laser scanning
BERCT	Backscattered energy ratio of canopy to total
CF	Canopy fraction
CHM	Canopy height model
DBH	Diameter at breast height
DBH_g	Basal-area-weighted mean diameter at breast height
DSM	Digital surface model
DTM	Digital terrain model
FMCW	Frequency-modulated continuous-wave
GNSS	Global navigation satellite system
H_g	Basal-area-weighted mean canopy height
HPBW	Half-power beamwidth
IMU	Inertial measurement unit
InSAR	Interferometric synthetic aperture radar
LAI	Leaf area index
LiDAR	Light detection and ranging
MLS	Mobile laser scanning
PLS	Personal laser scanning
PolInSAR	Polarimetric interferometric synthetic aperture radar
PolSAR	Polarimetric synthetic aperture radar
R^2	Coefficient of determination
r	Correlation coefficient

RMSE	Root mean square error
$RMSE_{rel}$	Relative root mean square error
SAR	Synthetic aperture radar
TLS	Terrestrial laser scanning
UAV	Unmanned aerial vehicle
ULS	UAV laser scanning

1 Introduction

1.1 Motivation and background

Forests, occupying approximately one-third of the terrestrial vegetated surface, play an important role in biodiversity and the functioning of forest ecosystems (Brockerhoff et al., 2017; Reichstein and Carvalhais, 2019). In addition, forests are crucial in reducing the amount of greenhouse gases through carbon sequestration (Pan et al., 2011). Boreal forests are particularly important because they constitute one of the largest forest biomes globally and store a substantial amount of terrestrial carbon (Astrup et al., 2018). Forests also provide wood for renewable products and energy, thus enabling a sustainable economy (Verkerk et al., 2011). Forest management strategies affect tree growth rate, wood quality, species richness, carbon balance, and long-term forest productivity (Burger, 2009; Chaudhary et al., 2016; Islam et al., 2024; Paradis et al., 2019). Therefore, accurate information on forest structure and related attributes, including canopy height, diameter at breast height (DBH), stem volume, and above-ground biomass (AGB), is essential for forest monitoring and management. This creates a need for accurate, efficient, and cost-effective forest inventory methods.

Conventional forest inventory relies on numerous manual measurements in forest sample plots. In these plots, directly measurable tree attributes, such as tree height and DBH, are recorded and used to derive forest attributes that cannot be measured directly. Although these field data are reliable, the process is labor-intensive and time-consuming, especially over large areas. In recent decades, remote sensing techniques, including optical sensors, light detection and ranging (LiDAR) systems, and microwave radio detection and ranging (radar) systems, have been increasingly applied in forest inventories, offering efficient methods to collect large-area data for forest attribute estimation and mapping (Hyyppä et al., 2000; Hyyppä et al., 2024; Lechner et al., 2020; Ma et al., 2024; McRoberts and Tomppo, 2007; Tian et al., 2023; Yu et al., 2015). Modern forest inventories integrate wall-to-wall airborne or spaceborne remote sensing data with accurate ground-truth measurements. These measurements are collected from field reference plots distributed across the area of interest through systematic sampling designs.

AGB estimation based on remote sensing technology generally follows two main approaches: signal-based retrieval and height- or structure-based modeling (Ma et

al., 2024; Tian et al., 2023). The signal-based approach relates AGB directly to remotely sensed reflectance or intensity features from optical, aerial, or SAR images (Nandy and Kushwaha, 2021; Shao and Zhang, 2016; Sinha et al., 2015). These features are sensitive to variations in forest structure and biomass and are commonly linked to field-measured AGB using empirical regression or machine-learning models. However, signal-based retrieval can be affected by illumination conditions, moisture, surface roughness, viewing geometry, and signal saturation in dense or high-biomass forests. In contrast, the height- or structure-based approach uses remote sensing data to derive canopy height, vertical structure, or other structural metrics, which are then converted to AGB using allometric equations or statistical models (Borsah et al., 2023; Hyyppä et al., 2000; Hyyppä et al., 2024; Karila et al., 2015; Næsset, 2002). Its accuracy depends on the sensor's ability to map the canopy surface, terrain elevation, or vertical canopy profile, which is strongly influenced by forest density, canopy gaps, and signal penetration.

Radar is an active remote sensing technique that transmits radio waves and receives signals backscattered from targets. Compared with passive optical sensors, radar is independent of solar illumination, and its radio wavelengths can penetrate cloud cover, enabling data acquisition under a wider range of weather and illumination conditions (Gupta et al., 2022; Hyyppä et al., 2024; Sinha et al., 2015). In forest inventory, the recorded radar response depends on the interaction between the transmitted signal and canopy components, which is controlled by factors such as wavelength, polarization, acquisition geometry, moisture conditions, and forest structure. Therefore, radar data can support forest attribute estimation through both backscatter-based signal retrieval and height- or structure-based modeling. Previous studies have mainly used P-, L-, C- and X-band radar signals for forest research, with longer wavelengths such as P- and L-band being particularly valuable because of their stronger interactions with branches, trunks, and in some cases the ground (Ghasemi et al., 2011; Ho Tong Minh et al., 2021; Hyyppä et al., 2000; Ramachandran et al., 2021; Richards et al., 1987; Santoro et al., 2019; Sinha et al., 2015; Tebaldini and Rocca, 2012). However, the long wavelengths of P- and L-band systems require large, heavy antenna structures, making them impractical for integration into lightweight, low-altitude autonomous platforms. Research on the penetration and application of Ku-band signals in forests remains limited, because their short wavelength is often assumed to restrict scattering mainly to the canopy surface, thereby limiting their sensitivity to forest vertical structure. Axelsson et al. (1999) found that tree heights derived from Ku-band helicopter-borne profiling radar data were generally lower and more variable than those from C-band data. Comite et al. (2021) reported that Sentinel-3 Ku- and C-band altimetry observables can be sensitive to forest AGB but may be strongly affected by topographic variation within the radar footprint. In addition, the penetration of microwave signals through forest canopies is influenced by structural properties such as stand density and canopy gaps (Askne and Santoro,

2012). The actual ability to derive canopy height profiles from radar measurements strongly affects forest variable estimation (Hyyppä et al., 2000). Therefore, the actual penetration performance and forest attribute estimation capability of Ku-band signals in low-density boreal forests with canopy gaps could be better than theoretical expectations. Compared to the well-studied P- and L-band signals, radar systems operating in the Ku band can use much smaller antennas, which facilitates the development of helicopter/drone-based radar systems for low-altitude forest inventory.

Synthetic Aperture Radar (SAR) is currently the dominant radar technique in forest remote sensing because it provides spatially continuous images containing backscatter intensity and phase information with practical antenna sizes. Owing to its all-weather observation capability and insensitivity to cloud cover, SAR has been adopted in many Earth Observation missions for large-scale environmental and forest monitoring. For example, the European Space Agency's (ESA) Biomass mission uses fully polarimetric P-band SAR to improve global forest biomass estimation and carbon-cycle understanding (ESA, 2025a). The Biomass mission also includes a dedicated tomographic phase to resolve the vertical distribution of forest backscatter, providing additional structural information for biomass estimation. The NASA–ISRO SAR (NISAR) mission carries L- and S-band SAR instruments for global monitoring of woody biomass and ecosystem disturbance (Rosen et al., 2025). The Japan Aerospace Exploration Agency's (JAXA) Advanced Land Observing Satellite-4 (ALOS-4) carries the wide-swath Phased Array type L-band SAR-3 (PALSAR-3), supporting forest monitoring and biomass estimation (JAXA, 2024). Looking ahead, ESA's planned ROSE-L (Radar Observing System for Europe in L-band) is scheduled for launch in 2028 and aims to monitor agriculture, forestry, and land use (ESA, 2025b). Despite these advances, resolving the vertical distribution of scattering within forest canopies remains difficult using conventional SAR observations, limiting the physical understanding of radar–forest interactions and their use in biomass estimation.

Profiling radar is another radar technique that records the energy of backscattered signals from a target as a function of range. Such range-resolved measurements can provide useful reference information for understanding radar penetration and scattering processes in forests, and may also support the interpretation and modeling of SAR-based forest observations. Early studies demonstrated the potential of nadir-looking profiling radar for forest applications. Bernard et al. (1987) first proposed deriving forest attributes, such as stand height and density, from radar backscatter profiles using the C-band ERASME system. Hallikainen et al. (1993) developed the Helsinki University of Technology Scatterometer (HUTSCAT), which operated at C- and X-band with multiple polarizations and incidence angles, and was used to estimate forest attributes including canopy height, diameter at breast height, and stem volume (Hyyppä and Hallikainen, 1993; Hyyppä and Hallikainen, 1996; Hyyppä et al., 1997). Axelsson et

al. (1999) measured boreal forests using a helicopter-borne profiling radar named NOPEX, which operated at C-, Ku-, and Ka-bands. These studies confirmed that nadir-looking radar profiles can provide information related to canopy height and forest density.

Nevertheless, the capability of Ku-band profiling radar for forest inventory remains insufficiently quantified. Previous studies indicated that Ku-band profiling measurements may contain useful forest structural information, but existing research has not systematically evaluated how deeply Ku-band profiling radar signals penetrate boreal forest canopies, how well they represent vertical canopy structure, and whether they can provide predictors for plot-level stem volume and AGB estimation. In addition, earlier profiling radar systems were constrained by the positioning and orientation technologies available at the time, which lacked the high-frequency inertial orientation corrections necessary to model beam-pointing variations. This limited accurate waveform georeferencing and spatial matching with field plots, forest stands, or coincident remote sensing reference data (Hyyppä and Hallikainen, 1993; Hyyppä and Hallikainen, 1996; Hyyppä et al., 1997). For example, although Hyyppä et al. (1997) used a global positioning system, the investigated stand boundaries had to be manually fine-tuned.

Against this background, the Finnish Geospatial Research Institute developed Tomoradar, a lightweight Ku-band frequency-modulated continuous-wave profiling radar equipped with a Global Navigation Satellite System (GNSS) and Inertial Measurement Unit (IMU) system providing centimeter-level trajectory information (Chen et al., 2017). Its lightweight design supports future UAV-mounted radar applications, making it relevant for flexible low-altitude forest inventory. The system provides an opportunity to study Ku-band backscattering in forests using accurately georeferenced range profiles together with matched LiDAR and field reference data. Therefore, this dissertation evaluates whether Tomoradar can retrieve ground and canopy elevations, characterize Ku-band signal penetration in boreal forest, and estimate plot-level forest attributes, including stem volume and AGB. The novelty of the dissertation lies in the systematic evaluation of a compact Ku-band profiling radar, from waveform-level forest structure detection to plot-level biomass estimation, thereby offering new evidence on its feasibility for low-altitude boreal forest inventory research.

1.2 Objectives and overview of the thesis

The general objective of this dissertation is to evaluate the feasibility of Ku-band profiling radar for boreal forest inventory. Specifically, the thesis investigates whether helicopter-borne Tomoradar measurements can provide reliable information on forest vertical structure, Ku-band canopy penetration, and plot-level forest attributes, including stem volume and above-ground biomass.

The specific objectives of the thesis are as follows:

Objective 1: To develop and evaluate waveform-based methods for retrieving terrain and canopy top elevation from helicopter-borne Ku-band profiling radar data, using existing DTM- and LiDAR-derived elevations as references for accuracy assessment (Publication I).

Objective 2: To quantify Ku-band signal penetration and vertical backscatter distribution in boreal forest by comparing Tomoradar waveforms with coincident LiDAR-derived canopy structure, including canopy height profiles, canopy fraction, and effective beamwidth characterization (Publications II–IV).

Objective 3: To assess the capability of Tomoradar-derived waveform features for estimating plot-level forest attributes, including basal-area-weighted mean canopy height, basal-area-weighted mean DBH, stem volume, and AGB, using field plot measurements as reference (Publication V).

This dissertation consists of five publications that address these objectives and together form a sequential research framework: first evaluating waveform-level ground and canopy detection, then analyzing Ku-band penetration and measurement geometry using LiDAR references, and finally extending the analysis to plot-level forest attribute estimation using field measurements. All publications used Tomoradar data collected during the same field campaign. Publications I–IV used helicopter-based LiDAR data collected simultaneously as reference or supporting data, whereas Publication V utilized manually measured field plots as field reference data. The study started from the estimation of terrain elevation and canopy top from individual radar waveforms, which revealed the feasibility of applying Ku-band profiling radar in forest inventory (Publication I). Publications I, III, and V form the core research line of the dissertation, while Publications II and IV provide complementary analyses of canopy height profiles and effective beamwidth, supporting the interpretation of Ku-band penetration and waveform–LiDAR comparison.

An overview of the publications in this thesis and the research links between the publications are given below:

In Publication I, the ground and canopy top elevations were extracted from backscatter waveforms recorded by the helicopter-borne Ku-band profiling radar Tomoradar. An accurate DTM and simultaneously collected ALS data were used as reference data for ground and canopy estimation accuracy evaluation, respectively. This study demonstrated that Tomoradar can retrieve ground level and canopy top elevation from individual waveforms, providing the waveform-level basis for subsequent penetration and biomass analyses.

In Publication II, the canopy height profiles (CHP) were derived from Tomoradar backscatter waveforms and compared to those generated by airborne LiDAR data. This comparison evaluated how Ku-band radar waveforms represent vertical canopy structure relative to laser scanning data and examined the influence of radar footprint definition.

In Publication III, the Ku-band signal penetration through forest canopy was investigated. The concept of Backscattered Energy Ratio of Canopy-to-Total (BERCT) was proposed as a metric derived from Tomoradar backscatter waveform energy distribution. The relationship between BERCT and LiDAR-derived canopy fraction was analyzed both qualitatively and quantitatively. Additionally, a regression model was fitted to numerically analyze the factors contributing to BERCT. The fitted model showed that the correlation coefficient (r) between BERCT and LiDAR-derived canopy fraction was 0.84, indicating that Tomoradar-derived energy distribution is closely related to canopy density represented by LiDAR canopy fraction.

In Publication IV, the effective beamwidth of Tomoradar in boreal forest was characterized by comparing Tomoradar waveforms with simulated waveforms and LiDAR-derived waveforms. The optimal beamwidth was estimated to improve spatial correlation between them. The findings refined the radar footprint definition required for reliable spatial matching between Tomoradar and LiDAR observations.

In Publication V, the random forest regression method was applied to estimate plot-level forest attributes, including basal-area-weighted mean canopy height, basal-area-weighted mean DBH, stem volume, and AGB, using features extracted from Tomoradar waveforms. The resulting top 15 features used in the model fitting indicated that the plot-level mean canopy height and heights at certain power percentiles were the major contributing features for the modeling. Additionally, the plot-level maximum heights were also estimated directly from Tomoradar waveforms. Both results were compared to the field measurement reference to present the estimation accuracy. This study demonstrated the feasibility of using Tomoradar waveform features for plot-level estimation of forest attributes, with height-related waveform metrics contributing most strongly to the models.

Besides this introduction, Section 2 reviews the relevant literature. Section 3 introduces the radar system, study area, and all the data used, including research data and ground truth data. Section 4 describes the major methods used in the study, and Section 5 summarizes the results of each topic, as well as the discussion, potential limitations and future work. Finally, some conclusions are drawn in Section 6.

2 Literature review

Remote sensing technologies have been used in forest above-ground biomass estimation for several decades. Currently, the three most widely applied remote sensing technologies are optical sensors, LiDAR, and radar. A review by Ullah et al. (2025) reported that 30% of biomass estimation studies used LiDAR data, 27% used optical data, and 6% relied on SAR data, while the remainder employed data fusion approaches. These technologies have developed rapidly in both sensor hardware and data processing methods, allowing for increasingly accurate estimation of forest attributes. In the following sections, optical sensors and LiDAR technology will be briefly introduced, followed by a more detailed discussion of radar-based remote sensing, which includes the technology used in this study.

2.1 Optical remote sensing

Optical satellite imagery, utilizing sunlight reflectance characteristics in the visible, near-infrared (NIR), and shortwave infrared (SWIR) wavelengths from multispectral and hyperspectral data, has been widely used in forest research for tree species classification and the estimation of forest structural variables, leaf area index (LAI), and AGB (Eckert, 2012; Minunno et al., 2025; Nandy and Kushwaha, 2021; Ozdemir and Karnieli, 2011; Song, 2013). Optical sensors are effective for large-scale forest studies, especially for forest classification or change detection because of the high spatial resolution and broad spectral range.

When analyzing forests using optical sensor data, the spectral reflectance captured by optical sensors is converted into forest-related indices. The commonly used vegetation indices (VIs) include the normalized difference vegetation index (NDVI), difference vegetation index (DVI), and enhanced vegetation index (EVI), which may have a saturation issue in dense forests due to the strong absorption of solar radiation in red wavelengths (Nandy and Kushwaha, 2021; Tian et al., 2023). In that case, more indices like renormalized DVI (RDVI) and modified simple ratio (MSR) are used to help with the biomass estimation. In terms of sparsely vegetated areas, the perpendicular VI (PVI), soil-adjusted VI (SAVI), and modified SAVI (MSAVI) are commonly used and have demonstrated reliable performance in vegetation estimation (Govender et al., 2007; McGwire et al., 2000; Tian et al., 2023). Besides, another important source of information is spatial texture calculated through spatial analysis of derived images, which reflects forest stand

structure and amount of forest AGB (Eckert, 2012; Ma et al., 2024; Tian et al., 2023).

Traditional optical sensors mainly acquire multispectral data, which usually contain 4-13 spectral bands spread between the visible band and the mid-infrared band (Ma et al., 2024). Most of the multispectral optical sensing data are satellite-based, offering large-scale forest monitoring. Widely used sensors such as Landsat and Sentinel-2 offer medium-level spatial resolution and support the estimation of AGB (Dube and Mutanga, 2015; López-Serrano et al., 2020; Wittke et al., 2019; Zheng et al., 2004), while the commercial datasets such as WorldView-2 provide high spatial resolution at about 2 meters, enabling highly accurate estimation of AGB (Eckert, 2012; Ozdemir and Karnieli, 2011; Wittke et al., 2019). With the development of optical sensors, optical data can be generated by collecting the reflectance of several hundred narrow and continuous spectral bands from the visible light to the thermal infrared bands (Govender et al., 2007). These data, known as hyperspectral optical data, have very high spectral resolution, typically including more than 200 bands on satellite platforms and more than 100 bands on airborne platforms. The high spectral resolution of hyperspectral data can capture more detailed information about the biochemical and structural properties of vegetation (Govender et al., 2007), making up for the lack of information from multispectral data due to the relatively coarse bands. Studies have demonstrated that hyperspectral data can estimate AGB with acceptable accuracy (Fassnacht et al., 2014; Halme et al., 2019; Jacon et al., 2021). However, it was also revealed that the extra information provided by hyperspectral optical data is more related to species-related variables (Fassnacht et al., 2014; Halme et al., 2019). Therefore, hyperspectral optical data provide limited improvement in AGB estimation accuracy but are more valuable for applications such as tree species classification and LAI estimation. A recent study also showed that hyperspectral data can support the early detection of bark beetle damage before visible symptoms appear (Cosimo et al., 2026).

Despite those advantages in terms of large-scale and temporal monitoring, as passive sensors, optical sensors are often constrained by atmospheric interference, cloud cover, and variable solar illumination, which affect image quality, introducing inconsistencies across time-series observations (Nandy and Kushwaha, 2021). Additionally, optical sensors usually capture reflectance from the canopy surface and have little access to understory vegetation, which affects the estimation of forest structural parameters like canopy height or volume, especially in dense forests (Zheng et al., 2024).

2.2 LiDAR data

LiDAR, also known as laser scanning, is one of the operationally mature remote sensing technologies for forest studies (Hyyppä et al., 2024; Rosette et al., 2012).

LiDAR data are acquired by active sensors emitting signals with wavelengths typically between 500 nm and 1550 nm (Hyyppä et al., 2024). Due to the interaction of laser pulses with different layers of forest, LiDAR data can provide detailed information on forest structure, enabling accurate estimation of forest attributes such as canopy height, basal area, crown size and stem volume, all of which are correlated with biomass (Borsah et al., 2023; Hyyppä et al., 2001; Næsset, 2002).

As an active remote sensing technology, conventional LiDAR systems emit laser pulses toward a target and record the energy and timing of laser echoes reflected from the illuminated area. The target range can be derived from the recorded time delay between pulse emission and reception. Based on the method of recording the returned signal, LiDAR systems are generally categorized into discrete-return (DR) LiDAR and full-waveform (FW) LiDAR. For each emitted laser pulse, DR LiDAR captures single or multiple discrete returns corresponding to detected peaks in the backscattered signal with energy intensities exceeding a threshold (Borsah et al., 2023; Rosette et al., 2012). The number of recorded returns is determined by the sensor design and configuration, as many systems store only a limited number of the strongest echoes from each emitted pulse. In forest applications, the first returns are typically associated with canopy surfaces, whereas the last returns often correspond to ground reflections (Borsah et al., 2023; Mallet and Bretar, 2009). These discrete returns form a three-dimensional (3D) point cloud containing the vegetation canopy and ground surface features, which has been intensively studied and applied in forest attribute estimation (Hyyppä et al., 2024).

In contrast, FW LiDAR records the complete backscattered signal of each emitted laser pulse as a continuous waveform over time, providing more detailed information about vertical vegetation structure and the physical backscattering properties. This richer signal enables more complex processing approaches, improving the reliability of feature detection. Similar 3D point clouds can be generated by extracting discrete echoes from the waveform; however, users can customize the extraction criteria such as amplitude thresholds or shape constraints, allowing for the extraction of weaker returns that might be missed by standard discrete-return systems. In addition, FW data can be analyzed directly in their raw form, such as through vertical waveform profiles, to derive forest structural attributes and biophysical parameters (Cao et al., 2014; Hyyppä et al., 2024; Mallet and Bretar, 2009).

In recent years, a new type of LiDAR system, called photon-counting LiDAR, has been introduced for large-area forest applications. These systems emit laser pulses with relatively low energy and use highly sensitive detectors to register the arrival time of individual photons. This approach enables very high point densities and efficient large-area coverage, but also increases sensitivity to noise from solar background and atmospheric scattering. A related development is multi-photon LiDAR, in which a return is recorded only when several photons are detected within a short time window. This reduces detection noise compared to single-photon

systems, but also decreases sensitivity to weak signals from the lower canopy or ground (Hyyppä et al., 2024; Wästlund et al., 2018; Yu et al., 2020).

Depending on the platform used for data acquisition, LiDAR systems can observe the Earth's surface from different viewing geometries and distances. LiDAR sensors can be mounted on a variety of platforms, including satellites, aircraft, unmanned aerial vehicles (UAVs), and ground-based systems that may operate either in static or mobile modes. Accordingly, LiDAR measurements are commonly categorized into spaceborne LiDAR, airborne laser scanning (ALS), UAV laser scanning (ULS), terrestrial laser scanning (TLS), and mobile laser scanning (MLS) (Borsah et al., 2023). These different platforms provide complementary capabilities for forest observations, ranging from large-area monitoring using satellite systems to highly detailed structural measurements obtained from ground-based or low-altitude platforms. As a result, the spatial resolution and footprint size of LiDAR measurements vary considerably among these systems.

Spaceborne LiDAR operates at high orbits, offering observation of forests at a global scale. The first satellite LiDAR to provide global-scale data was the Geoscience Laser Altimeter System (GLAS) onboard NASA's Ice, Cloud and land Elevation Satellite mission (ICESat; 2003–2009) (Hyyppä et al., 2024; Schutz et al., 2005; Wang et al., 2011). The GLAS sensor used laser pulses with a wavelength of 1064 nm to provide large-footprint (~70 m on ground) full-waveform data (Boudreau et al., 2008; Coops et al., 2021), which has been used in estimating canopy height (Lefsky, 2010; Simard et al., 2011), dominant height, crown closure (Mahoney et al., 2018), and biomass (Boudreau et al., 2008; Chi et al., 2015; Lefsky et al., 2005; Tang et al., 2022) at regional to global scales. Building on this foundation, the Global Ecosystem Dynamics Investigation (GEDI) onboard the International Space Station (ISS) was launched in late 2018 (Dubayah et al., 2020). Working with three active 1064 nm lasers, it provides about 25-m footprint full-waveform data, offering denser sampling and improved vertical resolution for biomass and canopy structure mapping (Coops et al., 2021). Forest vertical structure can be estimated solely using GEDI data (Rajab Pourrahmati et al., 2023) or by combining it with other space sensing data (Chen et al., 2021; Potapov et al., 2021; Schlund et al., 2023). In parallel, the next generation of the ICESat mission, ICESat-2, was also launched in 2018. On board there is an Advanced Topographic Laser Altimeter System (ATLAS), using a 532 nm photon-counting LiDAR that produces about 17-m-diameter footprints at the design altitude (Coops et al., 2021; Markus et al., 2017). Although the key mission of ICESat-2 is ice-related, it provides fine-scale data products for canopy height and terrain mapping (Neuenschwander and Pitts, 2019; Neuenschwander et al., 2023), enabling the estimation of ground elevation, forest canopy height, canopy cover and above-ground biomass (Narine et al., 2022; Varvia et al., 2024). GEDI provides detailed information on vertical forest structure, while ICESat-2 offers denser along-track sampling. Previous studies have

compared their performance in estimating ground elevation and canopy height (Liu et al., 2021; Zhu et al., 2023).

Compared with spaceborne LiDAR data, ALS data provide higher spatial resolution and greater flexibility in acquisition timing and flight configuration. Nowadays, the commonly used small-footprint ALS has a footprint size of 0.1-1 m (at 1 km flight height), enabling detailed characterization of forest canopy and terrain structure (Mandlburger, 2024). ALS has been used in forest inventories for decades, beginning with early studies on estimations of standwise mean height and volume (Næsset, 1997a, 1997b), and individual tree height and volume (Hyyppä and Inkinen, 1999; Hyyppä et al., 2001). With its ability to efficiently capture 3D forest structure over large areas, ALS has become a key data source for estimating AGB and other related forest attributes. A wide range of forest structural metrics including height percentiles, canopy cover fraction, crown diameters, leaf area index (LAI), and vertical profile indices are derived and serve as predictors for AGB estimation (Borsah et al., 2023; Hyyppä et al., 2008; Hyyppä et al., 2024).

Forest attribute estimation from ALS is commonly implemented using two methods: area-based approaches (ABAs, Næsset (2002)) and individual tree-based approaches (ITAs, Hyyppä and Inkinen (1999)). ITA is also described as individual tree detection (ITD) or individual tree crown (ITC) methods in other studies (Hyyppä et al., 2024; Lara-Gómez et al., 2023). In ABA, grid- or plot-level forest attributes are predicted from point clouds based on the statistical or machine learning models built between field measurements and ALS-derived metrics. Then forest attributes over larger area are then acquired by aggregating the grid-level results. In ITA, individual trees are first defined (typically using canopy height models and/or 3D point cloud segmentation), after which tree-level forest attributes are estimated and summed up to plot/stand level when needed (Hyyppä et al., 2012). ABA is widely used in regional and national scale forest inventories for its computational efficiency and relatively lower requirement on point density, while ITA is particularly useful when accurate individual tree attributes are required and data density and canopy conditions allow reliable crown segmentation. Early studies have shown that the two methods produced comparable accuracy when predicting plot-level forest attributes using ALS data, and increasing point density may improve the estimation accuracy of the ITA method (Yu et al., 2010). A more recent study by Lara-Gómez et al. (2023) suggested that selecting between ABA and ITA based on the tree density can improve overall estimation accuracy.

Recent advances in ALS-based forest inventories include the increasing use of photon-counting LiDAR and multispectral LiDAR data (Hyyppä et al., 2024). Studies estimating forest attributes using airborne photon-counting LiDAR data have been conducted in boreal forests in Finland and Sweden as well as in mixed boreal and coniferous forests in Canada. Results demonstrated that photon-counting ALS can support accurate estimation of forest attributes using ABA

modeling, with relatively minor sensitivity to point density and flight altitude (Wästlund et al., 2018; White et al., 2021; Yu et al., 2020). Multispectral ALS records laser returns at multiple wavelengths, offering more information for canopy component discrimination, thus supporting tree species classification, which can facilitate the estimation of other forest attributes (Yu et al., 2017). Overall, advances in sensor configurations, multi-wavelength capability, and flexible data collection strategies have reinforced ALS as a primary data source for regional or national scale forest inventories and a valuable complement to other remote sensing datasets. In this thesis, ALS serves as one of the reference datasets to benchmark forest structure and derived forest attributes against Ku-band profiling radar estimates.

UAV-borne LiDAR systems provide high spatial resolution data through direct measurement of trees, with flexible operational setups and low cost. ULS can be used as an alternative to ALS for small-area aerial surveys due to the high starting cost of ALS surveys (Antonova et al., 2019; Vandendaele et al., 2021). Hyyppä et al. (2020b) categorized ULS as a form of MLS, as the UAV-borne LiDAR systems can provide not only aerial data by flying above the canopy but also under-canopy data as a mobile platform, and the sensors used on UAVs are similar to those commonly used on mobile platforms (Liang et al., 2022). These studies show that ULS data can provide accurate estimates of canopy height, DBH, stem curves, and stem volume, making it an important platform for low-altitude sensing and a valuable source of reference data (Hyyppä et al., 2020b; Hyyppä et al., 2021; Hyyppä et al., 2024; Liang et al., 2022; Vandendaele et al., 2021).

TLS is a ground-based LiDAR system, typically mounted on a tripod to scan the surrounding area. TLS can acquire very dense data in a short time with high spatial resolution, achieving millimeter-level range resolution at a measurement distance of tens of meters (Liang et al., 2016). This capability allows detailed 3D measurements of forests at both tree and plot levels. Previous studies have employed TLS data to estimate forest attributes at tree and plot levels, including tree position and density, DBH, stem curve, stem volume, and biomass. Results indicate that DBH and stem curve can be measured with high accuracy, supporting reliable estimation of stem volume and biomass, whereas stem detection and tree height estimation remain more challenging due to occlusion effects (Hyyppä et al., 2024; Kankare et al., 2013; Liang et al., 2018; Liang et al., 2016; Stovall et al., 2017). Wang et al. (2019) further demonstrated that multi-scan TLS data can provide accurate tree height estimates for trees up to 15–20 m tall, with the threshold influenced by forest stand complexity.

MLS systems share similarities with TLS and ULS but offer greater flexibility in data acquisition. MLS can be broadly categorized into vehicle-based and portable personal laser scanning (PLS) systems. Early vehicle-based MLS for forest studies often relied on all-terrain vehicles (ATVs) or harvesters capable of operating within forest stands, while later developments have included conventional vehicles for

roadside tree surveys, particularly with the rapid development of autonomous driving technologies (Hyyppä et al., 2024; Liang et al., 2022). PLS systems, on the other hand, include backpack, handheld, and helmet-mounted scanners (Hyyppä et al., 2020a; Hyyppä et al., 2020b; Li et al., 2023; Mokroš et al., 2021). These different sensor integration methods provide varying levels of mobility and operability, allowing for forest inventory in areas that are otherwise difficult to reach. Tree position, DBH, stem curve, and stem volume are among the most commonly derived forest attributes from MLS data and are often estimated with high accuracy. In contrast, the tree height estimation remains more limited, as the acceptable accuracy strongly depends on tree height (Liang et al., 2022).

LiDAR has significantly enhanced forest biomass estimation capabilities by providing detailed three-dimensional characterization of forest structure. Although different LiDAR techniques, sensor resolutions, and platforms present unique strengths and limitations, integrating these systems strategically can optimize accuracy, coverage, and cost-effectiveness in forest inventory.

2.3 Radar data

Unlike passive optical sensors, radar systems do not depend on solar illumination and are generally less affected by cloud cover than optical or LiDAR systems. As active sensors, radar systems transmit radio waves and record backscatter from different forest layers, with the interaction depth strongly influenced by the operating wavelength. The following sections introduce key radar-forest interaction characteristics and biomass-retrieval concepts, and then review the main radar techniques used in forest remote-sensing research, including imaging SAR and its typical products as well as profiling radar, which provides waveform-based vertical profiles for canopy and ground characterization.

2.3.1 Radar–forest interaction and AGB retrieval

Radar signals at different wavelengths (frequencies) are backscattered from different layers of the forest due to their varying penetration capability. In general, longer wavelengths penetrate deeper into the forest canopy, even to the ground surface, while shorter wavelengths are primarily scattered by upper-canopy elements. The most commonly used radar frequency bands in forest remote-sensing research are P-band (30–100 cm), L-band (15–30 cm), C-band (3.8–7.5 cm), and X-band (2.5–3.8 cm) (Ghasemi et al., 2011; Sinha et al., 2015). Owing to their relatively long wavelengths, P-band signals can penetrate foliage and branches, and the resulting backscatter is dominated by contributions from trunks and the ground. With less penetration capability, L-band signals can penetrate the canopy and are backscattered mainly by tree trunks and large branches, with some contribution from the ground (Karam et al., 1995; Richards et al., 1987; Tebaldini

and Rocca, 2012). For shorter-wavelength bands, such as the C- and X-bands, canopy penetration is limited. Consequently, C-band signals are mainly backscattered from small branches (Askne and Santoro, 2012), whereas X-band signals are scattered by leaves and the upper canopy surface (Sinha et al., 2015). In addition, Ku-band (1.7–2.5 cm) and Ka-band (0.75–1.15 cm) were also explored for forest studies, though their short wavelengths are generally assumed to restrict interactions primarily to the canopy surface (Axelsson, 1995; Comite et al., 2021).

Due to their penetration characteristics, the P-band, L-band, and C-band are frequently used for biomass estimation, with the L-band generally being preferred because of its stronger interaction with trunks and branches (Sinha et al., 2015). However, actual penetration and the sensitivity of radar backscatter to forest attributes are strongly influenced by forest density, biomass level, forest type, and environmental conditions. Askne and Santoro (2012) suggested that the low density and canopy gaps in boreal forests allow for relatively deep penetration even at shorter wavelengths, such as the C-band. Fransson and Israelsson (1999) found that JERS-1 L-band backscatter was consistently more sensitive to boreal-forest stem volume than ERS-1 C-band backscatter. Similarly, Schlund and Davidson (2018) reported that biomass estimation is more accurate with P-band data for higher biomass forests, whereas L-band data perform better in lower biomass forests. Yu and Saatchi (2016) further showed that L-band backscatter is strongly affected by forest type and environmental conditions, indicating that accurate AGB estimation with L-band data requires appropriate forest type classification and model selection.

In addition to wavelength dependence, polarization also plays a key role in radar backscatter and biomass estimation. Polarization refers to the orientation of the electric field of the transmitted and received radar wave, with linear polarization being typical in forest inventory, namely horizontal (H) and vertical (V) orientations. By transmitting and receiving in either H or V orientation, a radar can generate four channels: the co-polarization channels HH and VV, and the cross-polarization channels HV and VH (Ghasemi et al., 2011). Studies indicate that co-polarized channels are more sensitive to surface scattering, particularly from the ground, while cross-polarized channels respond strongly to canopy volume scattering and thus to biomass. These effects are particularly evident at L-band (Askne and Santoro, 2012; Cartus et al., 2012; Ghasemi et al., 2011; Huang et al., 2015; Ramachandran et al., 2021; Sinha et al., 2015). However, Tebaldini and Rocca (2012) found that in boreal forests the P-band in HV polarization was mainly scattered by the ground, while the L-band maintained volume scattering. The diverse characteristics of polarimetric measurements provide complementary information on forest structure, facilitating the separation of scattering mechanisms, and enhancing the forest attribute retrieval.

In radar-based forest applications, AGB retrieval is strongly governed by the interaction between microwave signals and forest structural components, which is

controlled by sensor parameters such as wavelength, polarization, and acquisition geometry. For backscatter-based retrieval, AGB is related to radar backscatter intensity (σ^0) and its polarization and frequency. This approach can rely on a single channel (frequency/polarization) or integrate multi-frequency and multi-polarization measurements to better capture forest scattering mechanisms. In practice, AGB is retrieved using empirical regressions or machine learning models calibrated with field data. However, the sensitivity of σ^0 to environmental conditions (e.g., vegetation/soil moisture, surface roughness) and the well-known saturation behavior at higher biomass levels can constrain performance.

For height- or structure-based radar retrieval, canopy structure information (most commonly canopy height) is used as an intermediate variable for AGB estimation. In many SAR-based height approaches, canopy height is typically derived by differencing a radar-derived digital surface model (DSM) with a terrain model (DTM), with the latter often obtained from high-accuracy sources such as LiDAR. These height/structure metrics can then be converted to AGB through allometric equations or used as predictors in statistical models. The accuracy of this approach depends on where the radar signal is effectively scattered within the canopy.

Overall, radar observations capture both canopy scattering behavior and forest structural information, enabling forest attribute estimation across a range of sensor configurations and processing strategies.

2.3.2 Synthetic Aperture Radar

Among radar-based approaches, synthetic aperture radar (SAR) has been the most widely applied in forest research, primarily through spaceborne missions that provide large-scale and consistent observations. Conventional real-aperture radar requires either very short wavelengths or extremely long physical antennas to achieve high spatial resolution, which severely limits its application on airborne or satellite platforms. SAR overcomes this limitation by synthesizing a large effective aperture through the forward motion of the antenna combined with signal processing. This enables high-resolution imaging with practically sized antennas while still employing longer microwave wavelengths, which offer better penetration capability in forest canopies (Chan and Koo, 2008). During data acquisition, a SAR system records backscattered signals along its flight path. Coherent processing of these signals forms a two-dimensional image of the illuminated scene in range and azimuth, with each complex-valued pixel containing amplitude and phase information (Hyyppä et al., 2024; Rott, 2009). Over the past decades, SAR data have been widely applied to the retrieval of forest structural parameters such as canopy height, stem volume, and AGB, using different sensor configurations (platform, wavelength, polarization, incidence angle) together with various processing methods and models (Hyyppä et al., 2024).

Early applications of SAR in forest research primarily used backscatter intensity, which is sensitive to stand density, tree species composition, biomass, surface roughness, and vegetation and soil moisture (Hyyppä et al., 2024; Yu and Saatchi, 2016). SAR backscatter intensity has demonstrated capability for estimating AGB and related forest attributes across different forest types. For example, JERS-1 L-band backscatter showed a strong correlation ($r = 0.77$) with biomass in young regenerating tropical forests in Brazil (Kuplich et al., 2000). In a boreal forest, a stem-volume model based on multi-temporal JERS-1 L-band data achieved a validation correlation of $r = 0.78$ (Fransson and Israelsson, 1999). At the regional scale, ALOS PALSAR L-band HH and HV data were used to map AGB across the northeastern United States, with county-level validation yielding an RMSE of 12.9 t/ha (Cartus et al., 2012). To improve estimation accuracy, multi-source and multi-temporal approaches have been explored. For instance, Englhart et al. (2011) combined multi-temporal L- and X-band SAR to enhance AGB estimation in tropical forests, while Santi et al. (2017) combined L- and C-band SAR data to estimate growing stock volume, achieving $r = 0.86$ with an RMSE of 77 m^3/ha. Despite these advances, the relationship between backscatter intensity and forest attributes saturates at high levels of biomass or stem volume, limiting further reliable estimation. For biomass, Ningthoujam et al. (2016) found that airborne S-band SAR backscatter was sensitive to stand-level AGB mainly below approximately 100 t/ha, beyond which little additional sensitivity was observed. Sinha et al. (2015) summarized that C-band backscatter typically saturates at approximately 60–70 t/ha, whereas L- and P-band backscatter may saturate near 100 t/ha in complex heterogeneous tropical forests and around 250 t/ha in structurally simpler stands with few dominant species. In boreal forests, the reported ranges are approximately 100–150 t/ha for L-band and 100–300 t/ha for P-band. For boreal-forest stem volume, Fransson and Israelsson (1999) estimated saturation levels of approximately 64 m^3/ha for ERS-1 C-band and 143 m^3/ha for JERS-1 L-band.

When backscatter saturation limits intensity-based biomass estimation, interferometric SAR (InSAR) offers an alternative approach. InSAR uses the phase difference between two SAR acquisitions taken from slightly different positions or at different times, allowing the retrieval of relative elevation information (Rott, 2009). By separating the canopy return from the ground reference surface (often provided by an external DTM), InSAR can estimate canopy height and related forest attributes. A study conducted in a Finnish boreal forest investigated the relationship between the interferometric scattering phase center and canopy height using airborne X- and L-band InSAR data, achieving canopy height estimation with an RMSE of approximately 1.5 m using single-polarization X-band interferometry combined with an external DTM (Praks et al., 2012a). An early study using ERS-1/ERS-2 C-band VV tandem data in Swedish boreal forests showed that interferometric coherence could be related to stem volume, with a relative RMSE of approximately 20% for the best interferogram (Fransson et al., 2001). Extending

the evaluation to more diverse boreal forests in Central Siberia and considering earlier Scandinavian results, Santoro et al. (2007) concluded that relative RMSE values of approximately 15–25% were feasible for homogeneous stands larger than 2–5 ha under suitable acquisition conditions. A subsequent study using wintertime images showed that under optimal environmental conditions (subzero temperature, dry snow layer, moderate breeze), the best relative RMSE for stem volume estimation was 20%, whereas the value increased to approximately 30% under less favorable conditions (Askne and Santoro, 2012). The Shuttle Radar Topography Mission (SRTM) acquired X-band InSAR data with extensive spatial coverage. These data were subsequently used to estimate top height, mean height, stand density, stem volume, and biomass in spruce-dominated forests, with reported relative RMSE values of 6–9% for height, 10% for stand density, and 18–19% for volume and biomass (Solberg et al., 2010a), while the AGB estimation was also done in Scots pine-dominated plots, showing a different linear relation from spruce forests (Solberg et al., 2010b).

X-band SAR data from the German single-pass interferometry mission TanDEM-X (TDX) have been one of the most widely used SAR datasets. Several investigations have demonstrated its capability for tree height estimation, with errors typically within 0.7–3 m depending on forest type and season (Antonova et al., 2019; Olesk et al., 2015; Praks et al., 2012b). It has also been applied to AGB estimation, where the interferometric height and coherence showed strong predictive power, yielding stand-level accuracies with relative RMSEs of 16–25% in boreal and tropical forests (Askne et al., 2013; Persson et al., 2017; Persson and Fransson, 2017; Schlund et al., 2015; Solberg et al., 2013). However, accuracy decreased considerably in dense tropical forests (Solberg et al., 2017). In addition, comparisons between TanDEM-X InSAR and TerraSAR-X (TSX) stereo-radargrammetry for volume and biomass estimation indicated that InSAR generally outperforms radargrammetry at local scales (Karila et al., 2015; Rahlf et al., 2014). Nevertheless, InSAR is affected by temporal and volumetric decorrelation, particularly in dense forests where multiple scattering occurs, and the accuracy of canopy height retrieval often depends on the availability of high-quality external terrain models (Askne and Santoro, 2012; Praks et al., 2012b).

Polarimetric SAR (PolSAR) extends the information content of SAR by recording multiple polarization channels (HH, HV, VH, and VV), enabling the separation of scattering mechanisms such as surface, double-bounce, and volume scattering. These different scattering mechanisms are closely linked to forest structural attributes and biomass. Studies using fully polarimetric L-band data from ALOS/PALSAR and ALOS-2/PALSAR-2 have demonstrated the potential of polarimetric attributes for AGB estimation in tropical forests (Narvaes et al., 2023; Rajat et al., 2024). To further improve forest structure retrieval, PolSAR has been combined with interferometry in Polarimetric InSAR (PolInSAR). Praks et al. (2007) achieved correlation coefficients of 0.77 and 0.75 for canopy height

estimation in boreal forests using E-SAR airborne L- and X-band PolInSAR, respectively. Using the same airborne system with L- and P-band PolInSAR data over a boreal forest in northern Sweden, Neumann et al. (2012) found that stand-level AGB was most correlated with PolInSAR-derived forest height at L-band, and most correlated with polarimetric scattering-mechanism indicators at P-band. Hajnsek et al. (2009) reported height accuracy within 10% in pine forests using Indonesian Airborne Radar Experiment (INDREX-II) P- and L-band PolInSAR. In addition, Shiroma et al. (2016) demonstrated the use of repeat-pass dual-polarimetric P-band and single-pass three-baseline X-band PolInSAR for deriving DTM, DSM, and forest height.

Previous studies have shown that canopy height can be estimated with good accuracy from SAR-derived elevation, which is critical for biomass determination. Radargrammetry is another technique for deriving elevation from SAR data using stereoscopic geometry: two SAR images acquired from different incidence angles are matched, and elevation is derived from the observed parallax (Hyyppä et al., 2024). The method primarily uses image intensity and geometry, rather than coherence as in InSAR, making it less sensitive to temporal or volumetric decorrelation and potentially more robust in dense forest environments. A few studies have applied radargrammetry to TerraSAR-X images to estimate forest attributes in Finnish boreal forests, including canopy height, DBH, basal area, stem volume, and biomass. The corresponding relative RMSEs were approximately 14%, 19.7–22.2%, 29%, 30.2–34%, and 28%, respectively (Karila et al., 2015; Karjalainen et al., 2012; Wittke et al., 2019). A comparable study at two boreal-forest sites in Sweden reported relative RMSEs of 9.4% and 22.9% for canopy height and biomass estimation, respectively (Persson and Fransson, 2014). Rahlf et al. (2014) compared radargrammetry with InSAR, airborne laser scanning (ALS), and aerial photogrammetry in southern Norway for timber volume estimation, finding that ALS performed best (plot-level relative RMSE ~19%), followed by InSAR (42%) and radargrammetry (44%). Overall, radargrammetry is generally less accurate than InSAR, but can still provide useful structural information in the absence of phase-coherent data.

Unlike the previously discussed SAR methods, tomographic SAR (TomoSAR) reconstructs the vertical distribution of radar backscatter, thereby providing information on forest vertical structure. TomoSAR extends InSAR by coherently combining multiple SAR images acquired from slightly different cross-track positions, thereby synthesizing an aperture in the elevation direction and resolving scatterers at different heights within each range–azimuth resolution cell (Reigber and Moreira, 2000). The resulting vertical reflectivity profiles can distinguish scattering contributions from the ground and different forest layers, supporting the retrieval of ground elevation, canopy height, vertical structure, and AGB (Aghababaei et al., 2020; Tebaldini et al., 2021). Using airborne P-band TomoSAR data from two tropical forest sites, Ho Tong Minh et al. (2016) obtained canopy

height errors within 2.5 m and AGB errors of 16–18% at 1-ha resolution. Another airborne P-band study in tropical forest reported average relative uncertainties below 10% for both forest height and AGB over a biomass range of approximately 200–500 Mg/ha (Ramachandran et al., 2023). In boreal forests, Blomberg et al. (2021) showed that suppressing ground backscatter using P-band TomoSAR could reduce bias in AGB retrieval, although the benefit depended on topography and tomographic resolution. Building on these airborne studies, ESA's Biomass mission, launched in 2025, extends TomoSAR to systematic spaceborne forest observation. During its dedicated tomographic phase, stacks of seven repeated P-band SAR acquisitions are combined to generate three-dimensional maps of forest structure, with approximately 15–20 m vertical resolution and 200 m horizontal resolution, supporting global biomass estimation (ESA, 2025a). Although TomoSAR provides valuable information on the vertical distribution of forest backscatter, it requires multiple accurately calibrated, phase-coherent acquisitions. Its reconstruction quality depends strongly on the number, span, and distribution of baselines and on temporal coherence, resulting in substantially greater data acquisition and processing complexity (Aghababaei and Ferraioli, 2025).

Overall, SAR provides a diverse set of tools for forest inventory. Backscatter intensity enables relatively simple, large-scale estimation of forest biomass but becomes less sensitive as biomass increases because of signal saturation. InSAR, PolInSAR, and radargrammetry use interferometric phase, polarization, and stereoscopic geometry to derive elevation and structural information, thereby supporting canopy height and biomass estimation. TomoSAR further extends these capabilities by resolving the vertical distribution of radar backscatter, enabling three-dimensional characterization of forest structure as well as canopy-height and biomass retrieval. Despite these advances, SAR applications in forest research remain constrained by environmental conditions, demanding data-acquisition requirements, and the complexity of data processing and interpretation.

2.3.3 Profiling radar

Profiling radar is a different type of radar that records the whole backscattered signal as a function of target range. When applied to forest inventory, the radar system measures the vertical distribution of backscattered energy within forest canopies, producing a vertical profile where targets (e.g., canopy crown, ground) can be identified by their strong intensities, which is similar to FW LiDAR. The first profiling radar applied in forest study was the ERASME system, a C-band (5.35 GHz) FMCW radar introduced in Bernard et al. (1986). The system was mounted on a helicopter and configured to be nadir-looking during field measurements, demonstrating its ability to measure tree height and planting density (Bernard et al., 1987).

Subsequently, a similar system named Helsinki University of Technology SCATterometer (HUTSCAT) was developed for forest inventory (Hallikainen et al., 1993). HUTSCAT operated in the C- and X-band (5.4 and 9.8 GHz, respectively) with fully polarimetric capability (HH, HV, VV, VH), resulting in eight detection channels. Additionally, the system allowed the incidence angle to be adjusted mechanically from 0° to 45° and electronically from 0° to 60°, respectively. Installed on a helicopter, HUTSCAT detected forests at a range resolution of 65 cm, and produced vertical profiles of forest from various angles. Hyyppä and Hallikainen (1993) used HUTSCAT data at C-band and an incidence angle of 3 degrees to estimate mean tree height, dominant tree height, total basal area, and stem volume, achieving good level of accuracies and demonstrating the capability of airborne ranging radar in measuring forest attributes. Besides, Hyyppä and Hallikainen (1996) investigated the effects of different incidence angles (3°, 20°, 30°, and 40°) and dominant tree species (pine, spruce, and mixed) on the estimation of the four forest attributes mentioned above. The results indicated that estimates of mean tree height and dominant tree height were more accurate in pine-dominated plots than those in spruce-dominated plots, and the incidence angles had no effect on the conclusion. The estimation accuracy of basal area was independent of incidence angles, while the most accurate stem volume estimate was obtained by combining the derived mean tree height at an incidence angle of 3° and the basal area at the incidence angle of 20°. Hyyppä et al. (1997) conducted a comprehensive standwise forest inventory using C- and X-band HUTSCAT data with four polarization modes. They achieved satisfactory estimation accuracy for mean tree height, basal area, and stem volume, with standard errors of 1.6 m (13%), 4.3 m^2/ha (25%), and 31 m^3/ha (26%), respectively. The study concluded that due to the high correlation between polarization modes, the data from multiple polarization modes provided little additional information for the extraction of stand characteristics.

Another similar helicopter-borne FMCW profiling radar operating at C-, Ku- and Ka-bands (5, 14, and 35 GHz, respectively) with four polarization modes (HH, VV, VH, and HV) was developed by Axelsson (1993) and later named NOPEX (Northern Hemisphere Climate Processes Land-Surface Experiment) (Axelsson, 1995). Using its C-band nadir-looking measurements, Axelsson et al. (1999) estimated tree height and stem volume in boreal forests with standard deviations of 3.7 m and 71 m^3/ha, respectively. Comparison across the three frequency channels showed that tree heights derived from Ku- and Ka-bands were generally lower and revealed more structural variation, with RMS deviations of 1.3 m and 2.0 m relative to C band, respectively.

These earlier investigations highlighted the potential of profiling radar for retrieving forest attributes. Building on these developments and advances in positioning technology, FGI developed a lightweight Ku-band FMCW profiling radar, Tomoradar, equipped with a high-accuracy GNSS/IMU for precise

navigation (Chen et al., 2017). The system records echoes from both canopy and ground, which were validated against coincident laser scanning data. In this dissertation, Tomoradar data are employed for ground detection, as well as for estimating forest attributes including canopy height, DBH, stem volume, and forest biomass. Moreover, the penetration features of Ku-band signals through canopy were investigated with the support of laser scanning data.

In summary, while previous research confirmed the potential of profiling radar, the capabilities of Ku-band for forest inventory remain underexplored. The present dissertation addresses this gap through Tomoradar-based investigations of biomass estimation and signal penetration in boreal forests.

3 Materials

This study is primarily based on microwave radar data, with simultaneously acquired LiDAR data serving as reference for canopy height detection and Ku-band penetration modeling. Additional reference datasets include a high-accuracy DTM and field-based forest measurements, which were used for ground detection and forest attribute estimation. The following subsections provide detailed descriptions of these datasets.

3.1 Study areas and field reference

All five publications used data collected at a test site near Evo in southern Finland (61°19′N, 25°11′E). It is part of the southern boreal forest zone and primarily consists of Scots pine (*Pinus sylvestris*), Norway spruce (*Picea abies*), and deciduous trees, accounting for 40%, 36%, and 24% of the total volume, respectively. Unlike a completely homogeneous managed forest, this test site is a semi-managed site containing diverse vegetation structures. The collected data are categorized geographically into three distinct sections: east, west, and south. The first four publications mainly used data collected from the western area, while Publication V used data from all three sections.

The high-accuracy DTM used in Publications I and V was generated from classified ground returns of a LiDAR dataset acquired using the Leica ALS70-HA SN7202 system. The acquisition was conducted at an altitude of 900 m, producing an average point density of 6 points/m^2 and a footprint diameter of 13.5 cm on the ground (Yu et al., 2015).

The reference data used in Publication V were collected in the summer of 2014. During the manual field measurements, a total of 91 square sample plots, each measuring 32 by 32 m, were established at the test site. For all the trees with DBH greater than 5 cm, attributes including tree height, DBH, and tree species were measured and documented accurately. Tree height and DBH were measured using a hypsometer and a caliper, respectively, and the tree species were identified visually. The precise positions of trees were determined from a map generated using terrestrial laser scanning measurements coupled with GNSS. Subsequently, species-specific allometric equations, which are nationally recognized (Laasasenaho, 1982; Repola, 2008, 2009), were applied to calculate individual tree volume and biomass, based on recorded tree heights, DBH, and species classifications. The plot-level derived metrics, including the basal-area-weighted

mean canopy height (H_g), basal-area-weighted mean DBH (DBH_g), stem volume (V), and above-ground biomass (AGB), were aggregated by averaging or summing individual tree measurements. Additional field measurement details can be found in Yu et al. (2015). In Publication V, 55 of the 91 reference plots were used because corresponding Tomoradar measurements were only available for these plots (Feng et al., 2024).

3.2 Remote sensing data

The remote sensing dataset used in this dissertation consists of simultaneously acquired Ku-band profiling radar measurements and airborne LiDAR data, supported by high-precision GNSS-IMU positioning. The profiling radar (Tomoradar) provides range-resolved backscatter profiles sensitive to forest vertical structure and signal penetration, while the LiDAR system delivers high-resolution three-dimensional geometric reference data for canopy and terrain surfaces. The synchronized acquisition of both datasets enables direct comparison between radar waveforms and LiDAR-derived forest structural parameters, forming the basis for elevation retrieval, penetration analysis, and biomass modeling presented in subsequent chapters.

3.2.1 Tomoradar system overview

The primary remote sensing data used in this study were collected using a Ku-band FMCW profiling radar system, referred to as Tomoradar (Chen et al., 2017). The system concept, hardware architecture, and platform integration were originally documented in Chen et al. (2017), which provides the technical background for the Tomoradar measurements used in this dissertation. Here, only the main system characteristics relevant to the included studies are summarized.

The system is designed as a lightweight, airborne profiling system, originally developed for unmanned aerial vehicle (UAV) deployment. It operates at a center frequency of 14 GHz with a sweep bandwidth of 1 GHz, providing a vertical range resolution of approximately 15 cm. The selection of Ku band represents a practical trade-off between antenna aperture size, system weight, and achievable spatial resolution. Compared with lower-frequency systems, Ku band enables a compact antenna aperture suitable for lightweight airborne deployment, while still maintaining sensitivity to canopy structural variations in boreal forest environments.

The radar system is configured to observe in the nadir direction using parabolic dish antennas with a 6-degree half-power beamwidth (HPBW, 3 dB). This configuration is specifically suited for retrieving vertical forest structure parameters, such as ground elevation, canopy top height, and canopy vertical distribution, from distance-resolved backscatter waveforms. To support

polarimetric measurements, the system employs a bistatic dual-antenna configuration and is equipped with orthomode transducers (OMTs), enabling both horizontal and vertical polarization components for both transmission and reception, resulting in full polarimetric (HH, HV, VH, VV) data. Although full polarimetric capability is available, in this dissertation only data from the co-polarized HH channel were utilized due to its relatively stronger and more stable response in boreal forest environments.

In the transmit path, a digitally generated FMCW signal is upconverted to the Ku-band carrier frequency and amplified before being radiated by the transmit antenna. In addition, a directional coupler provides the transmitted signal to the receiving section as a reference signal for coherent demodulation. In the receive path, the backscattered signal collected by the receiving antenna is amplified and mixed with the reference signal to obtain an intermediate frequency (IF) signal, which contains the backscattering information. The IF signal passes through a distance corrector that compensates for the signal attenuation due to propagation range, and is subsequently recorded using a National Instruments PXIe-6115 digitizer at a sampling rate of 2.5 MS/s (Chen et al., 2017). Range profiles are later obtained from IF signals via frequency to range conversion, as described in Section 4. Figure 1 presents the system block diagram of Tomoradar.

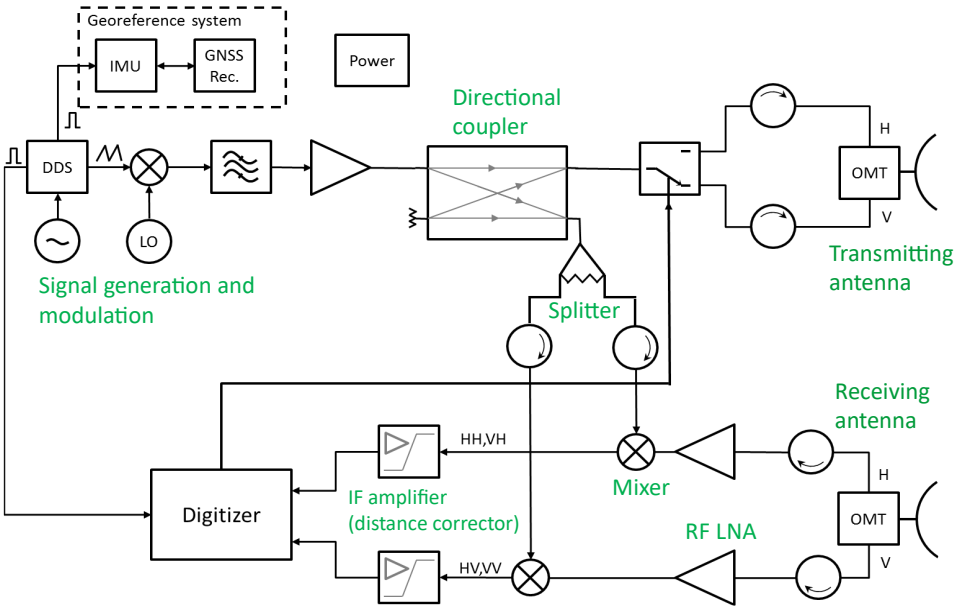


Figure 1 Block diagram of the Tomoradar system. In the diagram, DDS denotes direct digital synthesizer; LO, local oscillator; IMU, inertial measurement unit; GNSS, Global Navigation Satellite System; OMT, orthomode transducer; LNA, low-noise amplifier; RF, radio frequency; IF, intermediate frequency; and H and V, horizontal and vertical polarizations, respectively (Chen et al., 2017).

To ensure precise spatial referencing of individual radar waveforms, Tomoradar is integrated with a tightly coupled GNSS–IMU system providing centimeter-level positioning accuracy and high-frequency attitude measurements. The synchronization between radar acquisition and GNSS–IMU observations enables accurate georeferencing of each waveform, including compensation for platform motion and orientation variations during flight. This precise positioning capability represents a significant improvement over earlier profiling radar systems and is essential for reliable alignment of radar footprints with LiDAR point clouds and field reference plots. Overall, the principal system specifications of Tomoradar are summarized in Table 1, providing a concise reference for the key operational parameters.

Table 1 Tomoradar system technical specifications

Category	Parameter	Specified value
Radar configuration	Center frequency	14.0 GHz (Ku band, $\lambda \approx 2.14$ cm)
	Modulation type	FMCW (triangular)
	Modulation frequency	163 Hz
	Sweep bandwidth	1 GHz
	Measurement range	10–150 m
	Range resolution	0.15 m
Antenna characteristics	Antenna type	Parabolic dish (bistatic configuration)
	Antenna aperture	330 mm
	Incidence angle	Nominal incidence angle: 0° (nadir-looking configuration)
	Two-way beamwidth	6° (HPBW, 3 dB)
	Polarization modes	HH, VV, HV, VH
	Polarization isolation	>30 dB
Data recording	A/D converter	12 bits
	Sampling rate	2.5 MS/s
	Recorded signal	IF waveform
Georeferencing system	GNSS-IMU data rate	200 Hz (helicopter) / 125 Hz (UAV)
	Position accuracy	2 cm + 1 ppm
	Attitude accuracy	Roll/Pitch: 0.005° (helicopter) / 0.015° (UAV) Heading: 0.008° (helicopter) / 0.08° (UAV)

During the flight campaign conducted on September 20, 2016, the Tomoradar system was rigidly mounted on an external arm of a Bell 206 helicopter (Feng et al., 2018). The platform operated at flight altitudes of approximately 60–100 m above

ground level and ground speeds of 10–20 m/s. Under the nominal two-way HPBW of 6°, the resulting radar ground footprint diameter varied from 6 to 10 m.

3.2.2 Reference LiDAR data

In addition, a lightweight Velodyne VLP-16 LiDAR, operating at a measurement rate of 300,000 points/s, was mounted adjacent to Tomoradar to acquire high-resolution 3D point clouds simultaneously, ensuring spatial and temporal consistency across the datasets. Since LiDAR measurements are highly sensitive to canopy surface geometry, these data were intentionally collected to provide a reference for canopy height estimation. The small beamwidth of LiDAR pulses also enables accurate detection of forest structures such as canopy gaps, assisting in the analysis of forest vertical structure detected from Tomoradar data.

During the measurement, the LiDAR system operated with 16 laser beams distributed evenly over a vertical field of view of ±15°. Each transmitted laser pulse had a beam size of 12.7 mm (horizontal) × 9.5 mm (vertical) at the emission aperture, and the system recorded both the strongest and last return echoes. The scanner produced 360° horizontal scans, but for comparative forest structure analysis, only the forward-looking sectors (typically within ±8°) were considered to match the Tomoradar footprint geometry (Feng et al., 2018). The LiDAR data were used in Publications I–IV as reference or comparative data in the validation of radar-based measurements. Table 2 summarizes the characteristics of each data source, including key system parameters and their respective roles in this study.

Table 2 Summary of the data sources and sensor specifications used in this study

Data type	Sensor/Source	Key parameters	Publications
Ku-band radar	Tomoradar (FMCW profiling radar)	Center frequency: 14 GHz Bandwidth: 1 GHz Range resolution: 15 cm	I–V
LiDAR	Velodyne VLP-16	16 laser channels 300,000 points/s Vertical FOV: ±15°	I–IV
DTM	Leica ALS70-HA SN7202	Point density: 6 points/m^2	I, V
Field reference	Manual measurement	91 square plots (32 m × 32 m) Manually measured: tree height, DBH, species TLS/GNSS-derived: tree position Species-specific allometric equation derived: biomass and volume	V

4 Methods

This chapter introduces the methodological workflow applied to Tomoradar data for forest structure and biomass estimation, focusing on the approaches developed and implemented in Publications I, III, and V, which constitute the core methodological contributions of this dissertation. Publications II and IV are referenced for complementary findings and are summarized later without reproducing their methodological details.

The workflow begins with the preprocessing of raw radar waveforms to generate distance-resolved profiles and align them with reference LiDAR data. Terrain and canopy top elevations are then derived to characterize vertical forest structure, followed by an assessment of Ku band penetration through the canopy using LiDAR comparisons and effective beamwidth analysis. Finally, key plot-level forest attributes including canopy height, DBH, stem volume, and AGB are estimated using radar-derived features and machine learning models. The methodological components are described in detail in the following subsections.

4.1 Remote sensing data processing

Before forest attributes can be estimated, the Tomoradar backscatter waveforms must be processed to extract distance-resolved profiles of the forest structure. Based on the principle of FMCW radar, the target distance can be derived from the intermediate frequency contained in the recorded Tomoradar backscattered waveforms (Chen et al., 2017). Specifically, the relation between distance and the intermediate frequency can be expressed as follows:

$$f_b = \frac{\Delta f}{T_b}\frac{2R}{c}, \tag{1}$$

where f_b is the intermediate frequency, R is the target distance, c is the speed of light, Δf is the total frequency offset, and T_b is the chirp duration. Based on this relationship, the fast Fourier transform (FFT) is applied to convert the waveforms into the frequency domain, and the corresponding distance information is then derived, with amplitude values representing backscatter from different vertical layers. To reduce noise and improve interpretability, a smoothing filter is applied to the data.

For each Tomoradar backscattered waveform, a matching set of LiDAR points was identified within the radar footprint cylinder. A cylinder-shaped region was defined using the nadir beam geometry, with its footprint radius computed

dynamically from the recorded flight altitude and the radar's 6-degree beam divergence. The location and orientation of each radar footprint were determined using the GNSS-IMU data. All the LiDAR points within this spatial region were grouped as the corresponding LiDAR data for each Tomoradar waveform (Figure 2). This cylindrical selection was used in Publication I; Publications II–IV used a conical region to select the corresponding LiDAR points for more accurate comparison results.

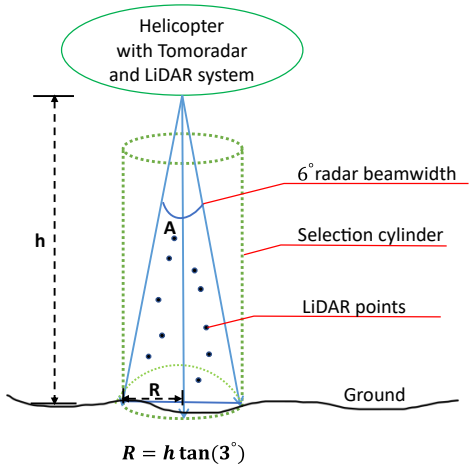


Figure 2 Selection of LiDAR points corresponding to a Tomoradar measurement. Here, h is the distance from the radar antenna to the ground, R is the radius of the Tomoradar footprint at ground level, and A denotes the highest LiDAR point within the cylindrical selection volume. The 3° term is the half-angle of the 6° radar beamwidth (Modified figure from Publication I).

4.2 Terrain and canopy top elevation estimation

Terrain and canopy elevations provide fundamental information for the calculation of other forest vertical structure features and parameters. Publication I investigated the extraction of ground level and canopy top elevation from Tomoradar backscatter waveforms.

After extracting the range information through the frequency components of the raw backscattered Tomoradar waveform, a vertical range profile with amplitude information of each layer is generated for each waveform. The targets, including canopy and ground, appear in the profile with high amplitude values.

As illustrated in Figure 3, the amplitude of the backscattered signal rises significantly above the noise level at locations corresponding to vegetation or ground surfaces. In cases where only the ground is detected (Figure 3(a)), the ground position in the backscatter waveform can be directly determined by identifying the peak amplitude along the backscattered radar profile. However, in most practical scenarios, both the ground and above-ground vegetation are

detected simultaneously (Figure 3(b)), which complicates the extraction and differentiation of target returns.

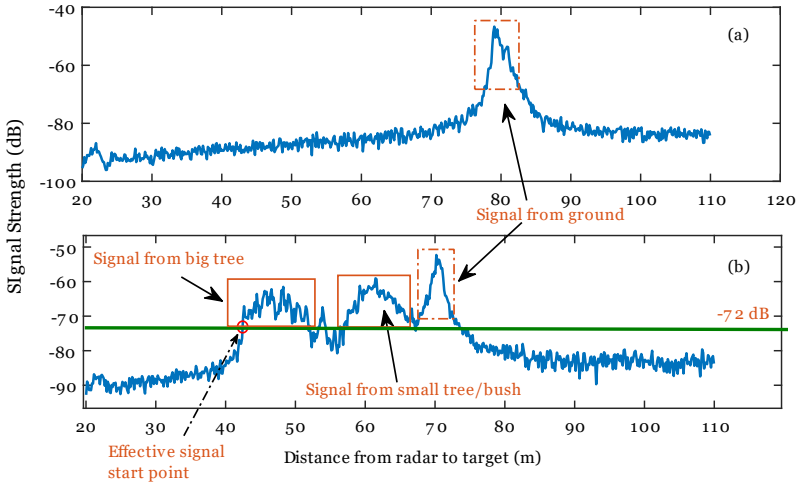


Figure 3 Tomoradar backscatter vertical range profiles of (a) a waveform only detecting ground and (b) a waveform detecting both complex vegetation and ground (Modified figure from Publication I).

To estimate the ground elevation from a backscatter waveform in such cases, candidate ground positions are first identified as local maxima within the amplitude profile. These candidate positions are then compared to the terrain elevation estimated from the previous waveform. Given the natural continuity of terrain, where elevation typically does not change dramatically over short distances, the candidate position closest to the previous ground level is selected as the terrain position detected by this waveform. Additionally, in situations where the above-ground vegetation is so dense that insufficient radar energy penetrates to the ground and is backscattered, the actual ground return may be absent from the waveform. To address this, the minimum distance between the detected peaks and the previous estimated ground position is evaluated. If this distance exceeds a preset threshold (1 m in this study), the peaks are assumed to represent backscatter from the canopy rather than the ground. Consequently, the waveform is considered to lack a valid ground return, and the previous terrain elevation is retained for continuity.

The accuracy of terrain elevation estimation was validated using a high-resolution DTM. Using the helicopter (Tomoradar) position and attitude information obtained from the GNSS and IMU data, the direction of the emitted radar signals was calculated. Based on this information, the intersection points between the transmitted signals and the DTM were determined, representing the reference locations where the transmitted signals intersected the ground surface. The distance from each radar position to the corresponding calculated ground-intersection point was used as the reference radar-to-ground distance. Finally, the

radar-to-ground distances estimated directly from the Tomoradar backscatter waveforms were compared with the corresponding reference distances, and the estimation accuracy was assessed statistically. Publication I includes the full details.

For canopy top elevation estimation, the canopy top was assumed to correspond to the position where significant backscatter began. To identify this position, an amplitude threshold was used to distinguish effective backscatter from noise. An initial threshold was derived using the three-standard-deviation criterion. Because this initial value did not produce satisfactory canopy top estimates, the threshold was increased stepwise, and the corresponding canopy top estimates were evaluated against LiDAR-derived canopy top elevations. A threshold of −72 dB yielded the lowest estimation RMSE and was therefore selected. The first waveform sample point exceeding this threshold was identified as the canopy top position (Figure 3(b)).

To verify the accuracy of the canopy top elevations estimated from Tomoradar data, LiDAR measurements were used as a reference. As described in Section 4.1, the corresponding LiDAR point cloud was extracted for each Tomoradar backscatter waveform. The LiDAR-derived canopy top elevation was defined as the elevation of the highest point within the corresponding point cloud (point A in Figure 2).

The canopy top elevations estimated from Tomoradar data were compared with LiDAR-derived values using both peak-to-peak and waveform-to-waveform approaches. In the peak-to-peak method, local maxima of canopy top elevations extracted from the LiDAR data were identified, and for each LiDAR-derived peak, the corresponding Tomoradar canopy top position was determined by searching for the nearest neighbor among all canopy top positions derived from Tomoradar waveforms. These matched peak pairs were evaluated using statistical metrics including correlation, mean and median elevation differences, and root mean square error (RMSE). In the waveform-to-waveform approach, all individual canopy top elevations derived from Tomoradar and LiDAR data were compared one by one across each file. The correlation coefficient and RMSE were calculated to provide a comprehensive analysis.

Publication I offers more details about the method. The same canopy top estimation method was also utilized in Publications III and V.

4.3 Ku-band signal penetration in boreal forests

It is generally believed that Ku-band signals, due to their shorter wavelength, will be backscattered by the canopy surface when emitted into the forest. However, the actual situation about how deeply Ku-band signal could penetrate the canopy remained under exploration.

The penetration of Ku-band microwave signals through forest canopy was investigated by analyzing the Backscattered Energy Ratio of Canopy-to-Total

(BERCT), derived from decomposed Tomoradar waveforms. A height threshold of 2 m was commonly used to distinguish between above-ground vegetation and ground. Thus, the waveform was segmented into two parts: the upper section ranging from the top of the canopy to the position that is 2 m above the ground (bottom of canopy section) representing backscatter from above-ground vegetation (canopy section), and the lower section ranging from the bottom of canopy to ground corresponding to ground returns (ground section). BERCT was defined as the ratio of integrated signal power from the canopy section to the total backscattered power. BERCT for each backscatter waveform can be calculated using the following equations:

$$R_{veg} = \frac{\sum E_{canopy}}{\sum E_{total}} = \frac{\sum_{z=2}^{z_{top}} E_P(z)}{\sum_{z=0}^{z_{top}} E_P(z)} \quad (2)$$

$$\sum E_{canopy} + \sum E_{ground} = \sum E_{total}, \quad (3)$$

where R_{veg} (BERCT) is the ratio of canopy backscatter power to total backscatter power; $E_P(z)$ is the backscatter power at height z; z denotes the height above ground measured in meters, with z = 0 representing ground level and z = 2 representing 2 m above ground; and z_{top} is the canopy top height; $\sum E_{canopy}$, $\sum E_{ground}$, and $\sum E_{total}$ are the backscatter powers summed over the canopy section, ground section and the total backscatter power, respectively.

As described above, for each Tomoradar waveform the corresponding LiDAR data were obtained by taking all the LiDAR returns within the Tomoradar waveform footprint cone. Similar to the processing of Tomoradar waveforms, the LiDAR returns were divided into two portions based on the positions of the returns. To assess the influence of canopy structure, canopy fraction was calculated from the LiDAR point cloud as the proportion of returns within the canopy group relative to the total returns. The canopy fraction can be calculated by the equation:

$$CF_{LiDAR} = \frac{P_C}{P_T}, \quad (4)$$

where P_C is the number of LiDAR returns from the canopy section, and P_T is the total number of returns from the canopy top to the ground within the Tomoradar waveform footprint cone.

Using LiDAR-derived canopy fraction as a reference, the Tomoradar-derived BERCT was compared and investigated. A linear regression was then performed between these two parameters to evaluate their correlation. Additionally, a multiple regression model incorporating canopy fraction, canopy height, and the distance between the radar and the canopy top was developed to quantify their associations with radar backscatter and evaluate Ku-band signal penetration through the boreal forest canopies. Figure 4 presents an example of one Tomoradar waveform and the corresponding LiDAR point cloud. The method was implemented and described in greater detail in Publication III.

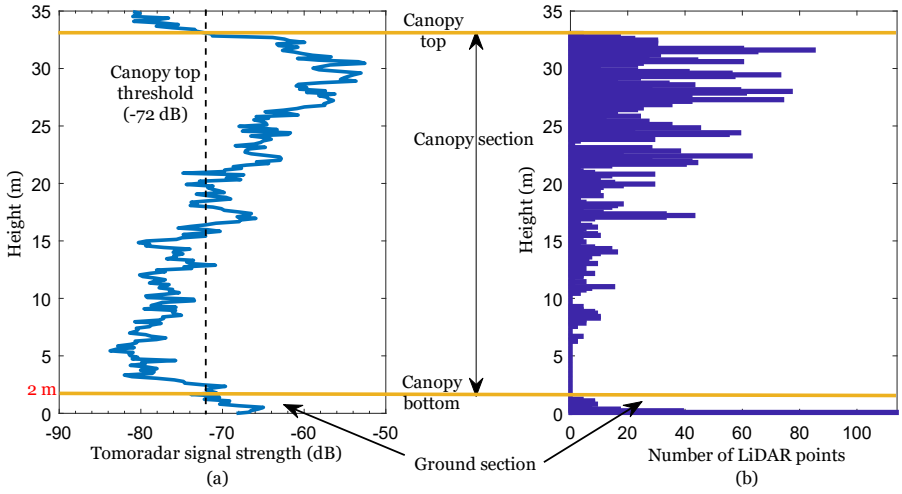


Figure 4 Comparison between (a) a single Tomoradar backscatter waveform containing both canopy and ground returns and (b) a histogram of the corresponding LiDAR returns within the Tomoradar footprint. The canopy section was defined as the section from the canopy top to the position that is 2 m above the ground level, which was estimated independently using the method described in Section 4.2. Returns below this position were assigned to the ground section (Modified figure from Publication I).

4.4 Plot-level forest attribute extraction

Publication V estimated plot-level forest attributes including H_g, DBH_g, stem volume (V), and AGB through the extracted plot-level forest vertical structure features and the method of random forest (RF). RF has shown good performance for AGB prediction using multisource remote sensing datasets that include SAR observations (Chen et al., 2019).

Before applying RF, various plot-level waveform features were calculated to serve as input predictors. For each waveform, the detected terrain elevation and canopy top position were first derived from DTM and Tomoradar data, respectively, using the method described in Section 4.2. The canopy segment was defined as the range between the canopy top and the position 2 m above the ground surface. Within this segment, a series of waveform features were extracted to characterize the vertical structure and energy distribution of the backscattered signal.

These features included the position and strength of the maximum canopy return, height percentiles corresponding to cumulative power levels (100%, 90%, ..., 20%, 10%), and energy distribution across evenly segmented canopy layers. Additionally, features such as the total energy within the canopy and the ratio of this energy to total waveform energy (canopy cover) were calculated. Structural metrics were also derived to describe canopy structural compactness and depth, including the ratio of canopy bottom to canopy top height, the heights corresponding to 55% and 25% cumulative power, and their respective ratios to the canopy top height. For each sample plot, the mean and standard deviation of these

waveform features across all waveforms in the plot were computed, resulting in a comprehensive feature set including 60 variables per plot. Table 3 summarizes these waveform features.

Table 3 Names and brief descriptions of plot-level features (Modified from Table 2 in Publication V).

Mean value features	Standard deviation value features	Brief descriptions of waveform features
M_Rmax_C	Std_Rmax_C	Strongest reflection signal strength (dB) in canopy section (Rmax_C)
M_H_Rmax_C	Std_H_Rmax_C	Height of the strongest canopy return (H_Rmax_C)
M_HP_C1~10	Std_HP_C1~10	Height percentiles of canopy part: height with cumulative power 100%, 90%, ..., 10% of canopy power (HP_C1, 2, …, 10)
M_EP_C1~10	Std_EP_C1~10	Energy in canopy height layers: energy of 1st, 2nd, …, 10th evenly divided height range of canopy part (EP_C1, 2, … , 10)
M_PC	Std_PC	Power of canopy section (PC)
M_P_tot	Std_P_tot	Total power of both canopy and ground (P_tot)
M_Cov	Std_Cov	Radar-derived canopy cover: PC/P_tot (Cov)
M_CB2CH	Std_CB2CH	Ratio between canopy bottom height and canopy top height (CB2CH)
M_H55 M_H25	Std_H55 Std_H25	Heights corresponding to cumulative power fractions of 55% (H55) and 25% (H25)
M_R_H55 M_R_H25	Std_R_H55 Std_R_H25	Ratios of H55 (R_H55) and H25 (R_H25) to canopy top height

To predict the plot-level forest attributes H_g, DBH_g, V, and AGB, an RF regression model was employed. The model was configured with 300 trees, a minimum of three samples per leaf node, and five randomly selected variables considered at each node split. To avoid overfitting and to ensure generalization, a repeated hold-out validation scheme was applied. In each iteration, two-thirds of the plots were randomly assigned as training data and one-third as test data. The process was repeated multiple times so that each plot contributed to both training and testing phases.

To evaluate the estimation accuracy, the four predicted plot-level forest attributes were compared to the manually collected ground truth data, and the following statistical metrics were calculated: bias, relative bias ($bias_{rel}$), RMSE, relative RMSE ($RMSE_{rel}$), and coefficient of determination (R^2). In addition, the maximum canopy height within each plot was also obtained from Tomoradar data and compared with corresponding reference values to further assess the reliability of the radar-based canopy height estimation.

5 Results and discussion

This chapter presents and synthesizes the results obtained from the analysis of Tomoradar data in boreal forest conditions. The findings are integrated following the methodological progression in Chapter 4, with emphasis on the core results from Publications I, III, and V, while complementary results from Publications II and IV are used to support the interpretation of penetration behavior and measurement geometry. Beyond reporting quantitative performance metrics, this chapter interprets the results in the context of boreal forest remote sensing and evaluates the feasibility of Ku-band profiling radar for forest inventory applications. The chapter concludes with a critical discussion of methodological limitations, practical implications, and directions for future research.

5.1 Terrain and canopy top elevation estimation

5.1.1 Terrain elevation estimation

As described in Section 4.2, terrain positions corresponding to radar signals backscattered by the ground were identified based on the waveform amplitude features. For each waveform, the distance between the detected ground point and the helicopter was derived and compared to the reference distances derived from a DTM. To assess the performance of terrain elevation detection, three sample Tomoradar data files were analyzed, each containing 10,002 waveforms. Both visual inspection and statistical analysis were conducted.

Figure 5 illustrates the comparison results in three stand profile diagrams, each colored by the backscattered signal strength. Since the radar system operated in a nadir-looking configuration, the yellow and blue regions at the top part of the diagrams are interpreted as canopy and low vegetation returns, while the black and red lines represent the terrain elevation derived from Tomoradar and GNSS+DTM data, respectively. The comparison shows that the estimated distances from the radar sensor to the ground generally align well with the reference values; however, in specific locations (labeled A, B, and C in the figure) the detected ground distances were underestimated.

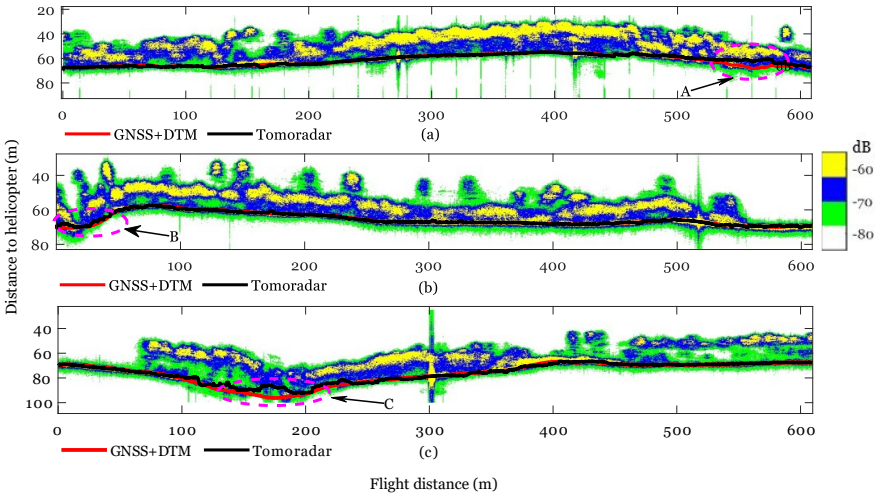


Figure 5 Three different stand profile diagrams produced from Tomoradar files with four colors representing the backscattered signal strength with the color scale on the right side. Each diagram contains the terrain position estimated from Tomoradar data (black line) and the corresponding reference (red line) produced by the GNSS and DTM. The letters mark locations where the estimates and reference values do not match (Modified figure from Publication I).

The statistical analysis shows that the RMSEs of ground range estimation for the three sample files were 1.49 m, 0.50 m, and 2.12 m (corresponding to diagrams a–c in Figure 5). After further checking the vegetation structure and helicopter attitude information offered by IMU data in the outlier parts (see Figure 6 in Publication I), it was found that these errors coincide with segments where the helicopter was turning. During the turning, the attitude of the helicopter changed significantly, resulting in large deviations (up to several tens of degrees) from the expected nadir incidence angle. The increased incidence angle led to larger signal footprints on the ground and consequently reduced detection accuracy. After excluding these unexpected data segments, the RMSEs improved to 0.43 m, 0.33 m, and 0.44 m for the three sample files, indicating that, under stable nadir-viewing conditions, the proposed method could achieve ground range estimation errors of less than 0.5 m.

Additionally, regions with greater estimation error often corresponded to areas with low vegetation, where the backscattered signal intensity from the vegetation closely resembled that from the ground. This similarity complicated accurate ground detection. Therefore, the performance of the proposed method is sensitive to the parameter settings, particularly the starting point of ground range detection and the threshold used to identify the backscatter power peak from the ground surface.

Through the study, the proposed approach using Tomoradar data achieves a ground range estimation RMSE of less than 0.5 m when operating under nadir

observation. By combining Tomoradar and the GNSS-IMU data, it is possible to construct an accurate ground model in boreal forest environments.

5.1.2 Canopy top elevation estimation

Forest canopy top elevation is an important variable for both canopy structure analysis and other forest attribute estimation. The canopy top position was extracted from each Tomoradar backscatter waveform, as well as the corresponding LiDAR point cloud. Figure 6 illustrates the canopy top estimation results from one minute of both Tomoradar (red dashed line) and LiDAR data (blue solid line), while the green dots represent the LiDAR point cloud collected simultaneously during a Tomoradar data collection process.

The figure shows that the canopy top elevations estimated from Tomoradar data generally follow the same trend as those derived from LiDAR measurements. However, the Tomoradar-derived canopy tops (red dashed line) exhibit a smoother profile compared to the more detailed LiDAR-derived canopy tops (blue solid line), which display greater local variation and finer structural peaks. This difference in resolution and level of detail is mainly due to the differing spatial characteristics of the two systems. Tomoradar uses a radar beam with a 6-degree beamwidth, resulting in a footprint spanning several meters on the ground. The backscattered waveform represents an average response over this area, which inherently introduces a spatial smoothing effect. In contrast, the LiDAR system emits narrow laser pulses with a much smaller beam divergence, allowing it to capture fine-scale variations in canopy structure with higher spatial resolution. As a result, the LiDAR canopy top profile preserves more localized features and canopy peaks, while the Tomoradar profile reflects a more generalized vertical structure.

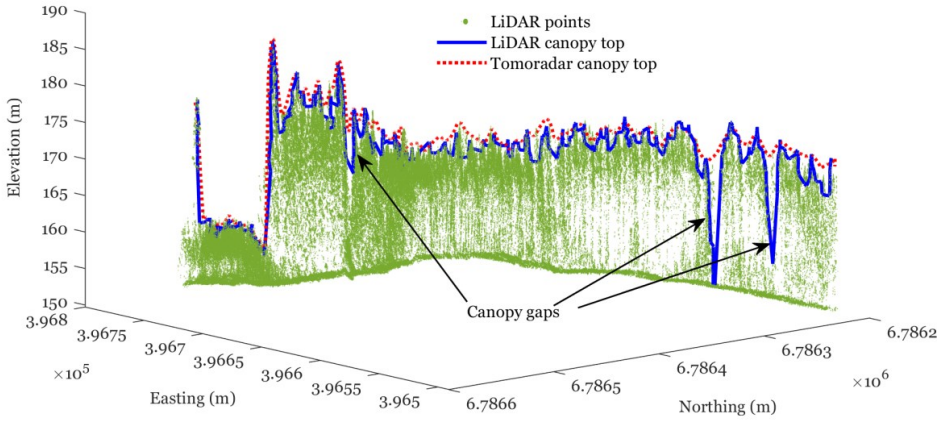


Figure 6 LiDAR point cloud (green dots) corresponding to one Tomoradar data file, together with canopy top elevations estimated from the Tomoradar data (red dashed line) and the LiDAR data (blue solid line). Horizontal coordinates are given in the ETRS-TM35FIN coordinate system, and elevations are the ellipsoidal heights (Modified figure from Publication I).

Another visible phenomenon is that, whenever there are canopy gaps, the canopy top elevations estimated from LiDAR data were much lower than those derived from Tomoradar data (Figure 6). The estimated elevation differences correlate with the canopy gap width and are mainly caused by additional backscatter received through the side lobes of the Tomoradar antenna. Although we assumed the backscattered energy was from the main lobe (defined by a 3 dB beamwidth), additional contributions from the side lobes extended the effective detection area beyond the main footprint. In contrast, the corresponding LiDAR points, which were selected from within the main lobe footprint, covered a narrower area. When the canopy gap is narrower than the Tomoradar main lobe footprint, both systems tended to ignore the gap, resulting in similar canopy top estimations (Figure 7(a)). Conversely, when the canopy gap is wider than the footprint covered by the side lobe, both systems will receive returns from the ground and the canopy top estimations are similar again (Figure 7(c)). However, when the canopy gap width falls between the footprint size of the Tomoradar main lobe and that of the side lobe, the situation is complicated. In such cases, the Tomoradar backscatter waveform may contain backscatter energy from nearby canopies or branches produced by the side lobes (Figure 7(b)), leading to an overestimation of the canopy top. Meanwhile, the LiDAR returns corresponding to the main lobe detection area will come only from the ground or lower vegetation within the gap, resulting in a significantly lower canopy top estimate. Figure 7 illustrates these scenarios.

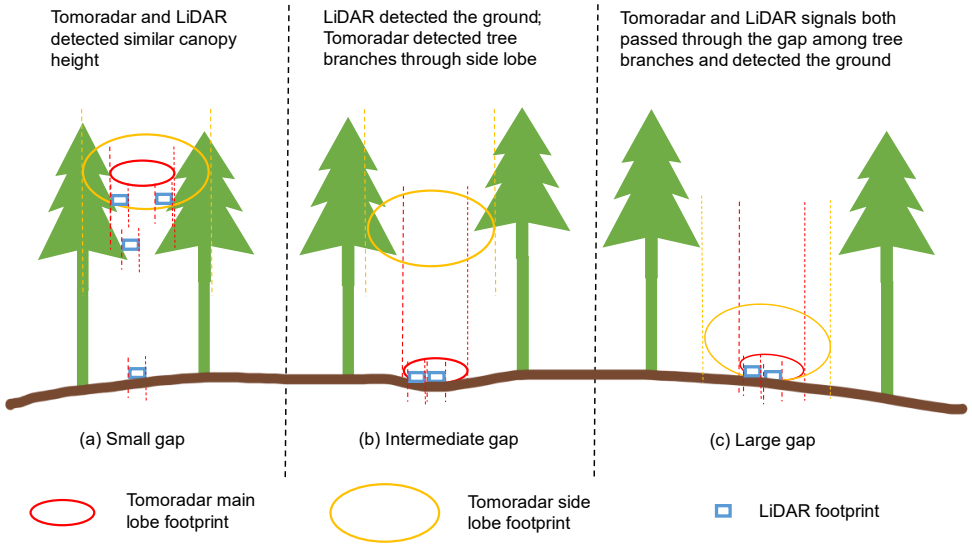


Figure 7 Different canopy elevation estimation scenarios based on canopy gap width: (a) canopy gap narrower than the Tomoradar main lobe footprint; (b) canopy gap wider than the Tomoradar main lobe footprint, but narrower than the side lobe footprint; (c) canopy gap wider than the Tomoradar side lobe. The red and yellow circles represent the Tomoradar main lobe and side lobe footprints, respectively. The blue rectangles represent LiDAR footprint.

Quantitative analysis was conducted using 17 datasets of both Tomoradar and LiDAR data. Using LiDAR data as the reference, the mean, median, and RMSE of canopy top elevation differences were calculated for each file based on matched canopy top peaks estimated from Tomoradar data. The best-performing dataset yielded a mean difference of 0.240 m, a median of 0.128 m, and an RMSE of 0.320 m, while the worst file produced a mean difference of 1.766 m, a median of 0.592 m, and an RMSE of 3.796 m. Overall, the average mean and median elevation estimation differences across all datasets are 0.737 m and 0.504 m, respectively, with an RMSE of 1.096 m. Further investigation revealed that the largest errors were primarily associated with canopy gaps, as previously discussed, and noise points in the LiDAR data. After removing these outlier peaks, the estimation accuracy improved, with the average mean and median elevation estimation differences reduced to 0.640 m and 0.493 m, respectively, and the RMSE improved to 0.852 m.

Similar numerical analysis was also conducted using waveform-to-waveform comparisons based on the same 17 datasets. Prior to the analysis, outliers associated with canopy gaps and LiDAR noise, which were previously identified during the peak-based comparison, were removed to improve robustness. The correlation coefficients and RMSEs of the comparison between canopy top elevations derived from Tomoradar and LiDAR data were calculated. The correlation coefficients were mostly between 0.90 and 0.98, with only two datasets falling below 0.90. The RMSE values ranged from 0.656 m to 0.914 m, with an overall average of 0.799 m. These results indicate that Tomoradar data can estimate canopy top elevation with an accuracy of approximately 0.8 m. However, as noted earlier, the presence of canopy gaps and the influence of side lobes significantly affect the estimation accuracy in certain cases. The detailed results for each file are provided in Publication I.

5.2 Ku-band signal penetration in boreal forests

Building upon the ground and canopy top elevation estimation from Section 4.2, this section presents a comprehensive qualitative and quantitative analysis of the backscatter profiles in the boreal forest at Ku band. The analysis focuses on the relationship between the backscattered energy ratio of canopy to total energy (BERCT) and the ratio of canopy returns to total returns (CF) derived from LiDAR data. Additionally, other forest parameters affecting BERCT were also analyzed by fitting a prediction model for BERCT.

According to Equations (2) and (4), the BERCT and CF were calculated for an approximately 600-m-long strip and the results are shown in Figure 8. In the figure, the stand profiles are colored by the backscatter signal strength, the distances to the radar sensor are scaled by the left y-axis, and the ground level is marked by a purple

solid line. The calculated BERCT and CF are scaled by the right y-axis and represented by an orange solid line and a black dashed line, respectively.

When we match the BERCT and the stand profile image, the BERCT varies as canopy height and canopy density change. When there is an increase in BERCT from A to B and from C to D, the corresponding detected canopy height also increases. When the canopy heights are similar at the positions marked by B, D, and E, the corresponding BERCTs are different. This is mainly because canopy density differs between these locations. The signal-strength colors show that the signal at position E is about 5–10 dB weaker than at position B. After position F, there is an open area without mature vegetation and the Tomoradar backscattered signal comes mostly from the ground, resulting in zero BERCT. Overall, the BERCT of Ku-band signals in boreal forest is related to the canopy height and density.

When we compared the BERCT and the LiDAR-derived CF from one strip, the BERCT highly aligns with the CF (Figure 8). The correlation coefficient between the two lines was 0.835, indicating that the BERCT correlates well with CF. The correlation is expected because both metrics reflect the relative distribution of returns between canopy and ground, although they arise from different measurement mechanisms. This result is influenced by both wavelength and forest canopy structure. The longer wavelength of the Ku-band Tomoradar signal allows part of the radar energy to be transmitted through foliage and scattered by lower-canopy elements or the ground. In contrast, LiDAR pulses generally reach the understory or ground through canopy gaps. Their narrow beam divergence and resulting small footprint allow some individual pulses to pass through small gaps without intercepting vegetation, producing numerous understory and ground returns in the LiDAR point cloud, as discussed in Publication I. In particular, within one Tomoradar waveform footprint, all the corresponding LiDAR returns are used to calculate CF, rather than only the highest return, as in the canopy elevation analysis. Therefore, the different effects of canopy gap on Tomoradar backscatter waveforms and LiDAR returns matter more.

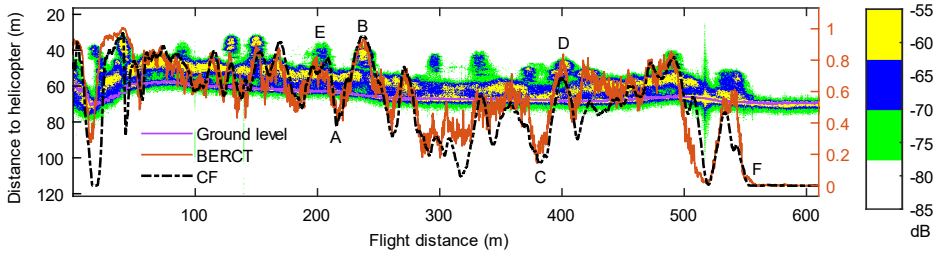


Figure 8 Tomoradar forest stand profile from a single flight strip, visualized by backscattered signal strength (color scale shown at right). The estimated ground level is shown in purple (scaled by the left y-axis). BERCT derived from Tomoradar data (orange solid line) and CF from LiDAR data (black dashed line) are overlaid and scaled by the right y-axis, using the stand profile as background for visual comparison.

Through the study in Publication III, the BERCT derived from Tomoradar data was linearly related to the LiDAR-derived canopy fraction and logarithmically related to canopy height h (m). In addition to these two variables, the fitted model for BERCT included the distance d (m) between the canopy surface and the radar sensor. Other potential influences, such as system errors, tree species, and humidity, were represented collectively by a constant term. Further analyses of these parameters were conducted in Publication III. A larger dataset (more than six strips of data, including 63,015 measurements) was used for the model fitting study, and the data were randomly split into equal model training and validation subsets. The obtained model is

$$BERCT = 0.8156 \times CF + 0.0423 \times \ln h + 165650 \times e^{-d} - 0.0281. \quad (5)$$

According to Equation (5), the LiDAR-derived canopy fraction was the dominant predictor of BERCT in the fitted model, which agrees with their definitions. The canopy height related to the canopy structure has a minor contribution, while the distance between radar sensor and canopy surface, as well as the other factors, also have small effects on the backscatter energy from canopy in Ku band.

Besides the canopy fraction analysis, Publication II further analyzed canopy vertical structure by deriving canopy height profiles (CHPs) from 6,766 Tomoradar measurements and the corresponding LiDAR data. Here, the CHP represents the relative distribution of the surface area of canopy components, including foliage and woody material, among different height layers. Using the LiDAR-derived CHPs as reference data, the Tomoradar footprint was initially defined based on the nominal 6° 3-dB beamwidth. With this footprint, 74.59% of the Tomoradar-derived CHPs showed at least moderate positive correlations with the corresponding LiDAR-derived CHPs. In the subsequent analysis, the footprint was expanded to an effective angular extent of 20°, encompassing more than 95% of the transmitted main-lobe energy. The percentage of CHP pairs showing at least moderate positive correlation consequently increased to 96.96%. In this case, 88.17% of the Tomoradar-derived CHPs had a strong correlation coefficient ($r > 0.6$) with those from LiDAR data.

Publications I and II revealed that Tomoradar backscatter waveforms often represent a larger effective footprint than that of a 6° half-power beamwidth (HPBW, 3 dB). This motivates an accurate characterization of the effective beamwidth when comparing waveform-derived forest attributes with LiDAR references. Publication IV investigated the effective beamwidth of Ku band by comparing Tomoradar waveforms and canopy top elevations with the corresponding LiDAR-derived values. It was found that the effective beamwidths of Tomoradar waveforms vary due to the diversity of the studied vegetation. Therefore, a new beamwidth definition named average effective beamwidth

(AEBW) was introduced, which is calculated from the actual effective beamwidths and their corresponding percentages to the total tested waveforms.

Through the study, the AEBW estimated from 8,565 Tomoradar measurements was about 8°, which is larger than the HPBW of 6°. When comparing the canopy tops derived from Tomoradar data and the LiDAR data within AEBW footprint size rather than the HPBW, the correlation coefficient increased from 0.89 to 0.98, while the standard deviation decreased from 3.79 m to 1.39 m. Therefore, using AEBW to determine the radar footprint should be more accurate for studies in boreal forests. However, according to the definition, the AEBW may vary with different vegetation types and radar antenna radiation patterns. Therefore, it has been suggested that the divergence angle of radar could be defined based on the fraction of total radiation energy, which is 91% in this study.

5.3 Plot-level forest attribute estimation

The previous studies have evaluated terrain elevation, canopy top elevation, and the Ku-band radar signal penetration through canopy in boreal forests. They all focused on single waveforms and used the corresponding LiDAR data or DTM as reference. In Publication V, not only canopy height, but also DBH, stem volume, and AGB were estimated at plot level using manually collected field data as the reference.

As introduced in Section 4.4, a total of 60 plot-level canopy features were used when applying the RF method for the estimation. For each forest attribute estimation, the importance of those features was calculated and the 15 highest-ranked features were used for the prediction. Overall, across all the top 15 important predictors for the four attributes, the plot-level feature mean values accounted for more than half of the 15 most important predictors of canopy height, stem volume, and AGB, while the standard deviations of the features played a greater role for the DBH estimation. When further checking the features, the mean values of the height percentiles of the canopy (M_HP_C) played an important role in the estimation, especially the heights with cumulative power of 100% and 90% (M_HP_C1, M_HP_C2). These two features have scores greater than 0.5 for almost all predicted attributes, except for AGB, where M_HP_C2 has a score of 0.48, ranking second. Based on the definition of M_HP_C, the M_HP_C1 is the same as the canopy height, which by nature is important for the forest attribute estimation. Besides, the energy percentiles of the canopy (EP_C) and the height of the position having the strongest reflected signal strength (H_Rmax_C) also played a role in prediction of all four attributes. The full list of the top 15 important features is provided in Table 5 of Publication V.

Through the reference data, the mean height and AGB of the studied 55 plots ranged from 12.72 to 31.35 m and 27.00 to 225.87 Mg/ha, respectively. The four forest attributes (H_g, DBH_g, V, and AGB) at plot level were estimated using the Tomoradar measurements from the 55 plots and compared to the manual

reference. The estimation accuracies are shown in Figure 9 and Table 4. According to Table 4, the estimation biases for H_g, DBH_g, V, and AGB are -0.17 m, -0.38 cm, -1.93 m^3/ha, and -1.36 Mg/ha, respectively, while the corresponding RMSEs are 2.17 m, 4.50 cm, 60.30 m^3/ha, and 28.04 Mg/ha. The R^2 values of linear fitting for the four attributes are 0.75, 0.63, 0.67 and 0.63, respectively. Additionally, the maximum canopy heights of the plots were estimated from Tomoradar data and compared to the manual reference, resulting in a bias and $bias_{rel}$ of -1.44 m and -5.23% with RMSE and $RMSE_{rel}$ of 2.19 m and 7.95%, and an R^2 of 0.89.

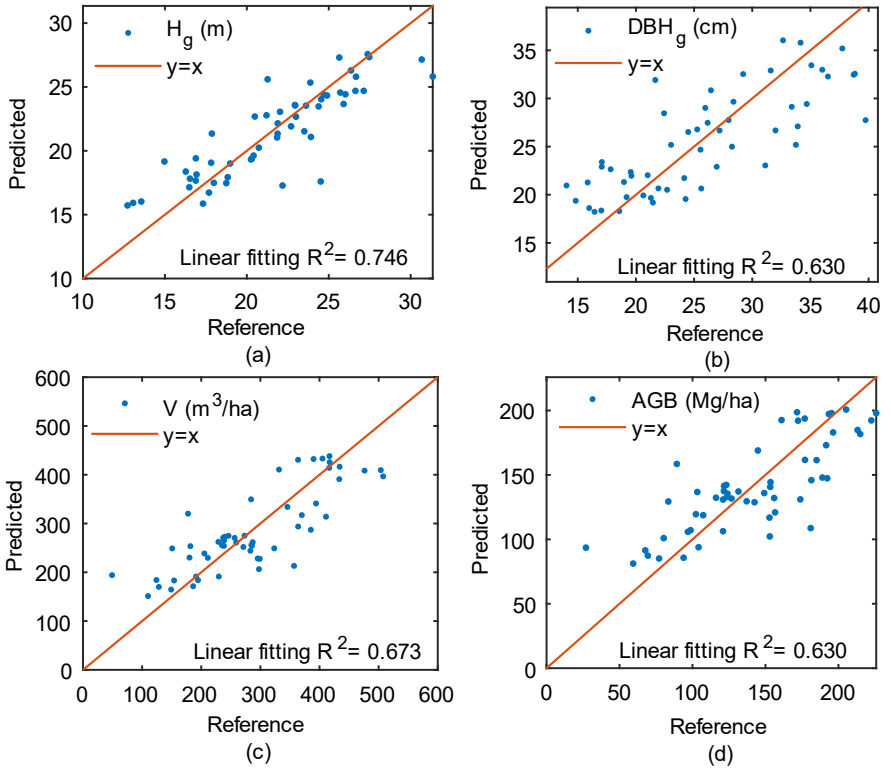


Figure 9 Scatter plots of predicted versus reference values for the four attributes (a) H_g, (b) DBH_g, (c) V, and (d) AGB. The coefficients of determination (R^2) from the linear fits, shown in each subplot, ranged from 0.630 to 0.746, with the highest value obtained for H_g (Publication V).

Table 4 Accuracy of plot-level forest attribute estimation based on mean and standard deviation of the features derived from Tomoradar waveforms. The 15 most important features were used (N = 55) (Publication V).

	Bias	$Bias_{rel}$ (%)	RMSE	$RMSE_{rel}$ (%)	R^2
H_g (m)	-0.17	-0.77	2.17	10.04	0.75
DBH_g (cm)	-0.38	-1.45	4.50	17.25	0.63
V (m^3/ha)	-1.93	-0.68	60.30	21.11	0.67
AGB (Mg/ha)	-1.36	-0.96	28.04	19.75	0.63

Theoretically, the profiling radar tends to underestimate the canopy height because of the penetration feature. However, since the applied RF method corrected the underestimation, the bias of mean canopy height (H_g) estimated using RF method was mainly caused by the prediction error rather than the penetration. When it comes to the plot-level maximum canopy height (close to the dominant height), the estimation bias from Tomoradar data was -1.44 m with a strong correlation to the reference. Compared to the mean canopy height, the maximum canopy height was derived directly from the original Tomoradar waveforms, and therefore contained the effects of penetration. Besides, there are three additional possible reasons for the underestimation: (1) the detected area of Tomoradar did not completely overlap with the area covered by the reference data. Tomoradar illuminated only portions of the plots and may have missed the tallest trees within the plots; (2) the backscattered data received by Tomoradar represented the combined response from the entire illuminated area rather than from individual trees; therefore, it was more strongly related to mean canopy height than to dominant height; (3) the threshold value used to determine the canopy height from Tomoradar waveforms was derived for the mean canopy height, not calibrated for the dominant height. However, the R^2 of the estimation still reached 0.89 with these challenges, indicating that the Ku-band profiling radar could accurately detect the maximum canopy height in boreal homogeneous forest, especially after appropriate calibration of the derived parameters.

A similar study was conducted by Hyyppä and Hallikainen (1996) using HUTSCAT data to estimate plot-level mean canopy height, stem volume, and dominant height, reporting RMSEs of 1.23 m, 44.9 m^3/ha, and 1.28 m, respectively. Compared with the HUTSCAT results, the Tomoradar-based random forest model achieved comparable accuracy for stem volume but yielded larger errors for mean canopy height and dominant height. Although Tomoradar provides a higher range resolution (0.15 m) than HUTSCAT (0.65 m), HUTSCAT likely offers a narrower antenna beam (HPBW < 5° versus ~6° for Tomoradar), which corresponds to a smaller beam footprint (i.e., finer lateral resolution) for a given observation range and can improve sensitivity to localized canopy-top features. In addition, potential antenna side lobe contributions in the Tomoradar system may introduce extra scattering from adjacent trees or terrain, increasing estimation uncertainty. Finally, despite the methodological similarity between the two profiling radar systems, differences in system configuration and operating frequency band, as well as data acquisition settings (e.g., observation range/geometry, plot size, and survey design), limit direct one-to-one performance comparisons.

Additionally, several forest inventory studies have been carried out over the Evo test site using various remote sensing datasets and the same field reference data. Karila et al. (2015) estimated forest attributes from German TanDEM-X (TDX) and TerraSAR-X (TSX) X-band data using 3D SAR techniques: TDX provides canopy-surface elevation primarily via single-pass InSAR (phase-based), whereas TSX was

processed using stereo radargrammetry (stereo measurement from SAR image geometry). In both cases, the SAR-derived elevations were converted to canopy heights using an external (ALS-based) DTM and then summarized into plot-level 3D height metrics for random forest (RF) modeling. Wittke et al. (2019) extended this comparison by including ALS (~17 pulses/m^2) and WorldView-2 (WV-2) stereo photogrammetry as additional 3D sources, and multitemporal Sentinel-2A as a 2D baseline based on spectral bands/indices (10/20/60 m native GSD, typically resampled to 10 m) without explicit height retrieval.

Overall, TDX InSAR, TSX stereo radargrammetry, ALS, and WV-2 stereo photogrammetry can be regarded as 3D/height-driven approaches, conceptually closer to Tomoradar, which extracts vertical structure from Ku-band profiling waveforms, whereas Sentinel-2 represents a 2D spectral approach. In many RF-based forest attribute models (including this study), canopy height is among the most influential predictors, which helps explain why methods providing reliable height or vertical-structure information often achieve higher accuracies. In our comparison, Tomoradar produced lower accuracies than ALS and WV-2, but higher accuracies than TSX and Sentinel-2A, with performance comparable to TDX. ALS and WV-2 stereo photogrammetry performed best because they provide detailed and spatially consistent plot-level 3D information (dense ALS sampling and high-resolution optical stereo matching). Although TSX stereo radargrammetry can generate 3D elevation points, its estimation accuracy can be limited by errors in matching corresponding features between the images in each stereo pair, with speckle further increasing the matching uncertainty, while Sentinel-2 has no direct height-sensing capability and relies on reflectance-based indices and multitemporal features for forest attribute estimation. The similarity between Tomoradar and TDX is consistent with both providing robust height-related information (waveform-derived vertical structure versus phase-based elevation retrieval). Further details of multi-sensor comparison for forest attribute estimation are provided in Publication V.

5.4 Scientific and practical implications

Generally, the studies in this dissertation contributed to the understanding of Ku-band profiling radar signal penetration through the forest canopy, particularly in boreal forests. This dissertation also demonstrated that helicopter-based Ku-band profiling radar can detect and estimate the terrain elevation, canopy top elevation, and other forest attributes with reasonable accuracy, offering a complementary source of structural information for forest inventory-related research. These results enhance the understanding of Ku-band radar interaction with boreal forest vegetation and demonstrate the feasibility of using airborne Ku-band profiling radar for forest structure and biomass-related studies. They also

provide empirical support for future Ku-band signal modeling and validation, as well as for multi-sensor forest inventory approaches involving LiDAR or radar data.

One of the core scientific implications is the ability of Ku-band signals to penetrate the forest canopy and interact with the ground surface. As discussed in Section 1.1, the longer wavelength P-, L-, or C-band radar signals are more commonly used in research related to forest inventory, and Ku-band signal was assumed to be mainly backscattered from the canopy surface due to the shorter wavelength. Thus, only limited studies have been conducted using Ku band, and the penetration capability of Ku-band signals within the forest canopy is underexplored. The results of Publication I indicate that Ku-band profiling radar can detect ground returns in boreal forest under suitable acquisition conditions, supporting the derivation of terrain information. When combined with canopy top detection, this capability can support canopy height estimation and reduce reliance on external terrain models.

Another key implication is that this dissertation provides high-quality empirical reference information for understanding Ku-band radar interaction with boreal forest canopies. In Publications II–IV, aided by LiDAR data, the vertical distribution of Ku-band backscatter, canopy penetration, and the effective beamwidth of the profiling radar were examined. The study proposed a reliable method to define the effective beamwidth of Ku-band profiling radar, offering a reference for future radar studies in forests. These results help clarify how short-wavelength radar signals interact with canopy elements and ground surfaces under boreal forest conditions. The comparison with LiDAR data also demonstrates the value of using independent three-dimensional reference data to interpret radar waveforms and to support future radar signal modeling and validation.

The penetration in forest canopy and resulting vertical profiles demonstrate the capability of Ku-band signals in measuring forest vertical structure, thereby supporting the accurate estimation of forest attributes, such as canopy height, mean DBH, stem volume, and AGB. The application of random forest method identified the most important radar-derived features contributing to forest attributes prediction, producing promising results, suggesting that other machine learning approaches could also be explored in future radar-based forest studies. Although the results are specific to the studied boreal forest conditions and the helicopter-borne Tomoradar configuration, the achieved accuracies indicate the potential of high-resolution Ku-band profiling radar as a complementary source of forest structural information.

From a practical perspective, the successful implementation of Tomoradar supports the further development of lightweight airborne profiling radar systems for forest applications. Although the measurements in this dissertation were conducted from a helicopter, the system was originally designed with UAV deployment in mind. Therefore, the findings provide technical and methodological support for future low-altitude radar measurements from lighter platforms,

particularly where flexible data acquisition, repeated flight lines, and integration with LiDAR or other remote sensing data are required.

Overall, these findings suggest that the current Tomoradar system is a complementary research instrument, rather than a replacement for established forest inventory methods. Field measurements provide direct reference attributes, LiDAR supplies detailed canopy and terrain geometry, and imaging SAR offers broad-area observations. Tomoradar adds finely detailed range-resolved Ku-band backscatter profiles to characterize canopy and ground scattering along selected flight paths. Currently, Tomoradar's most practical role is to support targeted experiments, radar-model development, and multi-sensor studies that supplement LiDAR- or SAR-based forest analyses, rather than to conduct independent comprehensive forest surveys.

5.5 Limitations and future research

This section outlines the key limitations encountered during this study and presents potential directions for future research based on the findings and challenges reported across the studies.

Through the estimation of forest canopy and ground elevation using Tomoradar data in Publication I, it was found that it is difficult for the Tomoradar system to detect narrow canopy gaps. Due to the radar's inherent feature that each Tomoradar waveform spatially integrates backscatter contributions from the antenna footprint, narrow gaps between tree crowns may be masked by returns from surrounding canopy elements, resulting in an overestimation of canopy continuity. Additionally, the side lobes in the radar beam introduced spurious returns in the vertical profiles, further obscuring small canopy gaps and complicating the vertical forest canopy structure analysis. This limitation suggests that a Ku-band profiling radar such as Tomoradar is more accurate in detecting forest canopies in sparser forests than in denser forests.

Moreover, platform instability presented a challenge. Whenever the helicopter changed directions during a field measurement flight, the attitude of the helicopter varied, leading to deviations from the expected nadir-looking geometry and thus affecting the effective beam pointing direction. As a result, the actual footprint shape, footprint size, and illuminated area may deviate from the nominal nadir-looking footprint. For the terrain elevation estimation, this issue was addressed by integrating the helicopter position and attitude information (pitch, roll, and yaw angles) from the onboard IMU, which improved the estimation accuracy. However, when comparing the forest canopy structure and top elevation with ALS data, the corresponding ALS data were selected from the constructed cylinder/cone based on the ground intersection and footprint size, which is different from the actual spatial covered area, thus introducing comparison differences. This could be improved by refining the selection area of corresponding reference data in future studies.

In the estimation of biomass in Publication V, there are mismatches between the radar data and the reference data, mainly caused by differences in their spatial coverage and acquisition time. The reference data were collected from an area that is larger and spatially different from the Tomoradar data, which may lead to a mismatch in study area. The reference sample plots were 32 m × 32 m in size, and the helicopter with Tomoradar system did not always fly exactly horizontally or vertically from one side of the plot to the other. In addition, Tomoradar has a ground footprint diameter of 6–10 m; thus, the measurements covered only part of each plot. Overall, this partial plot coverage may have increased the plot-to-footprint mismatch, thus degrading plot-level predictors, especially for the maximum canopy height estimation.

Since Tomoradar measurements were acquired in 2016, while the field reference data were collected in 2014, there was a two-year temporal mismatch. Forest growth, tree mortality, or harvesting during this interval may have altered canopy height, stem volume, and AGB, introducing systematic or plot-specific differences between the forest attributes derived from the radar data and the reference values. Available forest management records indicated no large-scale logging or other systematic management operations during this period, and the study area was dominated by mature stands, for which structural changes caused by growth over two years were expected to be relatively small. On this basis, the temporal mismatch was expected to have only a limited effect and was considered acceptable within the scope of this feasibility study. Although plot-level changes were not explicitly quantified, they may have some impacts on the prediction errors, but were not expected to affect the overall conclusions.

Furthermore, the distribution of tree species in the forest plot is uneven. This imbalance may have made the random forest model more representative of dominant species (such as pine and spruce), while reducing its reliability in less common or mixed-species stands. Additionally, forest attributes (stem volume, AGB) were also unevenly distributed among different tree species groups (Publication V). These tree species distribution imbalances also complicate the study of Ku-band profiling radar capability in estimating forest attributes for different tree species. To evaluate radar capabilities and conduct tree species-related studies more accurately, in future studies, the flight campaign paths could be designed to better match known reference plots and sample a more balanced range of tree species.

One motivation for developing Tomoradar was to obtain experimental Ku-band waveform observations for improving the understanding of radar signal interaction with forest canopies. The LiDAR-assisted analyses in this dissertation provide empirical information on Ku-band signals penetration, canopy and ground backscatter, and effective beamwidth under boreal forest conditions. These findings may support future modeling of Ku-band backscatter in forest and the interpretation of airborne or satellite SAR observations. However, using

Tomoradar-derived models or forest attributes to support the interpretation of SAR observations would require consideration of differences in frequency, observation geometry, spatial resolution, and spatial coverage. Among existing SAR techniques, TomoSAR is particularly relevant for comparison with profiling radar because both methods provide vertical profiles of radar backscatter, although through fundamentally different acquisition and processing approaches.

Tomoradar has two related spatial limitations, namely, measurements are acquired only along flight trajectories, and each waveform integrates backscatter over a finite antenna footprint. Although the system provides a range resolution of approximately 0.15 m along the radar line of sight, it cannot separate the horizontal origins of the backscatter contributions within a waveform. Publication II indicated that an effective angular extent of approximately 20° was required to encompass more than 95% of the transmitted main-lobe energy, demonstrating that the spatial support of a waveform can be considerably wider than the nominal 3-dB footprint, thereby reinforcing the difficulty of associating profile features with individual trees or crowns. In addition, mapping a large area with Tomoradar would require closely spaced parallel flight lines, increasing acquisition time and cost, although processing the individual waveforms is relatively straightforward. In comparison, TomoSAR coherently combines repeated SAR acquisitions of roughly the same swath from different baselines and reconstructs a vertical reflectivity profile for each of the many range–azimuth resolution cells throughout the swath. This provides height-resolved measurements across the imaged area rather than only along flight trajectories. While this mapping capability requires multiple phase-coherent acquisitions, suitable baseline geometry, accurate phase calibration, and substantially more complex processing; in addition, its elevation resolution depends on the acquisition configuration and temporal coherence.

Tomoradar and TomoSAR therefore have complementary roles: the former provides fine range-resolved observations at selected locations for investigating scattering processes and supplying reference information, while the latter provides spatially extensive three-dimensional mapping. Because differences in wavelengths, observation geometries, and spatial resolutions make direct comparison difficult, Tomoradar measurements should be treated as complementary radar reference information rather than as direct ground truth for TomoSAR. Future studies should therefore investigate feature- or model-level relationships rather than directly fusing the raw vertical profiles. Comparisons could focus on canopy height, ground-canopy separation, vertical distribution metrics, and biomass related estimates after adjusting the datasets to represent comparable ground areas. Tomoradar profiles could thereby support the interpretation and evaluation of TomoSAR-derived vertical structure. The dedicated tomographic phase of ESA's Biomass mission provides a specific opportunity for such research by enabling comparisons between airborne Ku-band profiles and spaceborne P-band tomographic structure and biomass products.

Besides those limitations that can be improved in future studies, there are also other potential directions for future study. One interesting study is a more comprehensive exploration of Tomoradar's capability under different polarization modes. Although the radar is capable of capturing fully polarimetric data, only the data collected in the HH polarization mode were used in the studies. Investigating the utility of other channels (e.g., VV, HV, VH) may reveal new relationships between Ku-band backscattering and forest structural attributes.

Another point related to the study data is that the single flight campaign data used in the study lack temporal variability in vegetation structure or environmental conditions. Future campaigns should consider multi-temporal acquisitions to assess how radar backscatter and structural metrics vary across different forest canopy shapes, and also enable forest change detection.

Another promising direction is the deeper integration of Tomoradar data with LiDAR observations. In this dissertation, LiDAR data were mainly used as reference or supporting data for evaluating canopy top elevation, canopy gaps, and Ku-band penetration. Future studies could move beyond validation and combine radar- and LiDAR-derived features directly in forest attribute modeling. LiDAR can provide accurate geometric information on canopy surface, canopy gaps, and terrain elevation, whereas Tomoradar waveforms provide complementary information on Ku-band backscatter distribution within the canopy. Such feature-level or model-level fusion may improve the estimation of forest structure and biomass, especially in stands where either sensor alone has limitations.

Finally, future research could also consider improvements in radar hardware design and acquisition geometry. As mentioned above, the current Tomoradar system observes the forest mainly in a nadir-looking profiling configuration and collects waveform data along the flight trajectory. Therefore, the spatial coverage is limited to a narrow footprint of several meters, although the system provides effective vertical profiling information. To improve area coverage and facilitate comparison with spatially continuous remote sensing products, future system development could explore wider spatial sampling strategies, for example through mechanical scanning or multi-angle acquisition designs. Mechanical scanning would be a relatively direct extension of the profiling concept, although it would likely provide coarser 2D mapping than imaging radar systems. Alternatively, a future Ku-band helicopter-borne or UAV-borne imaging radar could be developed based on related hardware concepts, but this would require SAR-specific system design, precise motion compensation, and dedicated image formation processing. Such development would represent a separate research direction rather than a direct extension of the profiling radar methods studied in this dissertation.

In addition to improving the radar hardware and acquisition geometry, adapting the system to different airborne platforms is another important direction for future research. Helicopter-based field measurements are expensive and involve greater operational and safety constraints, especially for low-altitude forest inventory.

Additionally, helicopter vibration and varying attitude can affect radar signal quality, and the flight paths are difficult to repeat precisely, limiting temporal studies. UAV, as a popular platform for many different applications, has been developed rapidly in recent years (Guimarães et al., 2020; Telli et al., 2023). The relatively low cost and operational flexibility of UAVs make them suitable for areas that are hard to reach. Moreover, their stable autopilot systems enable the repetition of identical flight trajectories for multi-temporal studies and other repeated-acquisition experiments. With rapid advancements in UAV technology, particularly in extended flight duration and increased payload capacity, drone-based radar systems have been developed (Kaniewski et al., 2019; Ruiz-Carregal et al., 2024). Consequently, the development of a lighter Ku-band profiling radar for drone platforms is a highly feasible and logical next step. Such a platform would preserve the vertical profiling capability demonstrated in this dissertation while improving the flexibility, repeatability, and cost-efficiency of local forest inventory campaigns.

Together, these directions suggest that future Ku-band profiling radar research should focus on more integrated, repeatable, and scalable forest measurements, supported by improved sensor design, multi-sensor fusion, and UAV-based acquisition.

6 Conclusions

This dissertation evaluated the feasibility of using helicopter-borne Ku-band profiling radar (Tomoradar) for boreal forest inventory. The study addressed three connected tasks: retrieving ground and canopy elevations from individual radar waveforms, characterizing Ku-band signal penetration and vertical backscatter distribution using LiDAR reference data, and estimating plot-level forest attributes from radar-derived waveform features.

The results demonstrate that Ku-band profiling radar can retrieve both topography and canopy top elevation across varying boreal forest conditions. Under stable nadir-looking acquisition geometry, terrain elevation was estimated with an average RMSE of approximately 0.40 m. Canopy top elevation was estimated with an average RMSE of approximately 0.80 m after removing outliers mainly associated with canopy gaps and LiDAR noise. These results demonstrate that Tomoradar waveforms contain usable information from both canopy and ground returns, supporting derivation of basic vertical structure metrics from Ku-band profiling radar measurements.

The dissertation also provides empirical evidence that Ku-band signals can produce detectable subcanopy and ground returns under the studied boreal forest conditions. The Backscattered Energy Ratio of Canopy-to-Total (BERCT) was introduced to describe the distribution of radar backscattered energy between canopy and ground components. The strong correlation between BERCT and LiDAR-derived canopy fraction ($r = 0.84$) indicates that the vertical distribution of Ku-band backscatter is closely related to canopy density and gap structure. Furthermore, the analyses reveal that canopy structure and radar footprint definition affect the interpretation of Tomoradar waveforms, emphasizing the importance of accurate georeferencing and effective beamwidth characterization in profiling radar forest applications.

At plot level, Tomoradar-derived waveform features successfully estimated basal-area-weighted mean height, basal-area-weighted mean DBH, stem volume, and above-ground biomass using random forest regression. The corresponding relative RMSEs were 10.04%, 17.25%, 21.11%, and 19.75%, with R^2 values of 0.75, 0.63, 0.67, and 0.63, respectively. Height-related waveform metrics, especially canopy height and power-percentile heights, were among the most important predictors, confirming that the biomass estimation capability of Tomoradar is primarily linked to its ability to capture forest vertical structure.

Overall, this dissertation demonstrates that compact Ku-band profiling radar can serve as a promising complementary research tool for ground detection, canopy structure characterization, signal penetration analysis, and plot-level forest attribute estimation in boreal forests. Future work should investigate the effects of profiling radar polarization mode, assess the potential of UAV-mounted platforms to improve cost efficiency and flexibility, and explore multi-sensor data fusion to further improve forest attribute estimation.

References

Aghababaei, H., & Ferraioli, G. (2025). TomoSAR from Theory to Practice – Overview of the Advancements and Challenges. *IGARSS 2025 - 2025 IEEE International Geoscience and Remote Sensing Symposium*, Brisbane, Australia, pp. 504-507. https://doi.org/10.1109/igarss55030.2025.11242958

Aghababaei, H., Ferraioli, G., Ferro-Famil, L., Huang, Y., Mariotti d'Alessandro, M., ..., Tebaldini, S. (2020). Forest SAR Tomography: Principles and Applications. *IEEE Geoscience and Remote Sensing Magazine*, *8*(2), 30-45. https://doi.org/10.1109/mgrs.2019.2963093

Antonova, S., Thiel, C., Höfle, B., Anders, K., Helm, V., ..., Boike, J. (2019). Estimating tree height from TanDEM-X data at the northwestern Canadian treeline. *Remote Sensing of Environment*, *231*, 111251. https://doi.org/10.1016/j.rse.2019.111251

Askne, J., Fransson, J., Santoro, M., Soja, M., & Ulander, L. (2013). Model-Based Biomass Estimation of a Hemi-Boreal Forest from Multitemporal TanDEM-X Acquisitions. *Remote Sensing*, *5*(11), 5574-5597. https://doi.org/10.3390/rs5115574

Askne, J., & Santoro, M. (2012). Experiences in Boreal Forest Stem Volume Estimation from Multitemporal C-Band InSAR. In I. Padron (Ed.), *Recent Interferometry Applications in Topography and Astronomy*. Intechopen. https://doi.org/10.5772/35102

Astrup, R., Bernier, P. Y., Genet, H., Lutz, D. A., & Bright, R. M. (2018). A sensible climate solution for the boreal forest. *Nature Climate Change*, *8*(1), 11-12. https://doi.org/10.1038/s41558-017-0043-3

Axelsson, S. R. J. (1993). Three-band FMCW-radar for scatterometry measurements and surface profiling. *Proceedings of IGARSS '93 - IEEE International Geoscience and Remote Sensing Symposium*, pp. 1644-1647. https://doi.org/10.1109/igarss.1993.322445

Axelsson, S. R. J. (1995). Radar profiling above pine forests. *1995 International Geoscience and Remote Sensing Symposium, IGARSS '95. Quantitative Remote Sensing for Science and Applications*, pp. 284-288. https://doi.org/10.1109/igarss.1995.520260

Axelsson, S. R. J., Eriksson, M., & Halldin, S. (1999). Tree-heights derived from radar profiles over boreal forests. *Agricultural and Forest Meteorology*, *98-99*, 427-435. https://doi.org/10.1016/s0168-1923(99)00113-6

Bernard, R., Frezal, M. E., Vidal-Madjar, D., Guyon, D., & Riom, J. (1987). Nadir looking airborne radar and possible applications to forestry. *Remote Sensing of Environment*, *21*(3), 297-309. https://doi.org/10.1016/0034-4257(87)90014-9

Bernard, R., Vidal-Madjar, D., Baudin, F., & Laurent, G. (1986). Data Processing and Calibration for an Airborne Scatterometer. *IEEE Transactions on*

Geoscience and Remote Sensing, *GE-24*(5), 709-716. https://doi.org/10.1109/tgrs.1986.289618
Blomberg, E., Ulander, L. M. H., Tebaldini, S., & Ferro-Famil, L. (2021). Evaluating P-Band TomoSAR for Biomass Retrieval in Boreal Forest. *IEEE Transactions on Geoscience and Remote Sensing*, *59*(5), 3793-3804. https://doi.org/10.1109/tgrs.2020.3020775
Borsah, A. A., Nazeer, M., & Wong, M. S. (2023). LIDAR-Based Forest Biomass Remote Sensing: A Review of Metrics, Methods, and Assessment Criteria for the Selection of Allometric Equations. *Forests*, *14*(10), 2095. https://doi.org/10.3390/f14102095
Boudreau, J., Nelson, R., Margolis, H., Beaudoin, A., Guindon, L., & Kimes, D. (2008). Regional aboveground forest biomass using airborne and spaceborne LiDAR in Québec. *Remote Sensing of Environment*, *112*(10), 3876-3890. https://doi.org/10.1016/j.rse.2008.06.003
Brockerhoff, E. G., Barbaro, L., Castagneyrol, B., Forrester, D. I., Gardiner, B., ..., Jactel, H. (2017). Forest biodiversity, ecosystem functioning and the provision of ecosystem services. *Biodiversity and Conservation*, *26*(13), 3005-3035. https://doi.org/10.1007/s10531-017-1453-2
Burger, J. A. (2009). Management effects on growth, production and sustainability of managed forest ecosystems: Past trends and future directions. *Forest Ecology and Management*, *258*(10), 2335-2346. https://doi.org/10.1016/j.foreco.2009.03.015
Cao, L., Coops, N., Hermosilla, T., Innes, J., Dai, J., & She, G. (2014). Using Small-Footprint Discrete and Full-Waveform Airborne LiDAR Metrics to Estimate Total Biomass and Biomass Components in Subtropical Forests. *Remote Sensing*, *6*(8), 7110-7135. https://doi.org/10.3390/rs6087110
Cartus, O., Santoro, M., & Kellndorfer, J. (2012). Mapping forest aboveground biomass in the Northeastern United States with ALOS PALSAR dual-polarization L-band. *Remote Sensing of Environment*, *124*, 466-478. https://doi.org/10.1016/j.rse.2012.05.029
Chan, Y. K., & Koo, V. C. (2008). An Introduction to Synthetic Aperture Radar (SAR). *Progress In Electromagnetics Research B*, *2*, 27-60. https://doi.org/10.2528/pierb07110101
Chaudhary, A., Burivalova, Z., Koh, L. P., & Hellweg, S. (2016). Impact of Forest Management on Species Richness: Global Meta-Analysis and Economic Trade-Offs. *Scientific Reports*, *6*, 23954. https://doi.org/10.1038/srep23954
Chen, H., Cloude, S. R., & White, J. C. (2021). Using GEDI Waveforms for Improved TanDEM-X Forest Height Mapping: A Combined SINC + Legendre Approach. *Remote Sensing*, *13*(15), 2882. https://doi.org/10.3390/rs13152882
Chen, L., Wang, Y., Ren, C., Zhang, B., & Wang, Z. (2019). Optimal Combination of Predictors and Algorithms for Forest Above-Ground Biomass Mapping from Sentinel and SRTM Data. *Remote Sensing*, *11*(4), 414. https://doi.org/10.3390/rs11040414
Chen, Y. W., Hakala, T., Karjalainen, M., Feng, Z. Y., Tang, J., ..., Hyyppä, J. (2017). UAV-Borne Profiling Radar for Forest Research. *Remote Sensing*, *9*(1), 58. https://doi.org/10.3390/rs9010058
Chi, H., Sun, G., Huang, J., Guo, Z., Ni, W., & Fu, A. (2015). National Forest Aboveground Biomass Mapping from ICESat/GLAS Data and MODIS

Imagery in China. *Remote Sensing*, *7*(5), 5534-5564. https://doi.org/10.3390/rs70505534
Comite, D., Pierdicca, N., Clarizia, M. P., Pascual, D., De Felice Proia, G., ..., Benveniste, J. (2021). Estimating Biomass From Sentinel-3 Altimetry Data: A Sensitivity Analysis. *2021 IEEE International Geoscience and Remote Sensing Symposium IGARSS*, pp. 2389-2392. https://doi.org/10.1109/igarss47720.2021.9554308
Coops, N. C., Tompalski, P., Goodbody, T. R. H., Queinnec, M., Luther, J. E., ..., Hermosilla, T. (2021). Modelling lidar-derived estimates of forest attributes over space and time: A review of approaches and future trends. *Remote Sensing of Environment*, *260*, 112477. https://doi.org/10.1016/j.rse.2021.112477
Cosimo, L. H. E., Lopez, J. G., Lindberg, E., & Huo, L. (2026). Linking hyperspectral remote sensing and tree hydraulic functioning for pre-emergence detection of bark beetle infestations. *ISPRS Journal of Photogrammetry and Remote Sensing*, *237*, 628-651. https://doi.org/10.1016/j.isprsjprs.2026.04.038
Dubayah, R., Blair, J. B., Goetz, S., Fatoyinbo, L., Hansen, M., ..., Silva, C. (2020). The Global Ecosystem Dynamics Investigation: High-resolution laser ranging of the Earth's forests and topography. *Science of Remote Sensing*, *1*, 100002. https://doi.org/10.1016/j.srs.2020.100002
Dube, T., & Mutanga, O. (2015). Evaluating the utility of the medium-spatial resolution Landsat 8 multispectral sensor in quantifying aboveground biomass in uMgeni catchment, South Africa. *ISPRS Journal of Photogrammetry and Remote Sensing*, *101*, 36-46. https://doi.org/10.1016/j.isprsjprs.2014.11.001
Eckert, S. (2012). Improved Forest Biomass and Carbon Estimations Using Texture Measures from WorldView-2 Satellite Data. *Remote Sensing*, *4*(4), 810-829. https://doi.org/10.3390/rs4040810
Englhart, S., Keuck, V., & Siegert, F. (2011). Aboveground biomass retrieval in tropical forests — The potential of combined X- and L-band SAR data use. *Remote Sensing of Environment*, *115*(5), 1260-1271. https://doi.org/10.1016/j.rse.2011.01.008
ESA. (2025a, Jul 3, 2025). *Biomass (Earth Explorer 7)*. eoPortal. Retrieved March 11, 2026 from https://www.eoportal.org/satellite-missions/biomass#eop-quick-facts-section
ESA. (2025b, Nov 14, 2025). *ROSE-L (Radar Observing System for Europe in L-band)*. eoPortal. Retrieved March 11, 2026 from https://www.eoportal.org/satellite-missions/rose-l#eop-quick-facts-section
Fassnacht, F. E., Hartig, F., Latifi, H., Berger, C., Hernández, J., ..., Koch, B. (2014). Importance of sample size, data type and prediction method for remote sensing-based estimations of aboveground forest biomass. *Remote Sensing of Environment*, *154*, 102-114. https://doi.org/10.1016/j.rse.2014.07.028
Feng, Z., Chen, Y., Hyyppä, J., Hakala, T., Zhou, H., ..., Karjalainen, M. (2018). Estimating Ground Level and Canopy Top Elevation With Airborne Microwave Profiling Radar. *IEEE Transactions on Geoscience and Remote Sensing*, *56*(4), 2283-2294. https://doi.org/10.1109/TGRS.2017.2778024
Feng, Z., Yu, X., Chen, Y., Puttonen, E., Hakala, T., ..., Hyyppä, J. (2024). Feasibility of using Ku-band helicopter-borne microwave radar for stem

volume and biomass estimation in boreal forest. *International Journal of Applied Earth Observation and Geoinformation*, *131*, 103966. https://doi.org/10.1016/j.jag.2024.103966

Fransson, J. E. S., & Israelsson, H. (1999). Estimation of stem volume in boreal forests using ERS-1 C- and JERS-1 L-band SAR data. *International Journal of Remote Sensing*, *20*(1), 123-137. https://doi.org/10.1080/014311699213640

Fransson, J. E. S., Smith, G., Askne, J., & Olsson, H. (2001). Stem volume estimation in boreal forests using ERS-1/2 coherence and SPOT XS optical data. *International Journal of Remote Sensing*, *22*(14), 2777-2791. https://doi.org/10.1080/01431160010006872

Ghasemi, N., Sahebi, M. R., & Mohammadzadeh, A. (2011). A review on biomass estimation methods using synthetic aperture radar data. *International Journal of Geomatics and Geosciences*, *1*, 776-788.

Govender, M., Chetty, K., & Bulcock, H. (2007). A review of hyperspectral remote sensing and its application in vegetation and water resource studies. *Water SA*, *33*(2), 145-151. https://doi.org/10.4314/wsa.v33i2.49049

Guimarães, N., Pádua, L., Marques, P., Silva, N., Peres, E., & Sousa, J. J. (2020). Forestry Remote Sensing from Unmanned Aerial Vehicles: A Review Focusing on the Data, Processing and Potentialities. *Remote Sensing*, *12*(6), 1046. https://doi.org/10.3390/rs12061046

Gupta, D. K., Prashar, S., Singh, S., Srivastava, P. K., & Prasad, R. (2022). Introduction to RADAR remote sensing. In P. K. Srivastava, D. K. Gupta, T. Islam, D. Han, & R. Prasad (Eds.), *Radar Remote Sensing - Applications and Challenges* (pp. 3-27). Elsevier. https://doi.org/10.1016/b978-0-12-823457-0.00018-5

Hajnsek, I., Kugler, F., Lee, S.-K., & Papathanassiou, K. P. (2009). Tropical-Forest-Parameter Estimation by Means of Pol-InSAR: The INDREX-II Campaign. *IEEE Transactions on Geoscience and Remote Sensing*, *47*(2), 481-493. https://doi.org/10.1109/tgrs.2008.2009437

Hallikainen, M., Hyyppä, J., Haapanen, J., Tares, T., Ahola, P., ..., Toikka, M. (1993). A helicopter-borne eight-channel ranging scatterometer for remote sensing. I. System description. *IEEE Transactions on Geoscience and Remote Sensing*, *31*(1), 161-169. https://doi.org/10.1109/36.210457

Halme, E., Pellikka, P., & Mõttus, M. (2019). Utility of hyperspectral compared to multispectral remote sensing data in estimating forest biomass and structure variables in Finnish boreal forest. *International Journal of Applied Earth Observation and Geoinformation*, *83*, 101942. https://doi.org/10.1016/j.jag.2019.101942

Ho Tong Minh, D., Le Toan, T., Rocca, F., Tebaldini, S., Villard, L., ..., Chave, J. (2016). SAR tomography for the retrieval of forest biomass and height: Cross-validation at two tropical forest sites in French Guiana. *Remote Sensing of Environment*, *175*, 138-147. https://doi.org/10.1016/j.rse.2015.12.037

Ho Tong Minh, D., Ngo, Y.-N., & Lê, T. T. (2021). Potential of P-Band SAR Tomography in Forest Type Classification. *Remote Sensing*, *13*(4), 696. https://doi.org/10.3390/rs13040696

Huang, W., Sun, G., Ni, W., Zhang, Z., & Dubayah, R. (2015). Sensitivity of Multi-Source SAR Backscatter to Changes in Forest Aboveground Biomass. *Remote Sensing*, *7*(8), 9587-9609. https://doi.org/10.3390/rs70809587

Hyyppä, E., Kukko, A., Kaijaluoto, R., White, J. C., Wulder, M. A., ..., Hyyppä, J. (2020a). Accurate derivation of stem curve and volume using backpack mobile laser scanning. *ISPRS Journal of Photogrammetry and Remote Sensing*, *161*, 246-262. https://doi.org/10.1016/j.isprsjprs.2020.01.018

Hyyppä, E., Yu, X., Kaartinen, H., Hakala, T., Kukko, A., ..., Hyyppä, J. (2020b). Comparison of Backpack, Handheld, Under-Canopy UAV, and Above-Canopy UAV Laser Scanning for Field Reference Data Collection in Boreal Forests. *Remote Sensing*, *12*(20), 3327. https://doi.org/10.3390/rs12203327

Hyyppä, J., & Hallikainen, M. (1993). A helicopter-borne eight-channel ranging scatterometer for remote sensing. II. Forest inventory. *IEEE Transactions on Geoscience and Remote Sensing*, *31*(1), 170-179. https://doi.org/10.1109/36.210458

Hyyppä, J., & Hallikainen, M. (1996). Applicability of airborne profiling radar to forest inventory. *Remote Sensing of Environment*, *57*(1), 39-57. https://doi.org/10.1016/0034-4257(95)00254-5

Hyyppä, J., Hyyppä, H., Inkinen, M., Engdahl, M., Linko, S., & Zhu, Y.-H. (2000). Accuracy comparison of various remote sensing data sources in the retrieval of forest stand attributes. *Forest Ecology and Management*, *128*(1-2), 109-120. https://doi.org/10.1016/s0378-1127(99)00278-9

Hyyppä, J., Hyyppä, H., Leckie, D., Gougeon, F., Yu, X., & Maltamo, M. (2008). Review of methods of small-footprint airborne laser scanning for extracting forest inventory data in boreal forests. *International Journal of Remote Sensing*, *29*(5), 1339-1366. https://doi.org/10.1080/01431160701736489

Hyyppä, J., & Inkinen, M. (1999). Detecting and estimating attributes for single trees using laser scanner. *The Photogrammetric Journal of Finland*, *16*(2), 27-42.

Hyyppä, J., Kelle, O., Lehikoinen, M., & Inkinen, M. (2001). A segmentation-based method to retrieve stem volume estimates from 3-D tree height models produced by laser scanners. *IEEE Transactions on Geoscience and Remote Sensing*, *39*(5), 969-975. https://doi.org/10.1109/36.921414

Hyyppä, J., Pulliainen, J., Hallikainen, M., & Saatsi, A. (1997). Radar-derived standwise forest inventory. *IEEE Transactions on Geoscience and Remote Sensing*, *35*(2), 392-404. https://doi.org/10.1109/36.563278

Hyyppä, J., Yu, X., Hakala, T., Kaartinen, H., Kukko, A., ..., Hyyppä, E. (2021). Under-Canopy UAV Laser Scanning Providing Canopy Height and Stem Volume Accurately. *Forests*, *12*(7), 856. https://doi.org/10.3390/f12070856

Hyyppä, J., Yu, X., Hyyppä, H., Vastaranta, M., Holopainen, M., ..., Alho, P. (2012). Advances in Forest Inventory Using Airborne Laser Scanning. *Remote Sensing*, *4*(5), 1190-1207. https://doi.org/10.3390/rs4051190

Hyyppä, J., Yu, X., Karjalainen, M., Liang, X., Jaakkola, A., ..., Hyyppä, E. (2024). Remote Sensing of Forests from LiDAR and Radar. In P. S. Thenkabail (Ed.), *Remote Sensing Handbook, Volume IV: Forests, Biodiversity, Ecology, LULC, and Carbon* (2 ed., pp. 47-95). CRC Press. https://doi.org/10.1201/9781003541172-3

Islam, M. R., Jönsson, A. M., Bergkvist, J., Lagergren, F., Lindeskog, M., ..., Kljun, N. (2024). Projected effects of climate change and forest management on carbon fluxes and biomass of a boreal forest. *Agricultural and Forest Meteorology*, *349*, 109959. https://doi.org/10.1016/j.agrformet.2024.109959

Jacon, A. D., Galvão, L. S., Dalagnol, R., & dos Santos, J. R. (2021). Aboveground biomass estimates over Brazilian savannas using hyperspectral metrics and machine learning models: experiences with Hyperion/EO-1. *GIScience & Remote Sensing*, *58*(7), 1112-1129. https://doi.org/10.1080/15481603.2021.1969630

JAXA. (2024). *About Advanced Land Observing Satellite-4 "DAICHI-4" (ALOS-4)*. Retrieved August 19, 2026 from https://global.jaxa.jp/projects/sat/alos4/

Kaniewski, P., Komorniczak, W., Leśnik, C., Cyrek, J., Susek, W., ..., Łabowski, M. (2019). S-band and Ku-band SAR system development for UAV-based applications. *Metrology and Measurement Systems*, *26*(1), 53-64. https://doi.org/10.24425/mms.2019.126326

Kankare, V., Holopainen, M., Vastaranta, M., Puttonen, E., Yu, X., ..., Alho, P. (2013). Individual tree biomass estimation using terrestrial laser scanning. *ISPRS Journal of Photogrammetry and Remote Sensing*, *75*, 64-75. https://doi.org/10.1016/j.isprsjprs.2012.10.003

Karam, M. A., Amar, F., Fung, A. K., Mougin, E., Lopes, A., ..., Beaudoin, A. (1995). A microwave polarimetric scattering model for forest canopies based on vector radiative transfer theory. *Remote Sensing of Environment*, *53*(1), 16-30. https://doi.org/10.1016/0034-4257(95)00048-6

Karila, K., Karjalainen, M., Yu, X., Vastaranta, M., Holopainen, M., & Hyyppä, J. (2015). Comparison of interferometric and stereo-radargrammetric 3D metrics in mapping of forest resources. *The International Archives of the Photogrammetry, Remote Sensing and Spatial Information Sciences*, *XL-7/W3*, 425-431. https://doi.org/10.5194/isprsarchives-XL-7-W3-425-2015

Karjalainen, M., Kankare, V., Vastaranta, M., Holopainen, M., & Hyyppä, J. (2012). Prediction of plot-level forest variables using TerraSAR-X stereo SAR data. *Remote Sensing of Environment*, *117*, 338-347. https://doi.org/10.1016/j.rse.2011.10.008

Kuplich, T. M., Salvatori, V., & Curran, P. J. (2000). JERS-1/SAR backscatter and its relationship with biomass of regenerating forests. *International Journal of Remote Sensing*, *21*(12), 2513-2518. https://doi.org/10.1080/01431160050030600

Laasasenaho, J. (1982). *Taper curve and volume functions for pine, spruce and birch*. [Doctoral dissertation, University of Helsinki]. https://urn.fi/URN:ISBN:951-40-0589-9

Lara-Gómez, M. Á., Navarro-Cerrillo, R. M., Clavero Rumbao, I., & Palacios-Rodríguez, G. (2023). Comparison of Errors Produced by ABA and ITC Methods for the Estimation of Forest Inventory Attributes at Stand and Tree Level in Pinus radiata Plantations in Chile. *Remote Sensing*, *15*(6), 1544. https://doi.org/10.3390/rs15061544

Lechner, A. M., Foody, G. M., & Boyd, D. S. (2020). Applications in Remote Sensing to Forest Ecology and Management. *One Earth*, *2*(5), 405-412. https://doi.org/10.1016/j.oneear.2020.05.001

Lefsky, M. A. (2010). A global forest canopy height map from the Moderate Resolution Imaging Spectroradiometer and the Geoscience Laser Altimeter System. *Geophysical Research Letters*, *37*(15). https://doi.org/10.1029/2010gl043622

Lefsky, M. A., Harding, D. J., Keller, M., Cohen, W. B., Carabajal, C. C., ..., de Oliveira, R. (2005). Estimates of forest canopy height and aboveground

biomass using ICESat. *Geophysical Research Letters*, *32*(22). https://doi.org/10.1029/2005gl023971
Li, J., Yang, B., Yang, Y., Zhao, X., Liao, Y., ..., Dong, Z. (2023). Real-time automated forest field inventory using a compact low-cost helmet-based laser scanning system. *International Journal of Applied Earth Observation and Geoinformation*, *118*, 103299. https://doi.org/10.1016/j.jag.2023.103299
Liang, X., Hyyppä, J., Kaartinen, H., Lehtomäki, M., Pyörälä, J., ..., Wang, Y. (2018). International benchmarking of terrestrial laser scanning approaches for forest inventories. *ISPRS Journal of Photogrammetry and Remote Sensing*, *144*, 137-179. https://doi.org/10.1016/j.isprsjprs.2018.06.021
Liang, X., Kankare, V., Hyyppä, J., Wang, Y., Kukko, A., ..., Vastaranta, M. (2016). Terrestrial laser scanning in forest inventories. *ISPRS Journal of Photogrammetry and Remote Sensing*, *115*, 63-77. https://doi.org/10.1016/j.isprsjprs.2016.01.006
Liang, X., Kukko, A., Balenovic, I., Saarinen, N., Junttila, S., ..., Hyyppä, J. (2022). Close-Range Remote Sensing of Forests: The state of the art, challenges, and opportunities for systems and data acquisitions. *IEEE Geoscience and Remote Sensing Magazine*, *10*(3), 32-71. https://doi.org/10.1109/mgrs.2022.3168135
Liu, A., Cheng, X., & Chen, Z. (2021). Performance evaluation of GEDI and ICESat-2 laser altimeter data for terrain and canopy height retrievals. *Remote Sensing of Environment*, *264*, 112571. https://doi.org/10.1016/j.rse.2021.112571
López-Serrano, P. M., Cárdenas Domínguez, J. L., Corral-Rivas, J. J., Jiménez, E., López-Sánchez, C. A., & Vega-Nieva, D. J. (2020). Modeling of Aboveground Biomass with Landsat 8 OLI and Machine Learning in Temperate Forests. *Forests*, *11*(1), 11. https://doi.org/10.3390/f11010011
Ma, T., Zhang, C., Ji, L., Zuo, Z., Beckline, M., ..., Xiao, X. (2024). Development of forest aboveground biomass estimation, its problems and future solutions: A review. *Ecological Indicators*, *159*, 111653. https://doi.org/10.1016/j.ecolind.2024.111653
Mahoney, C., Hall, R. J., Hopkinson, C., Filiatrault, M., Beaudoin, A., & Chen, Q. (2018). A Forest Attribute Mapping Framework: A Pilot Study in a Northern Boreal Forest, Northwest Territories, Canada. *Remote Sensing*, *10*(9), 1338. https://doi.org/10.3390/rs10091338
Mallet, C., & Bretar, F. (2009). Full-waveform topographic lidar: State-of-the-art. *ISPRS Journal of Photogrammetry and Remote Sensing*, *64*(1), 1-16. https://doi.org/10.1016/j.isprsjprs.2008.09.007
Mandlburger, G. (2024). Airborne Lidar: A Tutorial for 2025, Part I: Lidar basics. *LIDAR Magazine*, *14*(4). https://lidarmag.com/2024/12/30/airborne-lidar-a-tutorial-for-2025/
Markus, T., Neumann, T., Martino, A., Abdalati, W., Brunt, K., ..., Zwally, J. (2017). The Ice, Cloud, and land Elevation Satellite-2 (ICESat-2): Science requirements, concept, and implementation. *Remote Sensing of Environment*, *190*, 260-273. https://doi.org/10.1016/j.rse.2016.12.029
McGwire, K., Minor, T., & Fenstermaker, L. (2000). Hyperspectral mixture modeling for quantifying sparse vegetation cover in arid environments. *Remote Sensing of Environment*, *72*(3), 360-374. https://doi.org/10.1016/S0034-4257(99)00112-1

McRoberts, R., & Tomppo, E. (2007). Remote sensing support for national forest inventories. *Remote Sensing of Environment*, *110*(4), 412-419. https://doi.org/10.1016/j.rse.2006.09.034

Minunno, F., Miettinen, J., Tian, X., Häme, T., Holder, J., ..., Mäkelä, A. (2025). Data assimilation of forest status using Sentinel-2 data and a process-based model. *Agricultural and Forest Meteorology*, *363*, 110436. https://doi.org/10.1016/j.agrformet.2025.110436

Mokroš, M., Mikita, T., Singh, A., Tomaštík, J., Chudá, J., ..., Liang, X. (2021). Novel low-cost mobile mapping systems for forest inventories as terrestrial laser scanning alternatives. *International Journal of Applied Earth Observation and Geoinformation*, *104*, 102512. https://doi.org/10.1016/j.jag.2021.102512

Næsset, E. (1997a). Determination of mean tree height of forest stands using airborne laser scanner data. *ISPRS Journal of Photogrammetry and Remote Sensing*, *52*(2), 49-56. https://doi.org/10.1016/s0924-2716(97)83000-6

Næsset, E. (1997b). Estimating timber volume of forest stands using airborne laser scanner data. *Remote Sensing of Environment*, *61*(2), 246-253. https://doi.org/10.1016/s0034-4257(97)00041-2

Næsset, E. (2002). Predicting forest stand characteristics with airborne scanning laser using a practical two-stage procedure and field data. *Remote Sensing of Environment*, *80*(1), 88-99. https://doi.org/10.1016/s0034-4257(01)00290-5

Nandy, S., & Kushwaha, S. P. S. (2021). Forest Biomass Assessment Integrating Field Inventory and Optical Remote Sensing Data: A Systematic Review. *International Journal of Plant and Environment*, *7*(03), 181-186. https://doi.org/10.18811/ijpen.v7i03.1

Narine, L., Malambo, L., & Popescu, S. (2022). Characterizing canopy cover with ICESat-2: A case study of southern forests in Texas and Alabama, USA. *Remote Sensing of Environment*, *281*, 113242. https://doi.org/10.1016/j.rse.2022.113242

Narvaes, I. d. S., Santos, J. R. d., Bispo, P. d. C., Graça, P. M. d. A., Guimarães, U. S., & Gama, F. F. (2023). Estimating Forest Above-Ground Biomass in Central Amazonia Using Polarimetric Attributes of ALOS/PALSAR Images. *Forests*, *14*(5), 941. https://doi.org/10.3390/f14050941

Neuenschwander, A., & Pitts, K. (2019). The ATL08 land and vegetation product for the ICESat-2 Mission. *Remote Sensing of Environment*, *221*, 247-259. https://doi.org/10.1016/j.rse.2018.11.005

Neuenschwander, A. L., Pitts, K. L., Jelley, B. P., Robbins, J., Markel, J., ..., Sheridan, R. (2023). *ATLAS/ICESat-2 L3A Land and Vegetation Height, Version 6*. NASA National Snow and Ice Data Center Distributed Active Archive Center. https://doi.org/10.5067/ATLAS/ATL08.006

Neumann, M., Saatchi, S. S., Ulander, L. M. H., & Fransson, J. E. S. (2012). Assessing Performance of L- and P-Band Polarimetric Interferometric SAR Data in Estimating Boreal Forest Above-Ground Biomass. *IEEE Transactions on Geoscience and Remote Sensing*, *50*(3), 714-726. https://doi.org/10.1109/tgrs.2011.2176133

Ningthoujam, R., Balzter, H., Tansey, K., Morrison, K., Johnson, S., ..., Bermejo, J. (2016). Airborne S-Band SAR for Forest Biophysical Retrieval in Temperate Mixed Forests of the UK. *Remote Sensing*, *8*(7), 609. https://doi.org/10.3390/rs8070609

Olesk, A., Voormansik, K., Vain, A., Noorma, M., & Praks, J. (2015). Seasonal Differences in Forest Height Estimation From Interferometric TanDEM-X Coherence Data. *IEEE Journal of Selected Topics in Applied Earth Observations and Remote Sensing*, *8*(12), 5565-5572. https://doi.org/10.1109/jstars.2015.2501648

Ozdemir, I., & Karnieli, A. (2011). Predicting forest structural parameters using the image texture derived from WorldView-2 multispectral imagery in a dryland forest, Israel. *International Journal of Applied Earth Observation and Geoinformation*, *13*(5), 701-710. https://doi.org/10.1016/j.jag.2011.05.006

Pan, Y., Birdsey, R. A., Fang, J., Houghton, R., Kauppi, P. E., ..., Hayes, D. (2011). A large and persistent carbon sink in the world's forests. *Science*, *333*(6045), 988-993. https://doi.org/10.1126/science.1201609

Paradis, L., Thiffault, E., & Achim, A. (2019). Comparison of carbon balance and climate change mitigation potential of forest management strategies in the boreal forest of Quebec (Canada). *Forestry: An International Journal of Forest Research*, *92*(3), 264-277. https://doi.org/10.1093/forestry/cpz004

Persson, H., & Fransson, J. (2014). Forest Variable Estimation Using Radargrammetric Processing of TerraSAR-X Images in Boreal Forests. *Remote Sensing*, *6*(3), 2084-2107. https://doi.org/10.3390/rs6032084

Persson, H., Olsson, H., Soja, M., Ulander, L., & Fransson, J. (2017). Experiences from Large-Scale Forest Mapping of Sweden Using TanDEM-X Data. *Remote Sensing*, *9*(12), 1253. https://doi.org/10.3390/rs9121253

Persson, H. J., & Fransson, J. E. S. (2017). Comparison between TanDEM-X- and ALS-based estimation of aboveground biomass and tree height in boreal forests. *Scandinavian Journal of Forest Research*, *32*(4), 306-319. https://doi.org/10.1080/02827581.2016.1220618

Potapov, P., Li, X., Hernandez-Serna, A., Tyukavina, A., Hansen, M. C., ..., Hofton, M. (2021). Mapping global forest canopy height through integration of GEDI and Landsat data. *Remote Sensing of Environment*, *253*, 112165. https://doi.org/10.1016/j.rse.2020.112165

Praks, J., Antropov, O., & Hallikainen, M. T. (2012a). LIDAR-Aided SAR Interferometry Studies in Boreal Forest: Scattering Phase Center and Extinction Coefficient at X- and L-Band. *IEEE Transactions on Geoscience and Remote Sensing*, *50*(10), 3831-3843. https://doi.org/10.1109/tgrs.2012.2185803

Praks, J., Hallikainen, M., Antropov, O., & Molina, D. (2012b). Boreal forest tree height estimation from interferometric TanDEM-X images. *2012 IEEE International Geoscience and Remote Sensing Symposium*, pp. 1262-1265. https://doi.org/10.1109/igarss.2012.6351309

Praks, J., Kugler, F., Papathanassiou, K. P., Hajnsek, I., & Hallikainen, M. (2007). Height Estimation of Boreal Forest: Interferometric Model-Based Inversion at L- and X-Band Versus HUTSCAT Profiling Scatterometer. *IEEE Geoscience and Remote Sensing Letters*, *4*(3), 466-470. https://doi.org/10.1109/lgrs.2007.898083

Rahlf, J., Breidenbach, J., Solberg, S., Næsset, E., & Astrup, R. (2014). Comparison of four types of 3D data for timber volume estimation. *Remote Sensing of Environment*, *155*, 325-333. https://doi.org/10.1016/j.rse.2014.08.036

Rajab Pourrahmati, M., Baghdadi, N., & Fayad, I. (2023). Comparison of GEDI LiDAR Data Capability for Forest Canopy Height Estimation over Broadleaf

and Needleleaf Forests. *Remote Sensing*, *15*(6), 1522. https://doi.org/10.3390/rs15061522
Rajat, Priyanka, Musthafa, M., Kumar, P., Alsulamy, S., ..., Avtar, R. (2024). Development of L-band fully polarimetric SAR algorithm for forest biomass retrieval using 7SD and random forest regression. *Physics and Chemistry of the Earth, Parts A/B/C*, *136*, 103688. https://doi.org/10.1016/j.pce.2024.103688
Ramachandran, N., Saatchi, S., Tebaldini, S., Mariotti d'Alessandro, M., & Dikshit, O. (2021). Evaluation of P-Band SAR Tomography for Mapping Tropical Forest Vertical Backscatter and Tree Height. *Remote Sensing*, *13*(8), 1485. https://doi.org/10.3390/rs13081485
Ramachandran, N., Saatchi, S., Tebaldini, S., Mariotti d'Alessandro, M., & Dikshit, O. (2023). Mapping tropical forest aboveground biomass using airborne SAR tomography. *Scientific Reports*, *13*(1), 6233. https://doi.org/10.1038/s41598-023-33311-y
Reichstein, M., & Carvalhais, N. (2019). Aspects of Forest Biomass in the Earth System: Its Role and Major Unknowns. *Surveys in Geophysics*, *40*(4), 693-707. https://doi.org/10.1007/s10712-019-09551-x
Reigber, A., & Moreira, A. (2000). First demonstration of airborne SAR tomography using multibaseline L-band data. *IEEE Transactions on Geoscience and Remote Sensing*, *38*(5), 2142-2152. https://doi.org/10.1109/36.868873
Repola, J. (2008). Biomass equations for birch in Finland. *Silva Fennica*, *42*(4), 605-624, 236. https://doi.org/10.14214/sf.236
Repola, J. (2009). Biomass equations for Scots pine and Norway spruce in Finland. *Silva Fennica*, *43*(4), 625-647, 184. https://doi.org/10.14214/sf.184
Richards, J. A., Sun, G. Q., & Simonett, D. S. (1987). L-Band Radar Backscatter Modeling of Forest Stands. *IEEE Transactions on Geoscience and Remote Sensing*, *25*(4), 487-498. https://doi.org/10.1109/Tgrs.1987.289861
Rosen, P. A., Bawden, G. W., Barela, P., Chapman, B., Fattahi, H., ..., Shrikant, C. V. (2025). The NASA-ISRO SAR Mission: A summary. *IEEE Geoscience and Remote Sensing Magazine*, *13*(2), 8-34. https://doi.org/10.1109/mgrs.2025.3578258
Rosette, J., Suárez, J., Nelson, R., Los, S., Cook, B., & North, P. (2012). Lidar Remote Sensing for Biomass Assessment. In L. Fatoyinbo (Ed.), *Remote Sensing of Biomass - Principles and Applications*. IntechOpen. https://doi.org/10.5772/17479
Rott, H. (2009). Advances in interferometric synthetic aperture radar (InSAR) in earth system science. *Progress in Physical Geography: Earth and Environment*, *33*(6), 769-791. https://doi.org/10.1177/0309133309350263
Ruiz-Carregal, G., Lort Cuenca, M., Yam, L., Masalias, G., Makhoul, E., ..., Duro, J. (2024). Ku-Band SAR-Drone System and Methodology for Repeat-Pass Interferometry. *Remote Sensing*, *16*(21), 4069. https://doi.org/10.3390/rs16214069
Santi, E., Paloscia, S., Pettinato, S., Fontanelli, G., Mura, M., ..., Chirici, G. (2017). The potential of multifrequency SAR images for estimating forest biomass in Mediterranean areas. *Remote Sensing of Environment*, *200*, 63-73. https://doi.org/10.1016/j.rse.2017.07.038
Santoro, M., Cartus, O., Fransson, J. E. S., & Wegmüller, U. (2019). Complementarity of X-, C-, and L-band SAR Backscatter Observations to

Retrieve Forest Stem Volume in Boreal Forest. *Remote Sensing*, *11*(13), 1563. https://doi.org/10.3390/rs11131563
Santoro, M., Shvidenko, A., McCallum, I., Askne, J., & Schmullius, C. (2007). Properties of ERS-1/2 coherence in the Siberian boreal forest and implications for stem volume retrieval. *Remote Sensing of Environment*, *106*(2), 154-172. https://doi.org/10.1016/j.rse.2006.08.004
Schlund, M., & Davidson, M. (2018). Aboveground Forest Biomass Estimation Combining L- and P-Band SAR Acquisitions. *Remote Sensing*, *10*(7), 1151. https://doi.org/10.3390/rs10071151
Schlund, M., von Poncet, F., Kuntz, S., Schmullius, C., & Hoekman, D. H. (2015). TanDEM-X data for aboveground biomass retrieval in a tropical peat swamp forest. *Remote Sensing of Environment*, *158*, 255-266. https://doi.org/10.1016/j.rse.2014.11.016
Schlund, M., Wenzel, A., Camarretta, N., Stiegler, C., & Erasmi, S. (2023). Vegetation canopy height estimation in dynamic tropical landscapes with TanDEM-X supported by GEDI data. *Methods in Ecology and Evolution*, *14*(7), 1639-1656. https://doi.org/10.1111/2041-210x.13933
Schutz, B. E., Zwally, H. J., Shuman, C. A., Hancock, D., & DiMarzio, J. P. (2005). Overview of the ICESat Mission. *Geophysical Research Letters*, *32*(21). https://doi.org/10.1029/2005gl024009
Shao, Z., & Zhang, L. (2016). Estimating Forest Aboveground Biomass by Combining Optical and SAR Data: A Case Study in Genhe, Inner Mongolia, China. *Sensors*, *16*(6), 834. https://doi.org/10.3390/s16060834
Shiroma, G. H. X., Camara de Macedo, K. A., Wimmer, C., Moreira, J. R., & Fernandes, D. (2016). The Dual-Band PolInSAR Method for Forest Parametrization. *IEEE Journal of Selected Topics in Applied Earth Observations and Remote Sensing*, *9*(7), 3189-3201. https://doi.org/10.1109/jstars.2016.2520900
Simard, M., Pinto, N., Fisher, J. B., & Baccini, A. (2011). Mapping forest canopy height globally with spaceborne lidar. *Journal of Geophysical Research*, *116*(G4). https://doi.org/10.1029/2011jg001708
Sinha, S., Jeganathan, C., Sharma, L. K., & Nathawat, M. S. (2015). A review of radar remote sensing for biomass estimation. *International Journal of Environmental Science and Technology*, *12*(5), 1779-1792. https://doi.org/10.1007/s13762-015-0750-0
Solberg, S., Astrup, R., Bollandsås, O. M., Næsset, E., & Weydahl, D. J. (2010a). Deriving forest monitoring variables from X-band InSAR SRTM height. *Canadian Journal of Remote Sensing*, *36*(1), 68-79. https://doi.org/10.5589/m10-025
Solberg, S., Astrup, R., Breidenbach, J., Nilsen, B., & Weydahl, D. (2013). Monitoring spruce volume and biomass with InSAR data from TanDEM-X. *Remote Sensing of Environment*, *139*, 60-67. https://doi.org/10.1016/j.rse.2013.07.036
Solberg, S., Astrup, R., Gobakken, T., Næsset, E., & Weydahl, D. J. (2010b). Estimating spruce and pine biomass with interferometric X-band SAR. *Remote Sensing of Environment*, *114*(10), 2353-2360. https://doi.org/10.1016/j.rse.2010.05.011
Solberg, S., Hansen, E. H., Gobakken, T., Næsset, E., & Zahabu, E. (2017). Biomass and InSAR height relationship in a dense tropical forest. *Remote Sensing of Environment*, *192*, 166-175. https://doi.org/10.1016/j.rse.2017.02.010

Song, C. (2013). Optical remote sensing of forest leaf area index and biomass. *Progress in Physical Geography: Earth and Environment*, *37*(1), 98-113. https://doi.org/10.1177/0309133312471367

Stovall, A. E. L., Vorster, A. G., Anderson, R. S., Evangelista, P. H., & Shugart, H. H. (2017). Non-destructive aboveground biomass estimation of coniferous trees using terrestrial LiDAR. *Remote Sensing of Environment*, *200*, 31-42. https://doi.org/10.1016/j.rse.2017.08.013

Tang, Z., Xia, X., Huang, Y., Lu, Y., & Guo, Z. (2022). Estimation of National Forest Aboveground Biomass from Multi-Source Remotely Sensed Dataset with Machine Learning Algorithms in China. *Remote Sensing*, *14*(21), 5487. https://doi.org/10.3390/rs14215487

Tebaldini, S., Mariotti d'Alessandro, M., Le Toan, T., Villard, L., Ho Tong Minh, D., & Ferro-Famil, L. (2021). Polarimetric SAR Tomography for the Characterization of Forested Areas. *2021 IEEE International Geoscience and Remote Sensing Symposium IGARSS*, pp. 1534-1537. https://doi.org/10.1109/igarss47720.2021.9553140

Tebaldini, S., & Rocca, F. (2012). Multibaseline Polarimetric SAR Tomography of a Boreal Forest at P- and L-Bands. *IEEE Transactions on Geoscience and Remote Sensing*, *50*(1), 232-246. https://doi.org/10.1109/tgrs.2011.2159614

Telli, K., Kraa, O., Himeur, Y., Ouamane, A., Boumehraz, M., ..., Mansoor, W. (2023). A Comprehensive Review of Recent Research Trends on Unmanned Aerial Vehicles (UAVs). *Systems*, *11*(8), 400. https://doi.org/10.3390/systems11080400

Tian, L., Wu, X., Tao, Y., Li, M., Qian, C., ..., Fu, W. (2023). Review of Remote Sensing-Based Methods for Forest Aboveground Biomass Estimation: Progress, Challenges, and Prospects. *Forests*, *14*(6), 1086. https://doi.org/10.3390/f14061086

Ullah, S., Nazeer, M., Wong, M. S., & Amin, G. (2025). Remote sensing for aboveground biomass monitoring in terrestrial ecosystems: A systematic review. *Remote Sensing Applications: Society and Environment*, *39*, 101635. https://doi.org/10.1016/j.rsase.2025.101635

Vandendaele, B., Fournier, R. A., Vepakomma, U., Pelletier, G., Lejeune, P., & Martin-Ducup, O. (2021). Estimation of Northern Hardwood Forest Inventory Attributes Using UAV Laser Scanning (ULS): Transferability of Laser Scanning Methods and Comparison of Automated Approaches at the Tree- and Stand-Level. *Remote Sensing*, *13*(14), 2796. https://doi.org/10.3390/rs13142796

Varvia, P., Saarela, S., Maltamo, M., Packalen, P., Gobakken, T., ..., Korhonen, L. (2024). Estimation of boreal forest biomass from ICESat-2 data using hierarchical hybrid inference. *Remote Sensing of Environment*, *311*, 114249. https://doi.org/10.1016/j.rse.2024.114249

Verkerk, P. J., Anttila, P., Eggers, J., Lindner, M., & Asikainen, A. (2011). The realisable potential supply of woody biomass from forests in the European Union. *Forest Ecology and Management*, *261*(11), 2007-2015. https://doi.org/10.1016/j.foreco.2011.02.027

Wang, X., Cheng, X., Gong, P., Huang, H., Li, Z., & Li, X. (2011). Earth science applications of ICESat/GLAS: a review. *International Journal of Remote Sensing*, *32*(23), 8837-8864. https://doi.org/10.1080/01431161.2010.547533

Wang, Y., Lehtomäki, M., Liang, X., Pyörälä, J., Kukko, A., ..., Hyyppä, J. (2019). Is field-measured tree height as reliable as believed – A comparison study of tree height estimates from field measurement, airborne laser scanning and terrestrial laser scanning in a boreal forest. *ISPRS Journal of Photogrammetry and Remote Sensing*, *147*, 132-145. https://doi.org/10.1016/j.isprsjprs.2018.11.008

Wästlund, A., Holmgren, J., Lindberg, E., & Olsson, H. (2018). Forest Variable Estimation Using a High Altitude Single Photon Lidar System. *Remote Sensing*, *10*(9), 1422. https://doi.org/10.3390/rs10091422

White, J. C., Penner, M., & Woods, M. (2021). Assessing single photon LiDAR for operational implementation of an enhanced forest inventory in diverse mixedwood forests. *The Forestry Chronicle*, *97*(01), 78-96. https://doi.org/10.5558/tfc2021-009

Wittke, S., Yu, X., Karjalainen, M., Hyyppä, J., & Puttonen, E. (2019). Comparison of two-dimensional multitemporal Sentinel-2 data with three-dimensional remote sensing data sources for forest inventory parameter estimation over a boreal forest. *International Journal of Applied Earth Observation and Geoinformation*, *76*, 167-178. https://doi.org/10.1016/j.jag.2018.11.009

Yu, X., Hyyppä, J., Holopainen, M., & Vastaranta, M. (2010). Comparison of Area-Based and Individual Tree-Based Methods for Predicting Plot-Level Forest Attributes. *Remote Sensing*, *2*(6), 1481-1495. https://doi.org/10.3390/rs2061481

Yu, X., Hyyppä, J., Karjalainen, M., Nurminen, K., Karila, K., ..., Katoh, M. (2015). Comparison of Laser and Stereo Optical, SAR and InSAR Point Clouds from Air- and Space-Borne Sources in the Retrieval of Forest Inventory Attributes. *Remote Sensing*, *7*(12), 15933-15954. https://doi.org/10.3390/rs71215809

Yu, X., Hyyppä, J., Litkey, P., Kaartinen, H., Vastaranta, M., & Holopainen, M. (2017). Single-Sensor Solution to Tree Species Classification Using Multispectral Airborne Laser Scanning. *Remote Sensing*, *9*(2), 108. https://doi.org/10.3390/rs9020108

Yu, X., Kukko, A., Kaartinen, H., Wang, Y., Liang, X., ..., Hyyppä, J. (2020). Comparing features of single and multi-photon lidar in boreal forests. *ISPRS Journal of Photogrammetry and Remote Sensing*, *168*, 268-276. https://doi.org/10.1016/j.isprsjprs.2020.08.013

Yu, Y., & Saatchi, S. (2016). Sensitivity of L-Band SAR Backscatter to Aboveground Biomass of Global Forests. *Remote Sensing*, *8*(6), 522. https://doi.org/10.3390/rs8060522

Zheng, D., Rademacher, J., Chen, J., Crow, T., Bresee, M., ..., Ryu, S.-R. (2004). Estimating aboveground biomass using Landsat 7 ETM+ data across a managed landscape in northern Wisconsin, USA. *Remote Sensing of Environment*, *93*(3), 402-411. https://doi.org/10.1016/j.rse.2004.08.008

Zheng, J., Zhou, Z., Zhu, M., Wang, J., Wan, J., & Long, Y. (2024). Integration of Optical Remote Sensing and Laser Point Cloud for Forest Stock Estimation in Karst Mountainous Areas. *Forests*, *15*(12), 2106. https://doi.org/10.3390/f15122106

Zhu, X., Nie, S., Zhu, Y., Chen, Y., Yang, B., & Li, W. (2023). Evaluation and Comparison of ICESat-2 and GEDI Data for Terrain and Canopy Height Retrievals in Short-Stature Vegetation. *Remote Sensing*, *15*(20), 4969. https://doi.org/10.3390/rs15204969

Suomen Geodeettisen laitoksen julkaisut:
Veröffentlichungen des Finnischen Geodätischen Institutes:
Publications of the Finnish Geodetic Institute:

1. Y. VÄISÄLÄ: Tafeln für geodätische Berechnungen nach den Erddimensionen von Hayford. Helsinki 1923. 30 S.
2. Y. VÄISÄLÄ: Die Anwendung der Lichtinterferenz zu Längenmessungen auf grösseren Distanzen. Helsinki 1923. 22 S.
3. ILMARI BONSDORFF, Y. LEINBERG, W. HEISKANEN: Die Beobachtungsergebnisse der südfinnischen Triangulation in den Jahren 1920-1923. Helsinki 1924. 235 S.
4. W. HEISKANEN: Untersuchungen über Schwerkraft und Isostasie. Helsinki 1924. 96 S. 1 Karte.
5. W. HEISKANEN: Schwerkraft und isostatische Kompensation in Norwegen. Helsinki 1926. 33 S. 1 Karte.
6. W. HEISKANEN: Die Erddimensionen nach den europäischen Gradmessungen. Helsinki 1926. 26 S.
7. ILMARI BONSDORFF, V.R. ÖLANDER, Y. LEINBERG: Die Beobachtungsergebnisse der südfinnischen Triangulation in den Jahren 1924-1926. Helsinki 1927. 164 S. 1 Karte.
8. V.R. ÖLANDER: Ausgleichung einer Dreieckskette mit Laplaceschen Punkten. Helsinki 1927. 49 S. 1 Karte.
9. U. PESONEN: Relative Bestimmungen der Schwerkraft auf den Dreieckspunkten der südfinnischen Triangulation in den Jahren 1924-1925. Helsinki 1927. 129 S.
10. ILMARI BONSDORFF: Das Theorem von Clairaut und die Massenverteilung im Erdinnern. Helsinki 1929. 10 S.
11. ILMARI BONSDORFF, V.R. ÖLANDER, W. HEISKANEN, U. PESONEN: Die Beobachtungsergebnisse der Triangulationen in den Jahren 1926-1928. Helsinki 1929. 139 S. 1 Karte.
12. W. HEISKANEN: Über die Elliptizität des Erdäquators. Helsinki 1929. 18 S.
13. U. PESONEN: Relative Bestimmungen der Schwerkraft in Finnland in den Jahren 1926-1929. Helsinki 1930. 168 S. 1 Karte.
14. Y. VÄISÄLÄ: Anwendung der Lichtinterferenz bei Basismessungen. Helsinki 1930. 47 S.
15. M. FRANSSILA: Der Einfluss der den Pendel umgebenden Luft auf die Schwingungszeit beim v. Sterneckschen Pendelapparat. Helsinki 1931. 23 S.
16. Y. LEINBERG: Ergebnisse der astronomischen Ortsbestimmungen auf den finnischen Dreieckspunkten. Helsinki 1931. 162 S.
17. V.R. ÖLANDER: Über die Beziehung zwischen Lotabweichungen und Schwereanomalien sowie über das Lotabweichungssystem in Süd-Finnland. Helsinki 1931. 23 S.
18. PENTTI KALAJA, UUNO PESONEN, V.R. ÖLANDER, Y. LEINBERG: Beobachtungsergebnisse. Helsinki 1933. 240 S. 1 Karte.
19. R.A. HIRVONEN: The continental undulations of the geoid. Helsinki 1934. 89 pages. 1 map.
20. ILMARI BONSDORFF: Die Länge der Versuchsbasis von Helsinki und Längenveränderungen der Invardrähte 634-637. Helsinki 1934. 41 S.
21. V.R. ÖLANDER: Zwei Ausgleichungen des grossen südfinnischen Dreieckskranzes. Helsinki 1935. 66 S. 1 Karte.
22. U. PESONEN, V.R. ÖLANDER: Beobachtungsergebnisse. Winkelmessungen in den Jahren 1932-1935. Helsinki 1936. 148 S. 1 Karte.
23. R.A. HIRVONEN: Relative Bestimmungen der Schwerkraft in Finnland in den Jahren 1931, 1933 und 1935. Helsinki 1937. 151 S.
24. R.A. HIRVONEN: Bestimmung des Schwereunterschiedes Helsinki-Potsdam im Jahre 1935 und Katalog der finnischen Schwerestationen. Helsinki 1937. 36 S. 1 Karte.
25. T.J. KUKKAMÄKI: Über die nivellitische Refraktion. Helsinki 1938. 48 S.
26. Finnisches Geodätisches Institut 1918-1938. Helsinki 1939. 126 S. 2 Karten.
27. T.J. KUKKAMÄKI: Formeln und Tabellen zur Berechnung der nivellitischen Refraktion. Helsinki 1939. 18 S.
28. T.J. KUKKAMÄKI: Verbesserung der horizontalen Winkelmessungen wegen der Seitenrefraktion. Helsinki 1939. 18 S.
29. ILMARI BONSDORFF: Ergebnisse der astronomischen Ortsbestimmungen im Jahre 1933. Helsinki 1939. 47 S.
30. T. HONKASALO: Relative Bestimmungen der Schwerkraft in Finnland im Jahre 1937. Helsinki 1941. 78 S.
31. PENTTI KALAJA: Die Grundlinienmessungen des Geodätischen Institutes in den Jahren 1933-1939 nebst Untersuchungen über die Verwendung der Invardrähte. Helsinki 1942. 149 S.
32. U. PESONEN, V.R. ÖLANDER: Beobachtungsergebnisse. Winkelmessungen in den Jahren 1936-1940. Helsinki 1942. 165 S. 1 Karte.
33. PENTTI KALAJA: Astronomische Ortsbestimmungen in den Jahren 1935-1938. Helsinki 1944. 142 S.
34. V.R. ÖLANDER: Astronomische Azimutbestimmungen auf den Dreieckspunkten in den Jahren 1932-1938; Lotabweichungen und Geoidhöhen. Helsinki 1944. 107 S. 1 Karte.
35. U. PESONEN: Beobachtungsergebnisse. Winkelmessungen in den Jahren 1940-1947. Helsinki 1948. 165 S. 1 Karte.
36. Professori Ilmari Bonsdorffille hänen 70-vuotispäivänään omistettu juhlajulkaisu. Publication dedicated to Ilmari Bonsdorff on the occasion of his 70th anniversary. Helsinki 1949. 262 pages. 13 maps.
37. TAUNO HONKASALO: Measuring of the 864 m-long Nummela standard base line with the Väisälä light interference comparator and some investigations into invar wires. Helsinki 1950. 88 pages.
38. V.R. ÖLANDER: On the geoid in the Baltic area and the orientation of the Baltic Ring. Helsinki 1950. 26 pages.
39. W. HEISKANEN: On the world geodetic system. Helsinki 1951. 25 pages.
40. R.A. HIRVONEN: The motions of Moon and Sun at the solar eclipse of 1947 May 20th. Helsinki 1951. 36 pages.
41. PENTTI KALAJA: Catalogue of star pairs for northern latitudes from 55° to 70°for astronomic determination of latitudes by the Horrebow-Talcott method. Helsinki 1952. 191 pages.
42. ERKKI KÄÄRIÄINEN: On the recent uplift of the Earth's crust in Finland. Helsinki 1953. 106 pages. 1 map.
43. PENTTI KALAJA: Astronomische Ortsbestimmungen in den Jahren 1946-1948. Helsinki 1953. 146 S.
44. T.J. KUKKAMÄKI, R.A. HIRVONEN: The Finnish solar eclipse expeditions to the Gold Coast and Brazil 1947. Helsinki 1954. 71 pages.
45. JORMA KORHONEN: Einige Untersuchungen über die Einwirkung der Abrundungsfehler bei Gross-Ausgleichungen. Neu-Ausgleichung des südfinnischen Dreieckskranzes. Helsinki 1954. 138 S. 3 Karten.

46. Professori Weikko A. Heiskaselle hänen 60-vuotispäivänään omistettu juhlajulkaisu. Publication dedicated to Weikko A. Heiskanen on the occasion of his 60th anniversary. Helsinki 1955. 214 pages.
47. Y. VÄISÄLÄ: Bemerkungen zur Methode der Basismessung mit Hilfe der Lichtinterferenz. Helsinki 1955. 12 S.
48. U. PESONEN, TAUNO HONKASALO: Beobachtungsergebnisse der finnischen Triangulationen in den Jahren 1947-1952. Helsinki 1957. 91 S.
49. PENTTI KALAJA: Die Zeiten von Sonnenschein, Dämmerung und Dunkelheit in verschiedenen Breiten. Helsinki 1958. 63 S.
50. V.R. ÖLANDER: Astronomische Azimutbestimmungen auf den Dreieckspunkten in den Jahren 1938-1952. Helsinki 1958. 90 S. 1 Karte.
51. JORMA KORHONEN, V.R. ÖLANDER, ERKKI HYTÖNEN: The results of the base extension nets of the Finnish primary triangulation. Helsinki 1959. 57 pages. 5 appendices. 1 map.
52. V.R. ÖLANDER: Vergleichende Azimutbeobachtungen mit vier Instrumenten. Helsinki 1960. 48 pages.
53. Y. VÄISÄLÄ, L. OTERMA: Anwendung der astronomischen Triangulationsmethode. Helsinki 1960. 18 S.
54. V.R. ÖLANDER: Astronomical azimuth determinations on trigonometrical stations in the years 1955-1959. Helsinki 1961. 15 pages.
55. TAUNO HONKASALO: Gravity survey of Finland in years 1945-1960. Helsinki 1962. 35 pages. 3 maps.
56. ERKKI HYTÖNEN: Beobachtungsergebnisse der finnischen Triangulationen in den Jahren 1953-1962. Helsinki 1963. 59 S.
57. ERKKI KÄÄRIÄINEN: Suomen toisen tarkkavaaituksen kiintopisteluettelo I. Bench mark list I of the Second Levelling of Finland. Helsinki 1963. 164 pages. 2 maps.
58. ERKKI HYTÖNEN: Beobachtungsergebnisse der finnischen Triangulationen in den Jahren 1961-1962. Helsinki 1963. 32 S.
59. AIMO KIVINIEMI: The first order gravity net of Finland. Helsinki 1964. 45 pages.
60. V.R. ÖLANDER: General list of astronomical azimuths observed in 1920-1959 in the primary triangulation net. Helsinki 1965. 47 pages. 1 map.
61. ERKKI KÄÄRIÄINEN: The second levelling of Finland in 1935-1955. Helsinki 1966. 313 pages. 1 map.
62. JORMA KORHONEN: Horizontal angles in the first order triangulation of Finland in 1920-1962. Helsinki 1966. 112 pages. 1 map.
63. ERKKI HYTÖNEN: Measuring of the refraction in the Second Levelling of Finland. Helsinki 1967. 18 pages.
64. JORMA KORHONEN: Coordinates of the stations in the first order triangulation of Finland. Helsinki 1967. 42 pages. 1 map.
65. Geodeettinen laitos - The Finnish Geodetic Institute 1918-1968. Helsinki 1969. 147 pages. 4 maps.
66. JUHANI KAKKURI: Errors in the reduction of photographic plates for the stellar triangulation. Helsinki 1969. 14 pages.
67. PENTTI KALAJA, V.R. ÖLANDER: Astronomical determinations of latitude and longitude in 1949-1958. Helsinki 1970. 242 pages. 1 map.
68. ERKKI KÄÄRIÄINEN: Astronomical determinations of latitude and longitude in 1954-1960. Helsinki 1970. 95 pages. 1 map.
69. AIMO KIVINIEMI: Niinisalo calibration base line. Helsinki 1970. 36 pages. 1 sketch appendix.
70. TEUVO PARM: Zero-corrections for tellurometers of the Finnish Geodetic Institute. Helsinki 1970. 18 pages.
71. ERKKI KÄÄRIÄINEN: Astronomical determinations of latitude and longitude in 1961-1966. Helsinki 1971. 102 pages. 1 map.
72. JUHANI KAKKURI: Plate reduction for the stellar triangulation. Helsinki 1971. 38 pages.
73. V.R. ÖLANDER: Reduction of astronomical latitudes and longitudes 1922-1948 into FK4 and CIO systems. Helsinki 1972. 40 pages.
74. JUHANI KAKKURI AND KALEVI KALLIOMÄKI: Photoelectric time micrometer. Helsinki 1972. 53 pages.
75. ERKKI HYTÖNEN: Absolute gravity measurement with long wire pendulum. Helsinki 1972. 142 pages.
76. JUHANI KAKKURI: Stellar triangulation with balloon-borne beacons. Helsinki 1973. 48 pages.
77. JUSSI KÄÄRIÄINEN: Beobachtungsergebnisse der finnischen Winkelmessungen in den Jahren 1969-70. Helsinki 1974. 40 S.
78. AIMO KIVINIEMI: High precision measurements for studying the secular variation in gravity in Finland. Helsinki 1974. 64 pages.
79. TEUVO PARM: High precision traverse of Finland. Helsinki 1976. 64 pages.
80. R.A. HIRVONEN: Precise computation of the precession. Helsinki 1976. 25 pages.
81. MATTI OLLIKAINEN: Astronomical determinations of latitude and longitude in 1972-1975. Helsinki 1977. 90 pages. 1 map.
82. JUHANI KAKKURI AND JUSSI KÄÄRIÄINEN: The Second Levelling of Finland for the Aland archipelago. Helsinki 1977. 55 pages.
83. MIKKO TAKALO: Suomen Toisen tarkkavaaituksen kiintopisteluettelo II. Bench mark list II of the Second Levelling of Finland. Helsinki 1977. 150 sivua.
84. MATTI OLLIKAINEN: Astronomical azimuth determinations on triangulation stations in 1962-1970. Helsinki 1977. 47 pages. 1 map.
85. MARKKU HEIKKINEN: On the tide-generating forces. Helsinki 1978. 150 pages.
86. PEKKA LEHMUSKOSKI AND JAAKKO MÄKINEN: Gravity measurements on the ice of Bothnian Bay. Helsinki 1978. 27 pages.
87. T.J. KUKKAMÄKI: Väisälä interference comparator. Helsinki 1978. 49 pages.
88. JUSSI KÄÄRIÄINEN: Observing the Earth Tides with a long water-tube tiltmeter. Helsinki 1979. 74 pages.
89. Publication dedicated to T.J. Kukkamäki on the occasion of his 70th anniversary. Helsinki 1979. 184 pages.
90. B. DUCARME AND J. KÄÄRIÄINEN: The Finnish Tidal Gravity Registrations in Fennoscandia. Helsinki 1980. 43 pages.
91. AIMO KIVINIEMI: Gravity measurements in 1961-1978 and the results of the gravity survey of Finland in 1945-1978. Helsinki 1980. 18 pages. 3 maps.
92. LIISI OTERMA: Programme de latitude du tube zénithal visuel de l'observatoire Turku-Tuorla systéme amélioré de 1976. Helsinki 1981. 18 pages.
93. JUHANI KAKKURI, AIMO KIVINIEMI AND RAIMO KONTTINEN: Contributions from the Finnish Geodetic Institute to the Tectonic Plate Motion Studies in the Area between the Pamirs and Tien-Shan Mountains. Helsinki 1981. 34 pages.
94. JUSSI KÄÄRIÄINEN: Measurement of the Ekeberg baseline with invar wires. Helsinki 1981. 17 pages.
95. MATTI OLLIKAINEN: Astronomical determinations of latitude and longitude in 1976-1980. Helsinki 1982. 90 pages. 1 map.
96. RAIMO KONTTINEN: Observation results. Angle measurements in 1977-1978. Helsinki 1982. 29 pages.

97. G.P. Arnautov, Ye N. Kalish, A. Kiviniemi, Yu F. Stus, V.G. Tarasiuk, S.N. Scheglov: Determination of absolute gravity values in Finland using laser ballistic gravimeter. Helsinki 1982. 18 pages.
98. Leena Mikkola (editor): Mean height map of Finland. Helsinki 1983. 3 pages. 1 map.
99. Mikko Takalo and Jaakko Mäkinen: The Second Levelling of Finland for Lapland. Helsinki 1983. 144 pages.
100. Jussi Kääriäinen: Baseline Measurements with invar wires in Finland 1958-1970. Helsinki 1984. 78 pages.
101. Raimo Konttinen: Plate motion studies in Central Asia. Helsinki 1985. 31 pages.
102. Raimo Konttinen: Observation results. Angle measurements in 1979-1983. Helsinki 1985. 30 pages.
103. J. Kakkuri, T.J. Kukkamäki, J.-J. Levallois et H. Moritz: Le 250^{e} anniversaire de la mesure de l'arc du meridien en Laponie. Helsinki 1986. 60 pages.
104. G. Asch, T. Jahr, G. Jentzsch, A. Kiviniemi and J. Kääriäinen: Measurements of Gravity Tides along the "Blue Road Geotraverse" in Fennoscandia. Helsinki 1987. 57 pages.
105. Jussi Kääriäinen, Raimo Konttinen, Lu Qiankun and Du Zong Yu: The Chang Yang Standard Baseline. Helsinki 1986. 36 pages.
106. E.W. Grafarend, H. Kremers, J. Kakkuri and M. Vermeer: Adjusting the SW Finland Triangular Network with the TAGNET 3-D operational geodesy software. Helsinki 1987. 60 pages.
107. Matti Ollikainen: Astronomical determinations of latitude and longitude in 1981-1983. Helsinki 1988. 37 pages.
108. Markku Poutanen: Observation results. Angle measurements in 1967-1973. Helsinki 1988. 35 pages.
109. Jussi Kääriäinen, Raimo Konttinen and Zsuzsanna Németh: The Gödöllö Standard Baseline. Helsinki 1988. 66 pages.
110. Jussi Kääriäinen and Hannu Ruotsalainen: Tilt measurements in the underground laboratory Lohja 2, Finland, in 1977-1987. Helsinki 1989. 37 pages.
111. Mikko Takalo: Lisäyksiä ja korjauksia Suomen tarkkavaaitusten linjastoon 1977-1989. Helsinki 1991. 98 sivua.
112. Raimo Konttinen: Observation results. Angle measurements in the Pudasjärvi loop in 1973-1976. Helsinki 1991. 42 pages.
113. Raimo Konttinen, Jorma Jokela and Li Quan: The remeasurement of the Chang Yang Standard Baseline. Helsinki 1991. 40 pages.
114. Jussi Kääriäinen, Raimo Konttinen and Markku Poutanen: Interference measurements of the Nummela Standard Baseline in 1977, 1983, 1984 and 1991. Helsinki 1992. 78 pages.
115. Juhani Kakkuri (editor): Geodesy and geophysics. Helsinki 1993. 200 pages.
116. Jaakko Mäkinen, Heikki Virtanen, Qiu Qi-xian and Gu Liang-rong: The Sino-Finnish absolute gravity campaign in 1990. Helsinki 1993. 49 pages.
117. Raimo Konttinen: Observation results. Geodimeter observations in 1971-72, 1974-80 and 1984-85. Helsinki 1994. 58 pages.
118. Raimo Konttinen: Observation results. Angle measurements in 1964-65, 1971, 1984 and 1986-87. Helsinki 1994. 67 pages.
119. Jorma Jokela: The 1993 adjustment of the Finnish First-Order Terrestrial Triangulation. Helsinki 1994. 137 pages.
120. Markku Poutanen (editor): Interference measurements of the Taoyuan Standard Baseline. Helsinki 1995. 35 pages.
121. Jorma Jokela: Interference measurements of the Chang Yang Standard Baseline in 1994. Kirkkonummi 1996. 32 pages.
122. Olli Jaakkola: Quality and automatic generalization of land cover data. Kirkkonummi 1996. 39 pages.
123. Matti Ollikainen: Determination of orthometric heights using GPS levelling. Kirkkonummi 1997. 143 pages.
124. Tiina Kilpeläinen: Multiple Representation and Generalization of Geo-Databases for Topographic Maps. Kirkkonummi 1997. 229 pages.
125. Jussi Kääriäinen and Jaakko Mäkinen: The 1979-1996 gravity survey and the results of the gravity survey of Finland 1945-1996. Kirkkonummi 1997. 24 pages. 1 map.
126. Zhitong Wang: Geoid and crustal structure in Fennoscandia. Kirkkonummi 1998. 118 pages.
127. Jorma Jokela and Markku Poutanen: The Väisälä baselines in Finland. Kirkkonummi 1998. 61 pages.
128. Markku Poutanen: Sea surface topography and vertical datums using space geodetic techniques. Kirkkonummi 2000. 158 pages
129. Matti Ollikainen, Hannu Koivula and Markku Poutanen: The Densification of the EUREF Network in Finland. Kirkkonummi 2000. 61 pages.
130. Jorma Jokela, Markku Poutanen, Zhao Jingzhan, Pei Weili, Hu Zhenyuan and Zhang Shengshu: The Chengdu Standard Baseline. Kirkkonummi 2000. 46 pages.
131. Jorma Jokela, Markku Poutanen, Zsuzsanna Németh and Gábor Virág: Remeasurement of the Gödöllö Standard Baseline. Kirkkonummi 2001. 37 pages.
132. Andres Rüdja: Geodetic Datums, Reference Systems and Geodetic Networks in Estonia. Kirkkonummi 2004. 311 pages.
133. Heikki Virtanen: Studies of Earth Dynamics with the Superconducting Gravimeter. Kirkkonummi 2006. 130 pages.
134. Juha Oksanen: Digital elevation model error in terrain analysis. Kirkkonummi 2006. 142 pages. 2 maps.
135. Matti Ollikainen: The EUVN-DA GPS campaign in Finland. Kirkkonummi 2006. 42 pages.
136. Annu-Maaria Nivala: Usability perspectives for the design of interactive maps. Kirkkonummi 2007. 157 pages.
137. Xiaowei Yu: Methods and techniques for forest change detection and growth estimation using airborne laser scanning data. Kirkkonummi 2007. 132 pages.
138. Lassi Lehto: Real-time content transformations in a WEB service-based delivery architecture for geographic information. Kirkkonummi 2007. 150 pages.
139. Pekka Lehmuskoski, Veikko Saaranen, Mikko Takalo and Paavo Rouhiainen: Suomen Kolmannen tarkkavaaituksen kiintopisteluettelo. Bench Mark List of the Third Levelling of Finland. Kirkkonummi 2008. 220 pages.
140. Eija Honkavaara: Calibrating digital photogrammetric airborne imaging systems using a test field. Kirkkonummi 2008. 139 pages.
141. Markku Poutanen, Eero Ahokas, Yuwei Chen, Juha Oksanen, Marita Portin, Sari Ruuhela, Heli Suurmäki (editors): Geodeettinen laitos – Geodetiska Institutet – Finnish Geodetic Institute 1918–2008. Kirkkonummi 2008. 173 pages.

142. MIKA KARJALAINEN: Multidimensional SAR Satellite Images – a Mapping Perspective. Kirkkonummi 2010. 132 pages.
143. MAARIA NORDMAN: Improving GPS time series for geodynamic studies. Kirkkonummi 2010. 116 pages.
144. JORMA JOKELA AND PASI HÄKLI: Interference measurements of the Nummela Standard Baseline in 2005 and 2007. Kirkkonummi 2010. 85 pages.
145. EETU PUTTONEN: Tree Species Classification with Multiple Source Remote Sensing Data. Kirkkonummi 2012. 162 pages.
146. JUHA SUOMALAINEN: Empirical Studies on Multiangular, Hyperspectral, and Polarimetric Reflectance of Natural Surfaces. Kirkkonummi 2012. 144 pages.
147. LEENA MATIKAINEN: Object-based interpretation methods for mapping built-up areas. Kirkkonummi 2012. 210 pages.
148. LAURI MARKELIN: Radiometric calibration, validation and correction of multispectral photogrammetric imagery. Kirkkonummi 2013. 160 pages.
149. XINLIAN LIANG: Feasibility of Terrestrial Laser Scanning for Plotwise Forest Inventories. Kirkkonummi 2013. 150 pages.
150. EERO AHOKAS: Aspects of accuracy, scanning angle optimization, and intensity calibration related to nationwide laser scanning. Kirkkonummi 2013. 124 pages.
151. LAURA RUOTSALAINEN: Vision-Aided Pedestrian Navigation for Challenging GNSS Environments. Kirkkonummi 2013. 180 pages.
152. HARRI KAARTINEN: Benchmarking of airborne laser scanning based feature extraction methods and mobile laser scanning system performance based on high-quality test fields. Kirkkonummi 2013. 346 pages.
153. ANTERO KUKKO: Mobile Laser Scanning – System development, performance and applications. Kirkkonummi 2013. 247 pages.
154. JORMA JOKELA: Length in Geodesy – On Metrological Traceability of a Geospatial Measurand. Kirkkonummi 2014. 240 pages.
155. PYRY KETTUNEN: Analysing landmarks in nature and elements of geospatial images to support wayfinding. Kirkkonummi 2014. 281 pages.
156. MARI LAAKSO: Improving Accessibility for Pedestrians with Geographic Information. Kirkkonummi 2014. 129 pages.

The name of the series has changed the 1st of January in 2015.

FGI Publications:

157. LINGLI ZHU: A pipeline of 3D scene reconstruction from point clouds. Kirkkonummi 2015. 208 pages.
158. ROBERT E. GUINNESS: Context Awareness for Navigation Applications. Kirkkonummi 2015. 244 pages.
159. HANNU KOIVULA: Finnish permanent GNSS network FinnRef. Helsinki 2019. 141 pages.
160. PAULIINA KRIGSHOLM: Towards a future cadastral system: An exploration of the Finnish case. Helsinki 2020. 110 pages.
161. VEIKKO SAARANEN, PEKKA LEHMUSKOSKI, MIKKO TAKALO, PAAVO ROUHIAINEN: The Third Precise Levelling of Finland. Helsinki 2021. 307 pages.
162. JUHANI KAKKURI: Muistelmia geodeettien maailmasta = Memoirs From the World of Geodesy. Kirkkonummi 2021. 125 pages.
163. MIRJAM BILKER-KOIVULA: Geoid and postglacial rebound related gravity change in Finland. Helsinki 2021. 84 pages.
164. MATTI LEHTOMÄKI: Detection and Recognition of Objects from Mobile Laser Scanning Point Clouds: Case studies in a road environment and power line corridor. Helsinki 2021. 89 pages.
165. ROOPE NÄSI: Drone-based spectral and 3D remote sensing applications for forestry and agriculture. Helsinki 2021.78 pages.
166. MIKKO RÖNNEBERG: Approach for creating useful, gamified and social map applications utilising privacy-preserving crowdsourcing. Helsinki 2022. 112 pages.
167. SONJA LAHTINEN: Reference frame densifications for Nordic and Baltic countries. Helsinki 2022. 100 pages.
168. TIMO SAARI: Investigations of geoid models in Finland - Towards GNSS-related height system. Helsinki 2022. 76 pages.
169. ULLA KALLIO: Towards daily-based local ties at Fundamental Geodetic Sites - Development of local tie processes as a part of the renovations at Metsähovi Geodetic Research Station. Helsinki 2023. 119 pages.
170. RISTO KUITTINEN: Tutkijan muistelmia. Helsinki 2023. 170 pages.
171. SANNA KAASALAINEN, EIJA HONKAVAARA, MIKA SAAJASTO, ELIAS HAARNOJA, NIKO KOIVUMÄKI: GNSS security and resilience in Eastern Finland. Helsinki 2026. 48 pages.
172. JORMA JOKELA, PASI HÄKLI, TIMO SAARI, MARKKU POUTANEN: Interference measurements of the Nummela Standard Baseline in 2013 and 2024. Espoo 2026. 36 pages.
173. AIMAD EL ISSAOU: Automated pavement distress detection and quantification with multi-platform laser scanning. Helsinki 2026. 106 pages.
174. ZIYI FENG: Characterizing Boreal Forest Structure and Estimating Above-Ground Biomass with Helicopter-borne Ku-band Profiling Radar. Helsinki 2026. 67 pages.



Finnish Geospatial Research Institute FGI
Vuorimiehentie 5
FI-02150 Espoo
Finland

www.fgi.fi